GDAŃSK UNIVERSITY
OF TECHNOLOGY

FACULTY OF CIVIL AND
ENVIRONMENTAL
ENGINEERING

WILiŚ

The author of the PhD dissertation: Bartosz Sobczyk
Scientific discipline: Civil engineering

DOCTORAL DISSERTATION

Title of PhD dissertation: FEM analysis of composite materials failure in nonlinear six field shell theory

Title of PhD dissertation (in Polish): Analiza MES zniszczenia materiałów kompozytowych w ramach nieliniowej 6 parametrowej teorii powłok

Supervisor	Second supervisor
signature	*signature*
dr hab. inż. Wojciech Witkowski	
Auxiliary supervisor	Cosupervisor
signature	*signature*
dr inż. Agnieszka Sabik	

Gdańsk, year 2016

Contents

Acknowledgements

ABSTRACT

The dissertation deals with the problem of failure initiation in thin laminated composites. Known techniques of laminate structures modelling are briefly characterised. Eventually, shell based approach is chosen for the purpose of the description of the composite structures behaviour, as they predict their deformation and states of stress effectively in a global sense in the considered case. The nonlinear six parameter shell theory (6p theory) with asymmetric strain and stress measures is mainly used within the work and thus its main properties are described. Selected and commonly known methods of the damage onset description for laminated shells, based on the assumption of stress tensor symmetry, named as standard criteria, are studied and analyzed. These are: Tsai-Hill, Tsai-Wu, Hashin and Puck. Modifications of the aforementioned criteria meeting the requirements of the 6p theory are discussed and proposed, since no precise descriptions of the damage initiation in laminates are found in the literature when asymmetric strain and stress components are utilised. The modified criteria, allowing first ply failure (FPF) analysis of laminates, are implemented into non-commercial finite element method (FEM) code CAM. Finally, six numerical examples are solved using FEM to check if the FPF estimations resulting from the application of the standard and the modified criteria differ.

STRESZCZENIE

Niniejsza rozprawa dotyczy problemu inicjacji zniszczenia w laminatach kompozytowych o małej grubości całkowitej. W pracy przedstawiono znane techniki modelowania konstrukcji wykonanych z laminatów kompozytowych. Jednak do opisu zachowania analizowanych konstrukcji wybrano teorie powłokowe, gdyż są one wystarczająco dokładne na potrzeby odwzorowania globalnej pracy układu dla konstrukcji cienkich. W rozprawie wykorzystywana jest głównie nieliniowa 6 parametrowa teoria powłok, w której występują niesymetryczne miary odkształceń i naprężeń. W związku z tym jej główne cechy zostały zawarte w tekście. Omówiono wybrane i powszechnie znane standardowe metody szacowania inicjacji zniszczenia w laminatach: Tsai-Hill, Tsai-Wu, Hashin i Puck, w których zakłada się symetrię tensora naprężeń i odkształceń. Jako, że dokładne opisy sposobów przewidywania pierwszego uszkodzenia laminatów dla teorii z niesymetrycznymi składowymi odkształceń i naprężeń nie zostały znalezione w literaturze, zaproponowano modyfikacje rozważanych kryteriów standardowych. Kryteria zmodyfikowane, które pozwalają na analizę zniszczenia pierwszego włókna (FPF) zostały zaimplementowane do niekomercyjnego kodu metody elementów skończonych (MES) CAM. Na koniec rozwiązano, przy pomocy MES, sześć przykładów, w celu sprawdzenia czy występują różnice w oszacowaniach FPF kryteriów standardowych i zmodyfikowanych.

LIST OF THE MOST IMPORTANT SYMBOLS AND NOTATIONS

$\boldsymbol{Q(x)}$ – tensor of mean rotary deformation of the shell cross sections

$\boldsymbol{T(x)}$ – the structure tensor in the current configuration

$\boldsymbol{T_0(x)}$ – the structure tensor in the reference (initial) configuration

$\mathbf{e}$ – vector of shell strains

$\mathbf{s}$ – vector of shell stress and couple resultants

$\mathbf{c}$ – constitutive matrix

$\varphi_{(k)}$ – angle of fibre orientation in k^{th} lamina

$\left(a_{(k)}, b_{(k)}, c_{(k)}\right)$ – orthogonal material coordinate system of kth lamina

$\tilde{\mathbf{T}}_k$ – transformation matrix

$\underset{4\times4}{\mathbf{A}}$ – extensional stiffness matrix

$\underset{4\times4}{\mathbf{B}}$ – extension - bending coupling matrix

$\underset{4\times4}{\mathbf{D}}$ – bending stiffness matrix

$\underset{2\times2}{\mathbf{S}}$ – transverse shear stiffness matrix

$\underset{2\times2}{\mathbf{G}}$ – drilling resultants stiffness matrix

σ_{aa} – normal stress in the 1st material direction

σ_{bb} – normal stress in the 2nd material direction

σ_{ab} – in-plane shear stress in the in the 2nd material direction

σ_{ba} – in-plane shear stress in the in the 1st material direction

σ_a – transverse shear stress on the a-c plane

σ_b – transverse shear stress on the b-c plane

E_a – elastic modulus of lamina in the 1st material direction

E_b — elastic modulus of lamina in the 2nd material direction

G_{ab} — in-plane shear modulus of lamina

G_{ac} — lamina a-c plane transverse shear modulus

G_{bc} — lamina b-c plane transverse shear modulus

v_{ab} — major Poisson's ratio of a lamina

X_t — absolute value of a lamina tensile strength in the 1st material direction

X_c — absolute value of a lamina compressive strength in the 1st material direction

Y_t — absolute value of a lamina tensile strength in the 2nd material direction

Y_c — absolute value of a lamina compressive strength in the 2nd material direction

S_l — lamina in-plane shear strength

S_t — lamina transverse shear strength

σ_{nn} — normal stress component acting on lamina failure plane

σ_{nl} — shear stress component on failure plane in the fibre direction

σ_{nt} — shear stress component on failure plane perpendicular to σ_{nl}

θ_f — lamina failure plane inclination angle

η_{w1} — Puck's criterion weakening factor

1. INTRODUCTION

Engineers developed many materials over the centuries of mankind history. Some of them, such as steel, concrete or timber, have been applied for many years. For instance, the first use of concrete as structural material is dated to 7000 BC and was found in Yiftah el in Israel (see e.g. RACZKIEWICZ [2010]). These materials are used in civil engineering either separately or in combination of two or more constituents, forming composite structures. However, new material solutions are introduced. This is possible, because of a very rapid growth of science, industry and technology. The ongoing research aims to create new materials, which are light, have high strength and some particular desired properties or their use is economically reasonable. The new proposals may include for instance nanomaterials, reinforced plastics, functionally graded materials, structural foams, etc. Nevertheless, the Author is focused on the fibre reinforced plastics (FRP), namely polymer matrix laminated composites. The laminated composite can be divided into stack of single layers (laminas) bonded at their interface. Each lamina is made of one surface of reinforcement (e.g. uni or bidirectional) and the matrix, which surrounds the fibres (see for instance JONES R. M. [1999]). The concept of laminated composite structure is shown in Fig. 1.1.
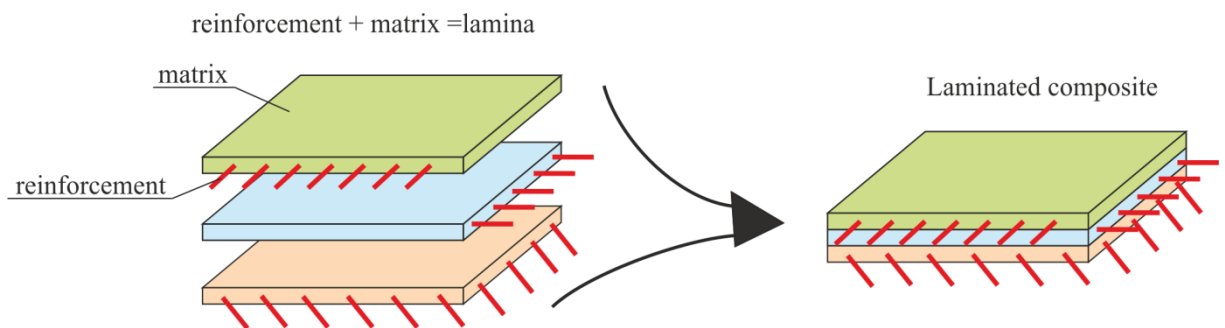
Fig. 1.1 The structure of laminated composite

Historically, laminated composites can be classified as very modern materials. Their production became possible as a consequence of the development of synthetic fibres manufacturing techniques after 2nd World War. At first glass fibres were invented. Shortly after, in the 1950s and 1960s also carbon fibres production was launched (see for instance GERMAN [2001]). Single fibres have very high longitudinal stiffness. However fibres alone can't sustain loads in off-fibres direction and are not able to carry more complex loading conditions. In order to overcome these drawbacks they have to be immersed in a matrix, forming a lamina, which can be further combined into a laminated composite. The matrix distributes loads between fibres in the lamina and also protects fibres against negative

environmental influences or damages due to for example impacts. There are different types of matrices e.g. polymer, metal or ceramic, that allow to form different types of composites. The polymer matrix composites are nowadays the most commonly applied ones (compare with GURIT [2015]). Typical stress-strain relations of: single fibres, homogenous matrix material and reinforced plastics composite are illustrated in Fig. 1.2.
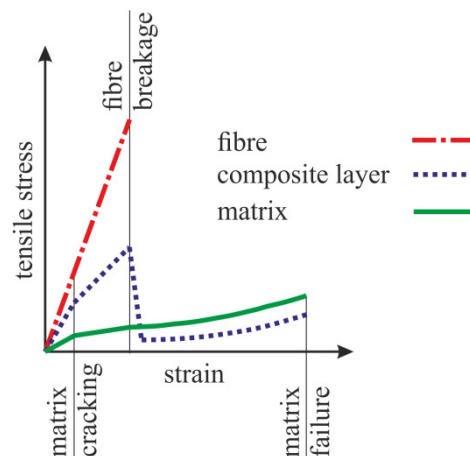

Fig. 1.2 Stress-strain relations of: single fibres, homogenous matrix material and reinforced plastics composite (created on the basis of GURIT [2015] and ASHBY M. F., JONES D. R. H. [2006])

The overall properties of the composite layer make it attractive to use them (see Fig. 1.2). The laminated composite has high load bearing capabilities together with low density, high resistance to environmental influences and short time of fabrication. In effect, the laminated composites can compete with other traditional materials, such as steel or concrete in the field of material and structural properties (GURIT [2015]). Generally, the manufacture cost of laminated composite structures may be higher, as compared with production cost of e.g. steel or concrete structures. On the other hand, the range of maintenance works for laminated composite structures is reduced, which means that higher production cost can be compensated by durable long-term efficient performance (TONY GEE PARTNERS [2012]). Hence, it can be stated that the overall properties of the laminated composites are competitive to the ones presented by standard materials and therefore can be applied in engineering practice.

1.1 Thesis motivation

Because of the avantages discussed above, the laminates are commonly applied, for example in marine, rail, automotive or aerospace industry, to produce sport equipments, everyday devices, or in civil engineering (see e.g. CAMPBELL F. C. [2010]).

The author of this thesis was involved in a research project, under which an U-shaped composite sandwich footbridge was developed and built (The National Centre for Research and Developement project, FOBRIDGE, PBS1/B2/6/2013). The outer skins of the sandwich are made of FRP. Design of such a bridge required some particular design approaches, in the field of among others laminated composite load capacity (see CHRÓSCIELEWSKI J., KLASZTORNY M., NYCZ D., SOBCZYK B. [2014]) Until then the bridges made of laminated composite are the main area of interest of the Author, which inspired him to deal with the problems described later in this thesis.

Owing to the above, some selected examples of designed and constructed bridges, containing FRP elements, are given below:

- the Beddington Trail highway bridge in Canada, in which carbon fibre reinforced plastics tendons were used in pretensioned concrete girders (HOFFARD T. A., MALVAR L. J. [2005]),

- the Salmon River Bridge, which is reported as the first, concrete bridge deck slab where fibre reinforced plastics (FRP) rods where used instead of regular steel ones (HOFFARD T. A., MALVAR L. J. [2005]),

- the Wickwire Run Bridge in West Virginia manufactured by Creative Pultrusions, which is made from modular FRP bridge decks, that are placed on steel girders (LOPEZ-ANIDO R., TROUTMAN D. L., BUSEL J. P.),

- tied arch pedestrian bridge in Lleida in Spain and cable-stayed footbridge in Kolding in Denmark, both made entirely by means of FRP pultruded profiles (SMITS J. [2014]),

- Halgavor suspension bridge with FRP deck, located in the south of Bodmin in Cornwall, UK (GUNAYDIN M., ADANUR S., ALTUNISIK A. C., SEVIM B. [2015]),

- truss bridge fully made of FRP composite, located at sewage plant in Łódź (ZOBEL H., KARWOWSKI W., ŻÓŁTOWSKI K., KOZAKIEWICZ A. [2005])

- composite road bridge in Błażowa, made of FRP girders and concrete slab (Combridge project, PONETA P., KULPA M., WŁASAK L., SIWOWSKI T. [2014])

- FOBRIDGE project pedestrian bridge with 14m long span, the full scale research object previously located at the Gdańsk University of Technology campus in Gdańsk, Poland (see Fig. 1.3), now mounted over the Radunia River in Pruszcz Gdański, it is a shell structure made of sandwich plates, with FRP skins and inner foam core (Pyrzowski Ł., Sobczyk B., Witkowski W., Chróścielewski J. [2015]).

Fig. 1.3 Full scale research object of pedestrian bridge, developed, under FOBRDIGE project at Gdańsk University of Technology, Gdańsk, Poland.

Obviously, the above short list does not cover all applications in bridge design. 355 bridges with FRP elements, among which 53 bridges are classified as fully made of FRP were reported already in 2011 (Potyrała P. B. [2011]). This number is still extensively growing.

The designed FRP structures need to enable safe and durable exploitation. Therefore various design aspects arise. One of them is the estimation of the structure load capacity, known as the FRP failure. Because the FRP material does not have a long history of application, the methods that define structural failure are still under investigation. It is also worth to mention, that the standard load capacity estimations procedures valid for instance for steel and concrete cannot be used in the analyzes of FRPs. This is because in the mechanics of FRPs we deal with an anisotropic or orthotropic continuum instead of an isotropic one. Two states of damage are distinguished in laminates: the First Ply Failure - FPF and the Last Ply Failure - LPF (see for instance Kaw A. K. [2006], German [2001]). FPF defines the moment of the initial failure in the whole structure, whereas LPF is reached when the structure cannot transfer no more load. The FPF method seems to be more appropriate for application in the design process, in which progressive failure cannot

occur, as it may lead to a very rapid and uncontrolled failure. The process of progressive material degradation, which is the essence of LPF calculations, is seldom used in practice. It is rather utilised in order to formulate reasonable conclusions on complex failure modes of FRP elements that may happen. On the basis of LPF behaviour some complicated material damage models can be developed and validated. This leads to the formulation of general rules of composite laminates behaviour after initial failure, which are required for proper design of civil engineering structures.

A lot of researchers have made contributions in the areas mentioned above. Among others: Hinton Sodden and Kaddour opened three World Wide Failure exercises in order to summarize existing information and to extend the base of knowledge on initial and progressive damage under two and three-dimensional loading conditions (see HINTON M. J., KADDOUR A. S., SODEN P. D. (EDS.) [2004], HINTON M. J., KADDOUR A. S. [2012], KADDOUR A. S., HINTON M. J., SMITH P. A., LI S. [2013]). However an effort is still required to understand behaviour of laminated composites since many aspects of this process are still not well identified, which motivates this thesis. Hence, this dissertation deals with the failure issues, that occur in composite laminates.

Composite laminates have a specific structure. As it was described earlier, they are made of very stiff fibres embedded in matrix. Since the fibres are thin, a single layer of laminate also has a small thickness and generally maintain high stiffness too. What is more, it is possible to apply different fibre orientations in different laminas. This means that reinforcement orientation of a designed structure can be precisely adjusted to some particular loading conditions. Thus, the total thickness of lamination lay-up will be small, while the structure will be able to carry significant loads. For example, the thickness of laminate skins in the Bradkirk Bridge in UK, which is a simply supported structure with 12m span length and sandwich type cross section, is approximately equal to 2.5mm (foam core is 100mm thick, CALVERT T. [2009]). The laminate skin in the regular midspan region of the FOBRIDGE research object (simply supported bridge, 14m span length, sandwich cross section, see Fig. 1.3) built in 2014, is approximately 4mm thick (foam core is up to 100mm thick). This gives cross section depth to span length ratio equal to: 0.00875 for Bradkirk bridge and 0.0077 for FOBRIDGE footbridge. Pressure vessels and tanks are another example of FRP laminates application. For instance centrifugally cast flat bottom, open top fibreglass tanks offered by Design Tanks company (Sioux Falls, SD, USA), have the wall thickness to tank radius ratio ranging from 0.0042 to 0.0083 for tanks with

capacity ranging from 3.785m^3 to 22.712 m^3 (the product information available online at: www.designtanks.com/UserFiles/Documents/

Resources/Company Literature/Design_Tanks_Catalog.pdf). Thus, it can be stated that structures made of FRP, either fully or partially like sandwich plates with FRP skins, generally have a wall thickness small enough, which allow to treat them as a shell-like body. From the reasons described in this paragraph it is intended here to analyze damage onset in shell structures using a chosen shell theory.

Different techniques are available to model multilayered shell structures (see e.g. REDDY J. N. [2004], KREJA I. [2011], WAGNER W. [2010]. Generally, it is possible to use two dimensional (2D) or three dimensional (3D) theories with different levels of complicity, which depends on the required results precision. The computations in this work are made with aid of 2D shell theory. There are many shell theories currently available. They can be classified with respect to the formulation procedure. Following for example CHRÓŚCIELEWSKI J., MAKOWSKI J., PIETRASZKIEWICZ W. [2004] direct and derived types of shell theories are distinguished. According to the direct approach, a shell is treated from the beginning as a 2D material continuum endowed with some kinematical and dynamical properties. It was firstly proposed in the works: COSSERAT E., COSSERAT F. [1908], COSSERAT E., COSSERAT F. [1909], more examples of approaches classified into this group can be found in CHRÓŚCIELEWSKI J., MAKOWSKI J., PIETRASZKIEWICZ W. [2004]. On the other hand the derived type theories assume that a shell is a 3D body with a particular geometry, namely with an easily determined thickness. Therefore, the continuum mechanics principles formulated for 3D body are reduced in a appropriate manner to the case of 2D shell. These kinds of approaches may be traced back to the works: LOVE A. E. H. [1889], LOVE A. E. H. [1927]. Different shell kinematics arises, depending on the chosen theory. If the direct theories are chosen, kinematics of Cosserat medium is introduced. Such a kinematics is accompanied with asymmetric strain and stress measures, because of the considered orientation and length of material fibres (see for instance ALTENBACH J., ALTENBACH H., EREMEYEV V. A. [2010]). On the other hand, these effects can be neglected in derived theories. Their basic examples are the 3-parameter Kirchoff-Love and 5-parameter Reissner-Mindilin theories (REDDY J. N. [2007], BÎRSAN M., NEFF P. [2014b]). Since the shell fibre which is normal to the reference surface before deformation cannot rotate around its axis by assumption, the in-plane strain and stress measures need to be symmetric.

In this work the nonlinear 6-parameter shell theory (6p theory) is used, which principals can be found e.g. in works of REISSNER E. [1974a] and LIBAI A., SIMMONDS J. G. [1998]. From the theoretical point of view the 6p theory is a mixed approach, which utilizes some assumptions dictated by both direct and derived ones. In this theory the 6th parameter is the rotation perpendicular to the shell reference surface, which is an independent variable, just as in Cosserat type surface kinematics. As a consequence the strain and stress measures become asymmetric. It is worth to mention that the meaning of the 6th parameter may be different in other approaches. It may also represent extension of shell normal fibre (see among others BAŞAR Y., DING Y. [1997]). The effect of fibre extension can be analyzed also by means of more kinematical variables, as presented e.g. in IBRAHIMBEGOVIĆ A. [2005] (7-parameter theory).

The application of the 6p theory is motivated by the fact that it is especially dedicated to the analysis of shells with intersection. Since the aforementioned FOBRIDGE structure is a bridge of such a type, the Author of this work wanted to analyze its behaviour inter alia with aid of more sophisticated theoretical approaches.

1.2 Aim of the thesis and theoretical assumptions

This thesis proposes application of particular material law, developed by CHRÓSCIELEWSKI J., KREJA I., SABIK A., WITKOWSKI W. [2011], which fulfils the requirements of the 6p theory, in FPF analysis. The constitutive relation is derived on the basis of asymmetric Cauchy-type plane stress relation, assuming the first order shear deformation kinematics theory (FSDT) for an equivalent single layer panel (ESL model), which will be described later. In effect, failure initiation in laminated composites is considered for the continua, in which the in-plane strain and stress resultants are asymmetric. To the best of the Author's knowledge, this has not been discussed until now. Therefore, this work fills the gap in 6p theory, regarding analysis of laminated composites.

The following assumptions, concerning the analysis of laminated composites are imposed here as a consequence of the application of the 6p theory and constitutive relation (CHRÓSCIELEWSKI J., KREJA I., SABIK A., WITKOWSKI W. [2011]):

- all composite layers are made of a finite number of individually homogenous layers,

- all layers are ideally bonded, which means that no slip between them is allowed,
- the material is linearly elastic-brittle,
- thin and moderately thick shells can be analysed,
- only small strains are allowed.

The above mentioned material law provides an efficient description of global behaviour of multilayered shells in 6p theory.

The stress state that appear in composite layers is utilized to estimate damage initiation with aid of proper failure criteria (JONES R. M. [1999]). The existing failure initiation theories are formulated assuming that the in-plane shear stress components are symmetric. Thus, it is not possible to use them directly in order to describe the onset of damage in the framework of the 6p theory. What is more, there are no available precise descriptions of failure initiation for shell theories with Cosserat type kinematics. Therefore, in this work modifications of existing failure initiation criteria are presented, that allow to meet requirements dictated by the formalism of the 6p theory. It is believed that the advanced 6p theory is able to recreate the stress state in shell structures, especially in those with folds and branches more precisely, as compared with the 5 parameter theories (5p theory). This should result in a more accurate prediction of FPF.

Some numerical experiments are carried out in order to assess whether there are any differences between FPF estimations, resulting from the application of the modified and classical criteria. These experiments include geometrically nonlinear static tests on shells with and without intersections.

1.3 Analysis tools

All simulations in this work are conducted numerically with aid of Finite Element Method (FEM). They are mainly performed in the Author's code developed from the CAM code, which was firstly used by CHRÓŚCIELEWSKI J., MAKOWSKI J., STUMPF H. [1992]. Originally, the code had material law implemented, valid for small strain analysis of shells made of isotropic materials. As far as laminated shells are concerned the code was successfully expanded in a way that the new material law for laminated composites was incorporated (see CHRÓŚCIELEWSKI J., KREJA I., SABIK A., WITKOWSKI W. [2011]). Finally, new procedures concerning determination of stress state in all layers and specification of

initial failure in laminates have been implemented in this thesis. This is original Author achievement. Some results in this field were published for instance in: CHRÓŚCIELEWSKI J., WITKOWSKI W., SOBCZYK B., SABIK A. [2015], SOBCZYK B. [2015] and CHRÓŚCIELEWSKI J., SABIK A., SOBCZYK B., WITKOWSKI W. [2016]. The Author's CAM results are compared with reference data available in the literature and are also confronted with ABAQUS (ABAQUS 6.14 MANUAL) calculations in order to check the difference between the output of theories with asymmetric (CAM) and symmetric (ABAQUS) strain and stress measures.

1.4 Thesis

Finally, as a consequence of the information given in the preceding subsections, a following thesis is formulated and is going to be considered within this work:

It is possible to determine the damage onset moment with aid of FEM algorithms under the nonlinear 6 parameter shell theory.

1.5 Plan of the dissertation

After introduction, two important issues are briefly described, correspondingly in chapter 2 and 3, viz. modelling techniques of laminated composites and the basics of the nonlinear 6-parameter shell theory. These two chapters do not elucidate all aspects underlying the discussed subjects, but intend to point out the most important theoretical issues, which are necessary to understand modifications of the failure initiation criteria.

Then, in chapter 4, failure initiation estimation methods are reviewed and the development of the classical Tsai-Hill, Tsai-Wu, Hashin and Puck criteria is described. After that, modifications of these criteria are proposed, in chapter 5, that allow FPF analysis within the framework of the 6p theory. This is the most important, original part of this work.

Numerical calculations are performed and described in chapter 6 to check, if there are any differences between FPF estimations resulting from the classical (5p theory) and modified (6p theory) approach.

Finally some essential conclusions and final remarks are formulated in chapter 7.

2. MODELLING OF LAMINATED COMPOSITES

The structure of laminate is quite complex (stiff fibres and resilient matrix are connected, see e.g. HASHIN Z. [1980]). Different phenomena that take place in various materials, including FRPs, can be analysed at different scales: micro, meso (multi) and macro (see for instance KREJA I. [2011]). The micro-mechanical modelling is very detailed and enables among others precise analysis of the stress state and failure at the fibre-matrix interface, in separate fibres within the matrix or at layers interface. On the other hand these highly local effects can be neglected when global response of the laminated structure is predicted, which can be determined via macro-mechanical models. Since the time consumption of micro-mechanical calculations is very high and the results of macro-mechanical analysis are sometimes not sufficient a compromise between these two approaches is reached leading to formulate meso-scale model. Some information on meso-scale models are available for instance in: ALLIX O. [2001], LADEVÈZE P., LUBINEAU G., MARSAL D. [2006], LUBINEAU G., LADEVÈZE P. [2008].

Correspondingly, REDDY J. N. [2004] distinguishes following types of theoretical models of laminates:

- Equivalent Single Layer (ESL) theories (two dimensional - 2D):

    o Classical lamination theory,

    o Shear deformation theories;

- Three-dimensional continuum theory (three dimensional - 3D):

    o Layerwise theories,

    o Traditional 3D continuum formulations;

- Multiple model methods (2D and 3D)

Some of them are described in the subsequent chapters.

2.1 Equivalent Single Layer models

The ESL theories transform 3D multilayered continuum into 2D one, through application of a shell fibre kinematics and some over the thickness integration procedures. Different kinematical assumptions can be applied, that consequently decide about the

usefulness of the theory. The ESL theory is classified into macro-mechanical models group. They are used to describe the global response of laminated structures and by assumption have some limitations, e.g. the subsequent layers are perfectly bonded. The ESL models are widely used in the global analysis of thin to moderately thick laminates.

The stiffness of the whole laminate in the ESL technique is described by statically equivalent single-layer shell. Its macro-mechanical properties are calculated as a weighted average of homogenized mechanical properties of each lamina of the laminate (see for instance REDDY J. N. [2004], KREJA I. [2011]). Therefore, the behaviour of multilayered laminate results from the behaviour of a single layer shell, which have particular properties, that depend on the lamination scheme.

According to such a definition of the problem, derivation of the kinematics in through the thickness direction of the laminate is required. Application of the Kirchoff-Love theory (see for example REDDY J. N. [2007]) is the simplest way to deal with this problem and in composite mechanics it is called Classical Lamination Theory - CLT (REDDY J. N. [2004]). In consequence, the shell straight fibre perpendicular to the shell reference surface before deformation, remains straight and perpendicular to the shell reference surface after deformation. Hence, shear strain in the planes perpendicular to the shell reference surface are equal to zero and shear stress resulting from constitutive law are zero as well (see e.g. JONES R. M. [1999]). Because of this feature, the CLT is not well suited to the analysis of laminated composites (KREJA I. [2011]), as they are susceptible to shear influences.

The next level of kinematics refinement is application of the First Order Shear Deformation Theory (FSDT), which is known also as the Reissner-Mindlin theory (RAMM E. [2000], REDDY J. N. [2007]). Here, the shell fibre after deformation does not remain normal to the shell reference surface, as opposed to CLT (REDDY J. N. [2004]). The transverse shear strain is constant in the shell thickness direction. Therefore, some shear correction factors (see REISSNER E. [1974b]) need to be associated with FSDT, because, in reality, the transverse shear stress distribution in the layer thickness direction is at least quadratic (REDDY J. N. [2004]). It is more difficult to define the correction factor for laminated composites, as compared with homogenous shells or plates (KREJA I. [2011], SABIK A. [2012]), thus introduction of the correction factor can be treated as a drawback of the method.

The shell kinematics can be further improved and expanded to Higher Order Shear Deformation Theories (HSDT), for example Second Order - SSDT or Third Order Shear Deformation Theory -TSDT, by including higher order terms in the kinematical assumptions (CARRERA E., BRISCHETTO S. [2009]). Basically, such a model is developed through the application of displacements and strains power series expansion, as a function of the shell thickness coordinate (KREJA I. [2011]). As a consequence, the restriction about straight fibres is relaxed. In such a case the distribution of transverse shear stress and strains in the thickness direction became quadratic or of higher order in each layer. Therefore the definition of shear correction factors in not necessary here (REDDY J. N. [2004]). On the other hand, the additional higher order terms are hard to describe from the physical point of view. Since the CLT and FSDT are able to describe the global behaviour of most laminates, the HSDT are used only in a limited group of cases, where their additional precision is required (REDDY J. N. [2004]). Because the application of additional higher order terms complicates the theoretical description and intensifies numerical effort, without satisfactory improvement of results, theories with a rank higher than three are not found to be applied (see for instance REDDY J. N. [2004]).

Kinematical models described earlier (e.g. FSDT) can be supplemented with some warping functions. This treatment is introduced in order to remove the limitations of HSDT and to include some additional effects that are observed in thick laminates and sandwich structures (TESSLER A., DI SCIUVA M., GHERLONE M [2010]) for example, among others, significant changes in the slope of displacement profile at the layer interface. In effect, the deformation pattern along the thickness coordinate becomes a so-called zig-zag profile (see e.g. SABIK A., KREJA I. [2008]). As compared with HSDT the theories with additional zig-zag warping functions are more precise in the description of laminate behaviour and less time consuming during calculations. However, the use of zig-zag theories in the case of large scale computations or engineering applications makes sense only when their analytical descriptions enable efficient finite element approximation (TESSLER A., DI SCIUVA M., GHERLONE M [2010]).

A comparison of the displacements and transverse shear stress distributions (resulting from constitutive law) in the thickness direction for some of the above described models is depicted in Fig. 2.1.
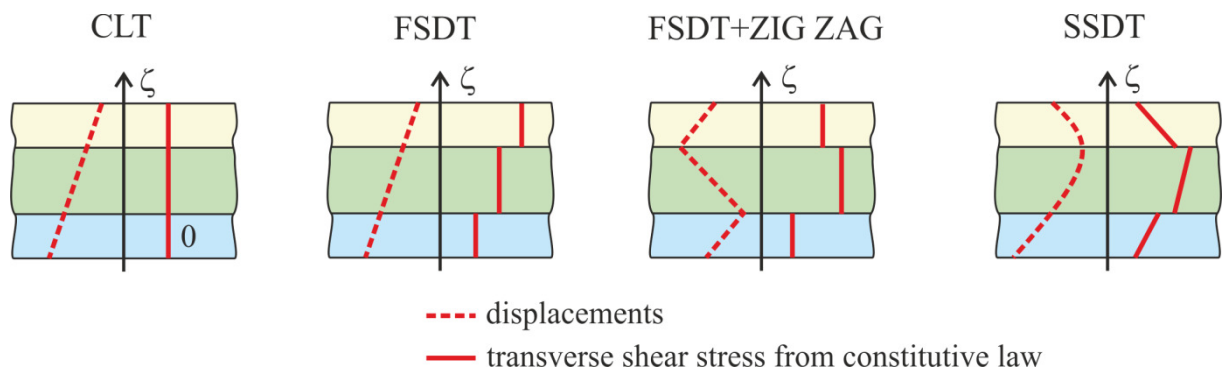
Fig. 2.1 Comparison of displacements and transverse shear stress distributions of ESL displacements models (created on the basis of CARRERA E., BRISCHETTO S. [2009]).

2.2 Layerwise theories

The next level of theory refinement includes the layerwise theories (LW) and enables meso and macro analyses. It is introduced, because among others results provided by ESL techniques are not sufficient to fully represent behaviour of laminated composites, for instance in the areas where concentrated loads are applied or geometric and material nonlinearities appear (REDDY J. N. [2004]).

In the LW approach each layer of the laminate is modelled separately. Appropriate continuity conditions are applied at the layers interface to maintain connection between them. Therefore the deformation profile of the stacking sequence is more precise and some limitations of ESL models are relaxed. However, as opposed to the ESL, the numerical level of complexity of LW task is greater here and is defined by the total number of layers (see e.g. KREJA I. [2011]). In the LW approach the laminate displacement variables are independent in each layer. Therefore, significant changes in the slope of displacements profile between layers, known as the zig-zag effect, can be easily recreated here. From these reasons the LW theories are commonly used in the analysis of moderately thick laminated composites (REDDY J. N. [2004]). An example of relation between displacements and transverse shear stresses, with respect to the laminate thickness, provided by LW theory calculations, assuming that TDST kinematics is utilised in each layer is shown in Fig. 2.2.
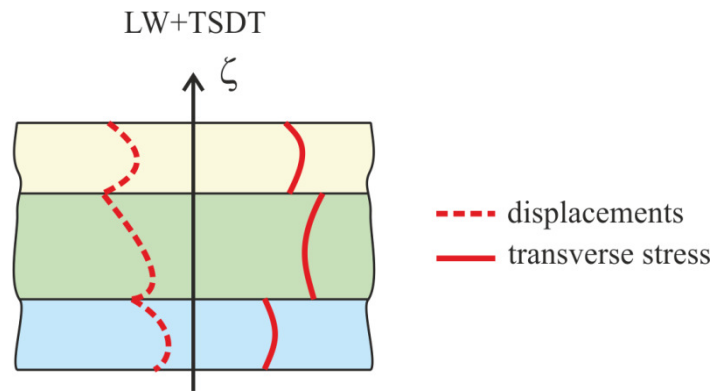
LW+TSDT

Fig. 2.2 Displacements and transverse shear stresses of laminate in LW calculations, assuming TDST in each layer (created on the basis of CARRERA E., BRISCHETTO S. [2009]).

2.3   3D formulations and multiple models

Finally, also 3D continuum models can be used to describe behaviour of multilayered medium on the micro, meso or macro scale. Regarding FEM approach, each layer of a laminate needs to be discretized with at least one finite element (WAGNER W. [2010], see also MEYER-PIENING H.-R. [2004]). This allow one to analyse laminates with different thickness, including precisely various effect of their deformation and stress distribution. However, in such a case the numerical cost increases drastically, as compared with 2D models, which generally preclude the application of this type of modelling in practical applications (KREJA I. [2011]). This is a consequence of the requirements about the size of solid finite elements. The laminas are thin, therefore the dimensions of the remaining finite element edges are affected by their thickness. According to ABAQUS 6,14 MANUAL, the default maximum value of hexahedral element aspect ratio is 10, where the aspect ratio defines the ratio between the longest and the shortest edge of the element. The use of multiple models is a compromise between high precision of results and very high numerical effort. In such a case, the 3D model is utilised only in the areas where the high results precision is required. In the remaining areas, where global behaviour is recreated a 2D ESL or LW model is used (REDDY J. N. [2004]).

3. NONLINEAR 6-PARAMETER SHELL THEORY BASICS

This chapter introduces basic information about the 6p theory and the associated material laws, which creates the theoretical background of finite element code CAM, mainly used in this work. However it does not pretend to be a thorough, concise and comprehensive description of all theoretical aspects of the 6p theory.

The works of REISSNER E. [1974a], SIMMONDS J. G. [1984] and LIBAI A., SIMMONDS J. G. [1998] may be mentioned as the foundations of the present 6 parameter theory. There are many papers discussing different aspects of the considered linear and nonlinear 6 parameter shell theories. The ones listed here can be treated as state of the art contribution in this area: EREMEYEV V. A., LEBEDEV L. P. [2011], EREMEYEV V. A, PIETRASZKIEWICZ W. [2011], EREMEYEV V. A., LEBEDEV L. P., CLOUD M. J. [2014], PIETRASZKIEWICZ W. [2011], ALTENBACH H., EREMEYEV V. A. [2014], PIETRASZKIEWICZ W., KONOPIŃSKA V. [2014], BÎRSAN M., NEFF P. [2014a], BÎRSAN M., NEFF P. [2014b], EREMEYEV V. A, PIETRASZKIEWICZ W. [2015], PIETRASZKIEWICZ W. [2015]. The kinematics of the present 6p theory is characterized by three rigid directors, similarly as in Cosserat kinematics. It should be mentioned that there are also different approaches, named as Cosserat ones. For instance GREEN A. E., NAGHDI P. M. WAINWRIGHT W. K. [1965] or GREEN A. E., NAGHDI P. M. [1982] use only one director, while EREMEYEV V. A., LEBEDEV L. P., ALTENBACH H. [2013] distinguish also introduction of one or more deformable directors, which are additional kinematical variables.

The approach of 6p theory was firstly adopted into the framework of FEM static calculations and described in following papers: CHRÓŚCIELEWSKI J., MAKOWSKI J., STUMPF H. [1992]; CHRÓŚCIELEWSKI J. [1996]; CHRÓŚCIELEWSKI J., MAKOWSKI J., STUMPF H. [1997]. Then it was extended onto dynamic problems, see e.g., CHRÓŚCIELEWSKI J., MAKOWSKI J., PIETRASZKIEWICZ W. [2000], LUBOWIECKA I. [2001] or LUBOWIECKA I., CHRÓŚCIELEWSKI J. [2002]. The book of CHRÓŚCIELEWSKI J., MAKOWSKI J., PIETRASZKIEWICZ W. [2004] is a summary of current state (as of 2004) of facts on static and dynamic problems of multifold shells, where also some numerical FEM examples were presented.

After 2004 further effort towards efficiency of 6p theory calculations was made. Some efficient low order finite elements for the analysis of shell structures were proposed in CHRÓŚCIELEWSKI J., WITKOWSKI W. [2006] and WITKOWSKI W. [2009].

The papers cited above consider the analysis of thin, elastic and isotropic shells. However, also other constitutive relations are available for this theory. CHRÓŚCIELEWSKI J., KREJA I., SABIK A., WITKOWSKI W. [2011] presented and successfully applied material law for orthotropic multilayered shells. The elastoplastic constitutive relation for isotropic shells, including micropolar effects via the characteristic length, was proposed for the 6p theory in the following papers: BURZYŃSKI S., CHRÓŚCIELEWSKI J., WITKOWSKI W. [2014a], BURZYŃSKI S., CHRÓŚCIELEWSKI J., WITKOWSKI W. [2014b], BURZYŃSKI S., CHRÓŚCIELEWSKI J., WITKOWSKI W. [2015]. It is also possible to analyze functionally graded materials by means of 6p theory (see DASZKIEWICZ K., CHRÓŚCIELEWSKI J., WITKOWSKI W. [2014] or BURZYŃSKI S., CHRÓŚCIELEWSKI J., DASZKIEWICZ K., WITKOWSKI W. [2016]).

It is worth to emphasize the reason for the application of 6p theory in FEM. Many shell finite elements have been developed for the purpose of computational structural analyses. Most of them are based on 5p theory. Such elements, for instance degenerated shell elements or Reissner-Mindlin type element (see for instance CHRÓŚCIELEWSKI J. [1996] and citations given there), have 5 degrees of freedom in each single node, namely 3 translations and 2 rotational parameters. This means that there is no rotation associated with direction perpendicular to the shell surface. Many civil engineering structures, that can be classified to the group of shell structures, have complex geometry with connections, branches, folds or intersections. Therefore the kinematical model associated with 5p theory is not sufficient to represent behaviour of such shell elements in FEM, because the lack of 3rd rotational degree of freedom can lead to false deformation patterns in the case of shell structures with folds or intersections (CHRÓŚCIELEWSKI J., MAKOWSKI J., PIETRASZKIEWICZ W. [2000], SCHMIDT B., DAMRATH R., PAHL P.J. [1977]). This problem can be solved through the application of appropriate numerical techniques, which generally involves introduction of artificial 6th degree of freedom (compare with ZIENKIEWICZ O. C., TAYLOR R. L. [2000] or ERHART T. [2013]).

The shell kinematics associated with the 6p theory is different. The 6th degree of freedom appears as a natural consequence of the following theoretical transformations. The equilibrium equations of 2D shell like body are derived from direct continuum mechanics laws of 3D body, by means of integration in through the thickness direction. On this basis 2D local equations of motion and boundary conditions are formulated, which are consequently used to build integral identity, interpreted as the principle of virtual work.

The identity gives the rise to the virtual strains and curvature measures energetically conjugated with stress and couple resultants. Thus, a particular shell kinematics of Cosserat type, composed of independent displacement and rotation fields is determined in a natural way, without any additional artificial assumptions. The only approximation appears on the level of constitutive equations.

3.1 Shell deformation and strain measures

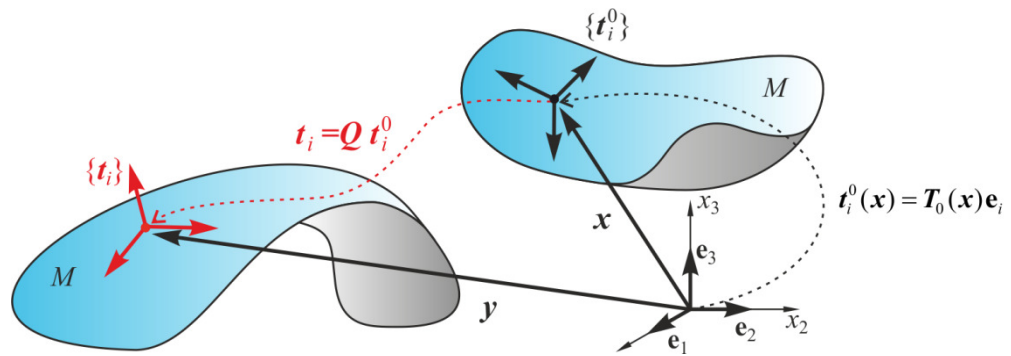The shell motion described by the 6p theory is shown in Fig. 3.1.

Fig. 3.1 Motion of the reference surface M.

The motion of the reference surface M is described by position vector field $y(x)$, which defines the translatory deformation:

$$y(x) = x + u(x) \tag{3.1}$$

and the proper orthogonal tensor field:

$$T(x) = T_0(x)Q(x). \tag{3.2}$$

Here, $Q(x)$ defines the mean rotary deformation of the shell cross sections, $T(x)$ is the structure tensor in current configuration, while $T_0(x)$ is the structure tensor in reference (initial) configuration.

The structure tensor defines geometry of the shell in different configurations. The tensor $T_0(x)$ can be represented by three directors (see Fig. 3.2):

$$t_\beta^0 = x,_\beta, \quad t_3^0 = \frac{t_1^0 \times t_2^0}{\| t_1^0 \times t_2^0 \|}, \quad \beta = 1, 2, \quad (.),_\beta = \frac{\partial(.)}{\partial s_\beta}. \tag{3.3}$$

The third director is assumed to remain normal to the reference surface, thus $\boldsymbol{t}^0 \equiv \boldsymbol{t}_3^0$. The directors $\{\boldsymbol{t}_i^0\}$ form a rigid orthogonal frame (see Fig. 3.2), that meets the following relations:

$$\boldsymbol{t}_i^0 \cdot \boldsymbol{t}_j^0 = \delta_{ij}, \ \| \boldsymbol{t}_i^0 \| = 1. \tag{3.4}$$
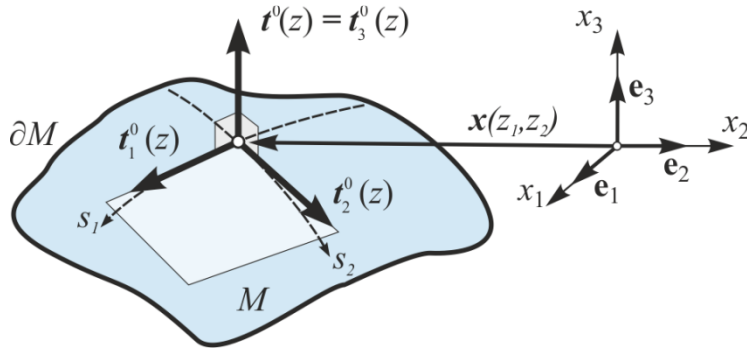

Fig. 3.2 Shell surface directors $\{\boldsymbol{t}_i^0\}$.

It should be mentioned here that the shell reference surface M in different configurations is formally described by means of orthogonal arc-length coordinates $\left(s^\gamma, s\right) = s^i$, where $\gamma = 1, 2$ and $i = 1, 2, 3$ (see Fig. 3.2). However, these are not directly required here, since only the surface tangent vectors are necessary for the purpose of shell motion description (CHRÓŚCIELEWSKI J., KREJA I., SABIK A., WITKOWSKI W. [2011]).

Owing to the above it is possible to determine the directors in the reference configuration (see Fig. 3.1), which in general can be defined in different ways (CHRÓŚCIELEWSKI J., MAKOWSKI J., PIETRASZKIEWICZ W. [2000]). Here, it is assumed that:

$$\boldsymbol{t}_i^0 = \boldsymbol{T}_0(\boldsymbol{x})\mathbf{e}_i, \ i = 1, 2, 3, \tag{3.5}$$

where $\{\mathbf{e}_i\}$ is a defined orthonormal basis in physical space. The structure tensor $\boldsymbol{T}_0(\boldsymbol{x})$ in 6p theory is a part of the input data of the problem to be solved.

Finally, the actual configuration (compare with Fig. 3.1) of shell geometry is defined:

$$\boldsymbol{t}_i(\boldsymbol{x}) = \boldsymbol{Q}(\boldsymbol{x})\boldsymbol{t}_i^0(\boldsymbol{x}) = \boldsymbol{Q}(\boldsymbol{x})\boldsymbol{T}_0(\boldsymbol{x})\mathbf{e}_i = \boldsymbol{T}(\boldsymbol{x})\mathbf{e}_i, \ i = 1, 2, 3. \tag{3.6}$$

Thus, it has been shown on the basis of (3.5) and (3.6), that the shell kinematics is created on the basis of three rigid directors, which corresponds with the Cosserat kinematics.

The relations between stresses and strains are the essential part of this research, therefore all the derivations and discussions about the definition of strains are omitted and only their final forms are presented. These derivations can be found e.g. in CHRÓŚCIELEWSKI J. [1996] or CHRÓŚCIELEWSKI J., MAKOWSKI J., PIETRASZKIEWICZ W. [2004].

In the shell base defined, as it is shown in e.g. CHRÓŚCIELEWSKI J. [1996], the virtual strain measures can be rewritten for stretching vector as:

$$\delta\boldsymbol{\varepsilon}_\beta(\boldsymbol{x}) = \boldsymbol{v}_{,\beta} + \boldsymbol{y}_{,\beta} \times \boldsymbol{w} = \boldsymbol{v}_{,\beta} + (\boldsymbol{t}_\beta + \boldsymbol{\varepsilon}_\beta) \times \boldsymbol{w} \;,\; \beta = 1, 2 \tag{3.7}$$

and for bending vector as:

$$\delta\boldsymbol{\kappa}_\beta(\boldsymbol{x}) = \boldsymbol{w}_{,\beta} \,,\; \beta = 1, 2 \,. \tag{3.8}$$

and the corresponding strain measures, that are related to (3.7) and (3.8) are defined as follows:

$$\boldsymbol{\varepsilon}_\beta = \boldsymbol{y}_{,\beta} - \boldsymbol{t}_\beta = \boldsymbol{u}_{,\beta} + (\mathbf{1} - \boldsymbol{Q})\boldsymbol{t}_\beta^0 \,,\; \beta = 1, 2 \,, \tag{3.9}$$

$$\boldsymbol{\kappa}_\beta = \mathrm{ad}^{-1}(\boldsymbol{Q}_{,\beta}\,\boldsymbol{Q}^{\mathrm{T}}) \,,\; \beta = 1, 2 \,. \tag{3.10}$$

Here, $\boldsymbol{v}$ and $\boldsymbol{w}$, denote correspondingly kinematically admissible field of virtual displacements and rotations.

Let us assume the following form of the generalized vector of displacement (CHRÓŚCIELEWSKI J., MAKOWSKI J., PIETRASZKIEWICZ W. [2004]):

$$\mathbf{u} = (\boldsymbol{u}, \boldsymbol{Q}) \,, \tag{3.11}$$

where: $\boldsymbol{u}$ denotes the vector field of translations, while $\boldsymbol{Q}$ represents the field of rotation tensors. The vector $\mathbf{u}$ satisfies the homogenous boundary conditions $\mathbf{u} = \mathbf{u}^*$ on ∂M_d. ∂M_d is a part of the ∂M boundary (see Fig. 3.**2**) where displacement boundary conditions are imposed. Then equations (3.7) and (3.8) can be rewritten in the following form:

$$\delta\mathbf{e} = \begin{Bmatrix} \delta\boldsymbol{\varepsilon}_1 \\ \delta\boldsymbol{\varepsilon}_2 \\ \delta\boldsymbol{\kappa}_1 \\ \delta\boldsymbol{\kappa}_2 \end{Bmatrix} = \begin{Bmatrix} \mathbf{v}_{,1} + (\mathbf{t}_1 + \boldsymbol{\varepsilon}_1) \times \mathbf{w} \\ \mathbf{v}_{,2} + (\mathbf{t}_2 + \boldsymbol{\varepsilon}_2) \times \mathbf{w} \\ \mathbf{w}_{,1} \\ \mathbf{w}_{,2} \end{Bmatrix}, \tag{3.12}$$

while equations (3.9) and (3.10) become:

$$\mathbf{e}(\mathbf{u}) = \begin{Bmatrix} \boldsymbol{\varepsilon}_\beta(\mathbf{u}) \\ \boldsymbol{\kappa}_\beta(\mathbf{u}) \end{Bmatrix} = \begin{Bmatrix} \boldsymbol{\varepsilon}_1(\mathbf{u}) \\ \boldsymbol{\varepsilon}_2(\mathbf{u}) \\ \boldsymbol{\kappa}_1(\mathbf{u}) \\ \boldsymbol{\kappa}_2(\mathbf{u}) \end{Bmatrix} = \begin{Bmatrix} \mathbf{u}_{,1} + (1-\mathbf{Q})\mathbf{t}_1^0 \\ \mathbf{u}_{,2} + (1-\mathbf{Q})\mathbf{t}_2^0 \\ \mathrm{axl}(\mathbf{Q}_{,1}\,\mathbf{Q}^T) \\ \mathrm{axl}(\mathbf{Q}_{,2}\,\mathbf{Q}^T) \end{Bmatrix}, \tag{3.13}$$

where $\mathrm{axl}(...)$ defines the axial vector of the skew tensor.

Consequently, stress measures, energetically coupled with (3.13), are defined:

$$\mathbf{s} = \begin{Bmatrix} \mathbf{n}^\beta \\ \mathbf{m}^\beta \end{Bmatrix} = \begin{Bmatrix} \mathbf{n}^1 \\ \mathbf{n}^2 \\ \mathbf{m}^1 \\ \mathbf{m}^2 \end{Bmatrix}. \tag{3.14}$$

The components of vector (3.13), in the (3.6) base can be rewritten in the following way:

$$\mathbf{e} = \{\varepsilon_{11}\ \varepsilon_{22}\ \varepsilon_{12}\ \varepsilon_{21}\,|\,\varepsilon_1\ \varepsilon_2\,\|\,\kappa_{11}\ \kappa_{22}\ \kappa_{12}\ \kappa_{21}\,|\,\kappa_1\ \kappa_2\}^T = \{\boldsymbol{\varepsilon}_m\,|\,\boldsymbol{\varepsilon}_s\,\|\,\boldsymbol{\varepsilon}_b\,|\,\boldsymbol{\varepsilon}_d\}^T. \tag{3.15}$$

where m denotes membrane in-plane action, s out of plane shear action, b holds for bending and d for drilling part of strain components. Similarly, components of (3.14) stress and couple resultants are defined:

$$\mathbf{s} = \{N^{11}\ N^{22}\ N^{12}\ N^{21}\,|\,Q^1\ Q^2\,\|\,M^{11}\ M^{22}\ M^{12}\ M^{21}\,|\,M^1\ M^2\}^T = \{\mathbf{s}_m\,|\,\mathbf{s}_s\,\|\,\mathbf{s}_b\,|\,\mathbf{s}_d\}^T. \tag{3.16}$$

Up to this point the whole theoretical derivation was analytically exact. The next chapter describes the material law which is the only field where some assumptions of the theory appear.

3.2 Constitutive relation

The general form of the linear constitutive relation, owing to the notation used here, becomes:

$$\mathbf{s} = \mathbf{C}\mathbf{e}(\mathbf{u}) \tag{3.17}$$

with $\mathbf{C}$ being a constitutive matrix with constant coefficients, to be defined in the next paragraph. The constant coefficients are used because it is intended here to carry out analyzes only to the growth of the first crack in the material. Obviously, if an analysis up to the total loss of material load capacity is performed, the coefficients of $\mathbf{C}$ matrix change in the course of calculations (REDDY J. N. [2004]).

The constitutive relations do not only describe the material properties of a continuum, but also allow to balance the amount of unknowns of the initial boundary value problem. The material law formulation is very complex, but with some general rules given for its determination. Particular relations are formulated for specific groups of material behaviour types, such as elastic, elasto-plastic, visco-elasto-plastic, etc. (RYMARZ C. [1993], SAWICKI. A. [1994], KREJA I. [2003]). What is more, different materials that are classified into the same group of behaviour type maintain the same form of constitutive equations description. However, distinct values of material constants are applied for them, e.g. for concrete or steel assuming linear response.

Formulation of specific relations can be done by means of observations and experiments at the macro level (phenomenological models). However in such a case it is almost impossible to include all material effects. Therefore some idealised models are used to approximate material behaviour. On the other hand the same observations can be performed for some identification experiments at the micro scale (physical models). In such a case it can be problematic to transform the micro results into some general rules for the macro mechanical behaviour (KREJA I. [2003]).

The aforementioned observations lead to the principals that need to be followed in constitutive relation definitions (see e.g. HAUPT P. [2000]):

- determinism - the state of stress is dependant only on the past history of a body motion,
- local action - the state of stress in a particle is determined by the motion of its vicinity and not by the motion of all particles of the body,
- frame-indifference - the material law does not depend on the reference coordinate system.

However, these are not the only requirements imposed on the constitutive relation. Also others must be fulfilled (see e.g. RYMARZ C. [1993], HAUPT P. [2000] and the references cited there), such as: compatibility with the balance relations, principle of irreversibility, principle of equipresence, the principle of fading memory.

In this work the material is assumed to undergo linear elastic small strain. The general form of constitutive relation is stated as in (3.17). The constitutive matrix **C** represents the particular properties of the applied material, which are determined with use of proper material constants (HIGHAM N. J., DENNIS M. R., GLENDINNING P., MARTIN P. A., SANTOSA F., TANNER J. (EDS.) [2015]).

3.2.1 Constitutive law of the layer

FRP laminates have a very specific structure, which has to be properly described with a constitutive relation. Although FRP laminate is a composite made of fibres and matrix, its properties can be homogenized, when it is not intended to represent the micromechanics of the composite. Fibres introduce some main directions of stiffness. Many FRP laminates are built of unidirectional or biaxial layers of reinforcement. Therefore, a single homogenized FRP layer represents features of anisotropic or orthotropic material GERMAN J. [2001].

It is assumed in this work, that a single lamina is made of transversely isotropic homogenous material. ESL technique and FSDT kinematics are used to determine the behaviour of multilayered medium. The stress state in the layer is described by asymmetric plane stress and transverse shear stress. Generally, each lamina of FRP composite can have different fibre orientation, defined with angle $\varphi_{(k)}$. Therefore, a particular orthogonal material coordinate system $\left(a_{(k)}, b_{(k)}, c_{(k)}\right)$ is introduced (CHRÓŚCIELEWSKI J., KREJA I., SABIK A., WITKOWSKI W. [2011]) in order to distinguish directions of orthotropy, where k denotes the number of considered layer, a describes the direction of reinforcement, and c is the axis normal to the shell reference surface. The material coordinate system, together with the $\{t_i^0\}$ triad, described in chapter 3.1, are depicted in Fig. 3.3. Fig. 3.4 presents the k layer as a part of the whole laminate with some symbols definitions, used for the purpose of material law formulation. The stress state in a layer, which is considered in the law is shown in Fig. 3.5 (the figure is created assuming that a $\varphi_{(k)} = 0$ layer is analyzed).
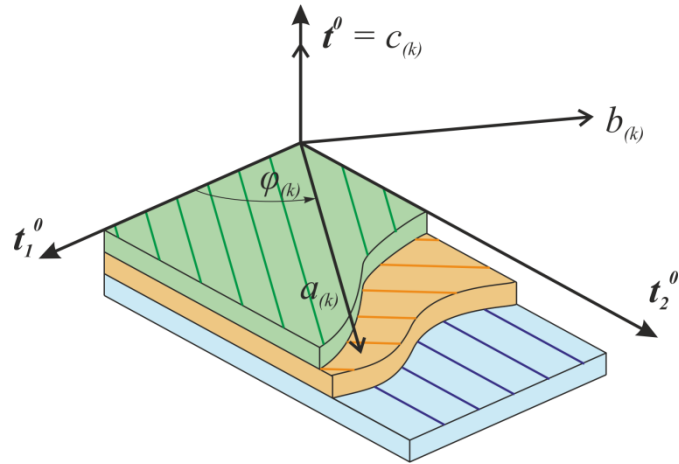
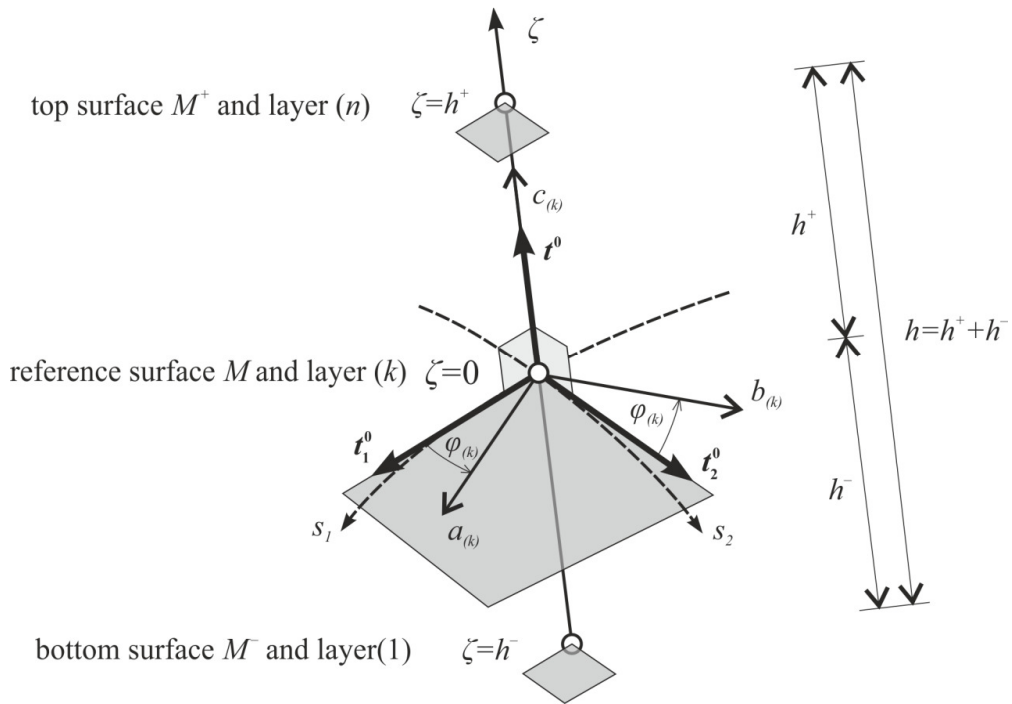Fig. 3.3 The material coordinate system of k layer

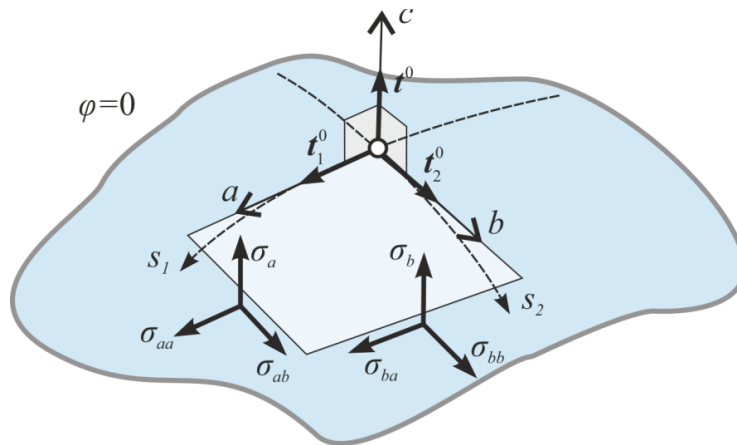Fig. 3.4 Layer k in the framework of shell notation

Fig. 3.5 The state of stress appearing in a $\varphi = 0$ layer

Owing to the above, the material law given in the material coordinate system of the layer similar as for 2D nonpolar orthotropic linearly elastic continuum can be used within the 6p theory. This law, refer to (3.18), (3.19) expressions, was proposed by CHRÓŚCIELEWSKI J., KREJA I., SABIK A., WITKOWSKI W. [2011] and successfully applied to the analysis of elastic shells:

$$
\begin{Bmatrix} \sigma_{aa} \\ \sigma_{bb} \\ \sigma_{ab} \\ \hline \sigma_{ba} \\ \sigma_{a} \\ \hline \sigma_{b} \end{Bmatrix}_k =
\begin{bmatrix}
\dfrac{E_a}{1-v_{ab}v_{ba}} & \dfrac{v_{ab}E_b}{1-v_{ab}v_{ba}} & 0 & 0 & 0 & 0 \\
\dfrac{v_{ba}E_a}{1-v_{ab}v_{ba}} & \dfrac{E_b}{1-v_{ab}v_{ba}} & 0 & 0 & 0 & 0 \\
0 & 0 & 2G_{ab} & 0 & 0 & 0 \\
0 & 0 & 0 & 2G_{ab} & 0 & 0 \\
\hline
0 & 0 & 0 & 0 & 2G_{ac} & 0 \\
0 & 0 & 0 & 0 & 0 & 2G_{bc}
\end{bmatrix}_k
\begin{Bmatrix} \varepsilon^{aa} \\ \varepsilon^{bb} \\ \varepsilon^{ab} \\ \hline \varepsilon^{ba} \\ \varepsilon^{a} \\ \hline \varepsilon^{b} \end{Bmatrix}_k , \qquad (3.18)
$$

where: E_a stands for elastic modulus in the fibre direction, E_b denotes elastic modulus in the direction perpendicular to fibres, G_{ab}, G_{ac} and G_{bc} define respectively, in-plane shear modulus, and two transverse shear moduli, finally, v_{ab}, v_{ba} are the Poisson ratios so that $E_a v_{ba} = E_b v_{ab}$ (without summation).

The relations (3.18) can be expressed in shorten notation:

$$
\begin{Bmatrix} \boldsymbol{\sigma}_m^{mat} \\ \hline \boldsymbol{\sigma}_s^{mat} \end{Bmatrix}_k =
\begin{bmatrix} \tilde{\boldsymbol{C}}_m & \boldsymbol{0}_{4\times2} \\ \hline \boldsymbol{0}_{2\times4} & \tilde{\boldsymbol{C}}_s \end{bmatrix}_k
\begin{Bmatrix} \boldsymbol{\varepsilon}_m^{mat} \\ \hline \boldsymbol{\varepsilon}_s^{mat} \end{Bmatrix}_k = \tilde{\boldsymbol{C}}_k
\begin{Bmatrix} \boldsymbol{\varepsilon}_m^{mat} \\ \hline \boldsymbol{\varepsilon}_s^{mat} \end{Bmatrix}_k , \qquad (3.19)
$$

assuming that the lower index m in (3.19) refers to the material system of a lamina.

3.2.2 Constitutive law of the laminate

In order to perform analysis of shells made of FRP laminates, the behaviour of the whole laminate needs to be described. Thus, a constitutive relation representing stiffness of all layers should be established. Owing to the fact that ESL technique is used in this work, it is required to transform the single layer stiffness (3.19) given in material coordinate system to the $\{\boldsymbol{t}_i^0\}$ coordinates. The following operation on stresses and strains has to be performed to achieve this goal:

$$\left\{\begin{matrix}\boldsymbol{\sigma}_m^{mat} \\ \boldsymbol{\sigma}_s^{mat}\end{matrix}\right\}_k = \left[\begin{array}{c|c}\tilde{\mathbf{T}}_m & \mathbf{0}_{4\times2} \\ \hline \mathbf{0}_{2\times4} & \tilde{\mathbf{T}}_s\end{array}\right]_k \left\{\begin{matrix}\boldsymbol{\sigma}_m \\ \boldsymbol{\sigma}_s\end{matrix}\right\}_k = \tilde{\mathbf{T}}_k \left\{\begin{matrix}\boldsymbol{\sigma}_m \\ \boldsymbol{\sigma}_s\end{matrix}\right\}_k \,, \tag{3.20}$$

$$\left\{\begin{matrix}\boldsymbol{\varepsilon}_m^{mat} \\ \boldsymbol{\varepsilon}_s^{mat}\end{matrix}\right\}_k = \left[\begin{array}{c|c}\tilde{\mathbf{T}}_m & \mathbf{0}_{4\times2} \\ \hline \mathbf{0}_{2\times4} & \tilde{\mathbf{T}}_s\end{array}\right]_k \left\{\begin{matrix}\boldsymbol{\varepsilon}_m \\ \boldsymbol{\varepsilon}_s\end{matrix}\right\}_k = \tilde{\mathbf{T}}_k \left\{\begin{matrix}\boldsymbol{\varepsilon}_m \\ \boldsymbol{\varepsilon}_s\end{matrix}\right\}_k \,, \tag{3.21}$$

where $\tilde{\mathbf{T}}_k$ is the transformation matrix defined as follows:

$$\tilde{\mathbf{T}}_k = \left[\begin{array}{cccc|cc}C^2 & S^2 & SC & SC & 0 & 0 \\ S^2 & C^2 & -SC & -SC & 0 & 0 \\ -SC & SC & C^2 & -S^2 & 0 & 0 \\ -SC & SC & -S^2 & C^2 & 0 & 0 \\ \hline 0 & 0 & 0 & 0 & C & -S \\ 0 & 0 & 0 & 0 & S & C\end{array}\right]_k = \left[\begin{array}{c|c}\tilde{\mathbf{T}}_m & \mathbf{0}_{4\times2} \\ \hline \mathbf{0}_{2\times4} & \tilde{\mathbf{T}}_s\end{array}\right]_k \tag{3.22}$$

and $S = \sin\left(\varphi_{(k)}\right)$; $C = \cos\left(\varphi_{(k)}\right)$ (see Fig. 3.3).

On this basis it is possible to define the constitutive matrix in the $\{t_i^0\}$ coordinate system (see for instance CHRÓŚCIELEWSKI J., KREJA I., SABIK A., WITKOWSKI W. [2011]):

$$\left\{\begin{matrix}\boldsymbol{\sigma}_m \\ \boldsymbol{\sigma}_s\end{matrix}\right\}_k = \left[\begin{array}{c|c}\tilde{\mathbf{T}}_m^{-1}\tilde{\mathbf{C}}_m\tilde{\mathbf{T}}_m & \mathbf{0}_{4\times2} \\ \hline \mathbf{0}_{2\times4} & \tilde{\mathbf{T}}_s^{-1}\tilde{\mathbf{C}}_s\tilde{\mathbf{T}}_s\end{array}\right]_k \left\{\begin{matrix}\boldsymbol{\varepsilon}_m \\ \boldsymbol{\varepsilon}_s\end{matrix}\right\}_k = \left[\begin{array}{c|c}\mathbf{C}_m & \mathbf{0}_{4\times2} \\ \hline \mathbf{0}_{2\times4} & \mathbf{C}_s\end{array}\right]_k \left\{\begin{matrix}\boldsymbol{\varepsilon}_m \\ \boldsymbol{\varepsilon}_s\end{matrix}\right\}_k . \tag{3.23}$$

Consequently, integration in the through the thickness direction of appropriate stress is performed for the whole stacking sequence, containing a total number of n_l layers. This allow formulation of stress and couple resultants (3.16). Thus, according to FSDT kinematics, the ESL material law, being the only field where some assumptions of the 6p theory appear, is defined (compare also with Fig. 3.4) in the following form:

$$\mathbf{s}_m = \sum_{k=1}^{n_l}\left(\int_{\zeta_k^-}^{\zeta_k^+} \{\mathbf{C}_m\}_k \left(\boldsymbol{\varepsilon}_m + \zeta\boldsymbol{\varepsilon}_b\right)\mu\,d\zeta\right) = \underset{4\times4}{\mathbf{A}}\,\boldsymbol{\varepsilon}_m + \underset{4\times4}{\mathbf{B}}\,\boldsymbol{\varepsilon}_b\,, \tag{3.24}$$

$$\mathbf{s}_s = \sum_{k=1}^{n_l}\left(\int_{\zeta_k^-}^{\zeta_k^+} (\alpha_s)_k \{\mathbf{C}_s\}_k \boldsymbol{\varepsilon}_s\,\mu\,d\zeta\right) = \underset{2\times2}{\mathbf{S}}\,\boldsymbol{\varepsilon}_s\,, \tag{3.25}$$

$$\mathbf{s}_b = \sum_{k=1}^{n_l}\left(\int_{\zeta_k^-}^{\zeta_k^+} \{\mathbf{C}_m\}_k \left(\zeta\boldsymbol{\varepsilon}_m + (\zeta)^2\boldsymbol{\varepsilon}_b\right)\mu\,d\zeta\right) = \underset{4\times4}{\mathbf{B}}\,\boldsymbol{\varepsilon}_m + \underset{4\times4}{\mathbf{D}}\,\boldsymbol{\varepsilon}_b\,, \tag{3.26}$$

$$\mathbf{s}_d = \alpha_t \sum_{k=1}^{n_l} \left(\int_{\zeta_k^-}^{\zeta_k^+} (\alpha_t)_k \{\mathbf{C}_d\}_k \boldsymbol{\varepsilon}_d \, \mu \, d\zeta \right) = \underset{2\times2}{\mathbf{G}} \boldsymbol{\varepsilon}_d. \tag{3.27}$$

In the above formulas $(\alpha_s)_k$ are the shear correction factors of the layer k, ζ_k^+ and ζ_k^- indicate the distance between the reference surface and the top and the bottom of the k layer respectively, while μ is the determinant of the shifter tensor, defined as (refer to Fig. 3.4):

$$\mu_{\alpha\beta} = \delta_{\alpha\beta} - \zeta \, b_{\alpha\beta}^0, \qquad \mu = \det \mu_{\alpha\beta} = 1 - 2\zeta H + \zeta^2 K. \tag{3.28}$$

where H is the mean curvature and K denotes the Gaussian curvature of M. It is assumed in (3.27) that $\mathbf{C}_d = \zeta^2 \mathbf{C}_s$. The $(\alpha_t)_k$ appearing in (3.27) is the drilling correction factor of the layer k, similar to the $(\alpha_s)_k$. In the computations performed in this work $(\alpha_t)_k = 1$ is used, similarly as in CHRÓŚCIELEWSKI J., KREJA I., SABIK A., WITKOWSKI W. [2011], because the drilling correction factor will be imposed globally to the shell cross section, via the parameter α_t. Its value has not yet been precisely defined. The values of α_t varying from 10^{-10} to 10^{+10} were investigated in numerical experiments (see e.g. CHRÓŚCIELEWSKI J., MAKOWSKI J., STUMPF H. [1992] or CHRÓŚCIELEWSKI J., MAKOWSKI J., STUMPF H. [1997]). According to this works, the difference between obtained deformations and internal energy of shells in different analysis cases is negligible for α_t between 0 and 1. Thus, taking into account the aforementioned information $\alpha_t = 0.01$ is used in all numerical calculations.

Since, thin shells are analysed, e.g. shells with thickness, which is smaller than typical dimension $h \leq L$ and shell curvature radius $h \leq R_{\min}$, the determinant of the shifter tensor is assumed to be $\mu \approx 1$ (CHRÓŚCIELEWSKI J., KREJA I., SABIK A., WITKOWSKI W. [2011]). Therefore, the matrices $\underset{4\times4}{\mathbf{A}}$, $\underset{4\times4}{\mathbf{B}}$, $\underset{4\times4}{\mathbf{D}}$, $\underset{2\times2}{\mathbf{S}}$, $\underset{2\times2}{\mathbf{G}}$ can be shorten:

$$\underset{4\times4}{\mathbf{A}} = \sum_{k=1}^{n_l} \{\mathbf{C}_m\}_k \left(\zeta_k^+ - \zeta_k^- \right), \tag{3.29}$$

$$\underset{4\times4}{\mathbf{B}} = \tfrac{1}{2} \sum_{k=1}^{n_l} \{\mathbf{C}_m\}_k \left((\zeta_k^+)^2 - (\zeta_k^-)^2 \right), \tag{3.30}$$

$$\underset{4\times4}{\mathbf{D}} = \tfrac{1}{3} \sum_{k=1}^{n_l} \{\mathbf{C}_m\}_k \left((\zeta_k^+)^3 - (\zeta_k^-)^3 \right), \tag{3.31}$$

$$\underset{2\times2}{\mathbf{S}} = \sum_{k=1}^{n_l} (\alpha_s)_k \{\mathbf{C}_s\}_k \left(\zeta_k^+ - \zeta_k^- \right), \tag{3.32}$$

$$\underset{2\times2}{\mathbf{G}} = \tfrac{1}{3}\alpha_t \sum_{k=1}^{n_l} (\alpha_t)_k \{\mathbf{C}_s\}_k \left((\zeta_k^+)^3 - (\zeta_k^-)^3 \right). \tag{3.33}$$

It is worth to emphasize, that all the integrals in the theoretical approach presented here can be solved analytically.

4. FAILURE CRITERIA IN LAMINATED COMPOSITES

In this chapter a literature review of the failure initiation estimation methods is given. Then the development of Tsai-Hill, Tsai-Wu, Hashin and Puck criteria is described in details and the failure envelopes of the chosen criteria are compared.

The failure hypotheses are used to judge whether the complex state of stress is safe or not. They are widely known in the mechanics of homogenous, isotropic materials and commonly described even in student coursebooks see e.g. BIELEWICZ E. [1998], JASTRZĘBSKI P., MUTERMILCH J., ORŁOWSKI W. [2011]. Their well known examples are: Galileo, de St. Venant, Tresca, Mohr or Huber Mises Hencky (HMH). The failure hypothesis are developed on the basis of particular assumptions. These may be attributed to the material properties and material behaviour with respect to directions in the considered stress space or to the differences in the response under tension and compression. Therefore, an experimental verification needs to be performed to judge their applicability. The following hypotheses, created for the purpose of failure estimation in isotropic materials, were positively checked in experiments: Tresca hypothesis of maximal shear stress, used in the analysis of materials having the same strengths in tension and compression; Mohr hypothesis of maximal shear stress, considered for materials with different values of strengths in tension and compressions and HMH elastic strain energy of distortion hypothesis for materials with similar tension−compression properties.

The process of new hypotheses development should fulfil the following conditions (see e.g. LEWIŃSKI J., WILCZYŃSKI A.P., WITEMBERG-PERZYK D. [1994]):

- the failure theory should be written with aid of stress tensor invariants

- the third stress tensor invariant should not be used to formulate a hypothesis

- the theory should not base on stress tensor components raised to the power higher than 4.

Since a laminate layer is an orthotropic material, the hypotheses formulated for isotropic continua cannot be utilised directly. Nevertheless, some of the concepts used during their formulation are applied in the failure analysis of laminates. For instance, modified HMH theory, extended to the analysis of orthotropic materials with different strengths in tension and compression, proposed by Tsai and Hill is called the Tsai-Hill

criterion. On the other hand the Mohr hypothesis is used to develop matrix failure (named also as inter fibre failure) expressions of Puck criterion.

The nomenclature in the failure analysis of laminates is also different, as compared with isotropic materials. The failure hypothesis are rather named as failure initiation criteria. JONES R. M. [1999] argues that the word "theory" should not be used when speaking about failure hypotheses, since they are a kind of approximation of the reality and not a precise theoretical derivation. The failure surface definitions for laminates are in many cases adopted to fit into the experimental data. Therefore, the word criterion is more suitable in this case. On the other hand, Puck (PUCK A., SCHÜRMANN H. [1998]) does not hesitate to use the word "theory", when describing matrix failure modes of his criterion. In this work the concept proposed by Jones is followed.

Failure initiation in fibrous laminated composites is broadly investigated. This is because of its significance regarding safety of designed laminated structures. Since laminated composite is a multilayered medium, a particular approach of failure analysis ought to be applied. On the one hand, the damage onset determination can be performed for the whole laminate as for a quasi homogenous element (VASILIEV V. V., MOROZOV E. V. [2013]). This however is not an appropriate approach in the design process, because it requires analysis of an enormous number of different stacking sequences, under various loading sets. It can be eventually applied, when some elements with repeatable lamination sequences are produced on industrial scale (VASILIEV V. V., MOROZOV E. V. [2013]). According to PUCK A., SCHÜRMANN H. [2002], the failure needs to be traced in separate layers. In such a case failure initiation and consequent progressive damage is represented more reliably. This is the most common way currently utilised by researchers and engineers (see for instance HINTON M. J., KADDOUR A. S., SODEN P. D. (EDS.) [2004]).

As reported in work of CAMANHO P. P. [2002] the main interest in this subject started in 1960s. Since then many failure initiation criteria were developed. Generally, they can be classified into two main groups, namely, criteria that do not and do determine the mode of failure (see for instance CAMANHO P. P. [2002]).

It is possible to distinguish different tensorial and polynomial failure criteria in the first group (CAMANHO P. P. [2002]), such as for example: Hoffmann, Tsai-Hill, Tsai-Wu. These criteria include different combinations of some stress tensor components, and are

usually formulated in a way to fit the failure curve into some experimental results. Hence, they do not have a physical reasoning (JONES R. M. [1999]).

The second group of criteria distinguishes two different modes, namely, fibre and matrix failure. This is a more realistic approach, which therefore can be successfully used in the analysis of the laminate progressive damage analysis (CAMANHO P. P. [2002]). This group can be further divided into: non-interactive and interactive criteria. The non-interactive ones do not include the interaction between different components of strain or stress tensor components. The basic criteria classified into this category are: maximum stress or maximum strain. The interactive ones include the aforesaid interaction. Some representative examples here are: Hashin, Puck, Chang or LaRC. Similar classifications with slightly changed criteria groups names, are described among others in the works of SUN C.T., QUINN B.J., TAO J., OPLINGER D.W., HUGHES W. J. [1996] or KULA K. [2007]

Some comprehensive literature reviews containing descriptions of also other failure initiation criteria are e.g.: NAHAS M. N. [1986], PARIS F. [2001], YU M.-H. [2002], HINTON M. J., KADDOUR A. S., SODEN P. D. (EDS.) [2004] or ROHWER K. [2015]. The total number of failure initiation criteria is hard to establish. PARIS F. [2001] listed 18 references to papers proposing failure criteria and 8 to works revising current approaches. These were selected from over 400 of papers written in this field in years 1993-1998.

Because many theories had been available M. J. Hinton, A. S. Kaddour and P. D. Sodden announced in 1996 the first World Wide Failure Exercise (WWFE). The first concept of this exercise was raised in 1992 during an expert meeting in United Kingdom (HINTON M. J., KADDOUR A. S., SODEN P. D. (EDS.) [2004]). Experimental data resulting from 14 test cases of laminated composite coupons were presented, in order to validate and improve existing failure initiation and evolution approaches under different in-plane loads. The full review of the Exercise results is available in HINTON M. J., KADDOUR A. S., SODEN P. D. (EDS.) [2004]. Hinton, Kaddour and Sodden analyzed and examined the contribution submitted to the exercise and formulated some recommendations for designers and researchers concerning application of analyzed criteria (see chapter 7.1 of HINTON M. J., KADDOUR A. S., SODEN P. D. (EDS.) [2004] or HINTON M. J., KADDOUR A. S., SODEN P. D. [2004]). In effect, 5 of them were selected as the leading ones: Zinoviev, Bogetti, Puck, Cuntze and Tsai-Wu. Zinoview used the maximum stress criterion, while Bogetti prefers the 3D version of the maximum strain one in order to estimate failure initiation. Puck

distinguished the failure phenomenon between fibre failure (FF) and inter fibre failure (IFF), which is treated as the matrix failure mode. The FF prediction is generally represented by the maximum stress criterion. The IFF modes are divided into three types, depending on the angle of the fracture plane to occur (PUCK A., SCHÜRMANN H. [1998]). They are expressed by means of quite advanced formulas. This concept is evaluated on the basis of Mohr fracture criteria (MOHR O. [1900]). The Cuntze criterion also distincts failure modes: two FF and three IFF. The theoretical reasoning of this criterion is based on the appropriate combination of unidirectional material (UD) stress invariants and application of Mohr Coulomb hypothesis (HINTON M. J., KADDOUR A. S., SODEN P. D. (EDS.) [2004]). This results in the maximum stress condition for FF, similarly as in Puck criterion and some more sophisticated expressions for IFF. The Tsai-Wu criterion is the general interactive polynomial criterion, which main concept is described earlier in this work, i.e. tensorial criterion concept. It is worth to note that three (maximum stress, maximum strain and Tsai-Wu) of five criterions are some basic criteria with a long history of application. Although the first WWFE was finished over 10 years ago these results are still presented and discussed - HINTON M. [2011]. Moreover, two subsequent failure exercises were opened - HINTON M. J., KADDOUR A. S. [2012] and KADDOUR A. S., HINTON M. J., SMITH P. A., LI S. [2013].

It should be also mentioned that some existing criteria were not investigated in the Exercise, as their authors decline to participate in it, as for example Hashin. He wrote to the organisers, that he does not know how to predict failure in laminates, he only can determine failure of unidirectional fibre composites (see HINTON M. [2011]). This is quite confusing, because the Hashin criterion is still available in some leading FEM codes as e.g. Abaqus. Moreover, the criterion is often successfully used in various failure analysis, see for instance: SANTIUSTE C. SÁNCHEZ-SÁEZ S., BARBERO E. [2010], WANG L., ZHENG CH., LUO H., WEI S., WEI Z. [2015], WARREN K. C., LOPEZ-ANIDO R. A., S. S. VEL, BAYRAKTAR H. H. [2016]. What is more, new criteria were developed after the first WWFE was finished. An important criterion called LaRC was created at the NASA Langley Research Center. It is outlined in the paper: DAVILA C. G., CAMANHO P. P., ROSE C. A. [2005]. It contains six expressions, including three modes of fibre failure and three modes of matrix damage. It was derived with the aid of the ideas proposed by Hashin and Puck, regarding the fracture plane concepts, including Mohr-Coulomb stress interaction in the plane of failure. Some results given in DAVILA C. G., CAMANHO P. P., ROSE C. A. [2005] or LEONE

F. A., DAVILA C. G., GIROLAMO D. [2015] show that it is properly established and is in good correspondence with the experimental data.

The short discussion on laminate failure initiation criteria given above reveals that a lot of effort has been made in this field, however an universal hypothesis which can be applied in general conditions has still not been developed. The results presented by SUN C.T., QUINN B.J., TAO J., OPLINGER D.W., HUGHES W. J. [1996] and repeated by CAMANHO P. P. [2002] show the percentage of different failure criteria industrial use Fig. 4.1.
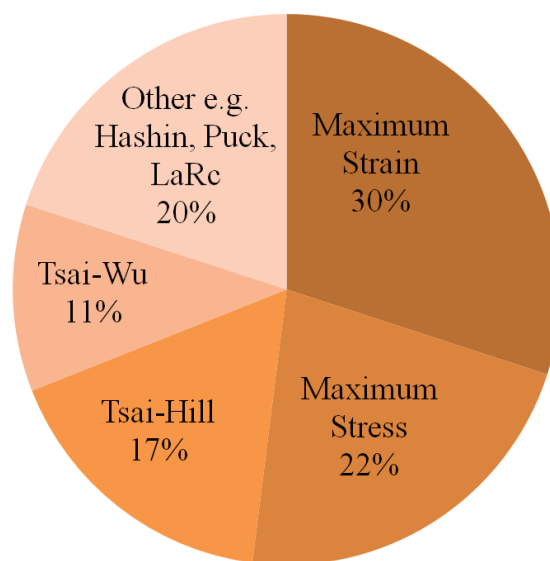
Fig. 4.1 Industrial use of different failure criteria (created from the data given in SUN C.T., QUINN B.J., TAO J., OPLINGER D.W., HUGHES W. J. [1996]).

According to Fig. 4.1 the basic criteria, as Maximum Stress or Strain, Tsai-Wu or Tsai-Hill are mostly used instead of the sophisticated ones, e.g. Hashin, Puck, etc. (classified into Other in Fig. 4.1). This is attributed to the fact that the more advanced theories require more complex descriptions or, in some cases, additional material constants, which are difficult to measure (for instance fracture energies in LaRC criteria DAVILA C. G., CAMANHO P. P., ROSE C. A. [2005]). Nevertheless, the recently developed criteria seems to be more appropriate to estimate initial failure of laminate, because they are usually based on some theoretical foundations, as it will be described later.

Tsai-Hill, Tsai-Wu, Hashin and Puck criteria are described in details. They are chosen, because the basic criteria are commonly used in practice, while the more complicated sophisticated ones are attractive from the point of view of FPF estimations.

These criteria are then modified in order to apply them in FEA of laminated structures performed by means of 6p theory.

4.1 Tsai-Hill criterion

The Tsai-Hill criterion was developed from HMH yield criterion (see e.g. LI Z. X., ZHUO X., VU-QUOC L, IZUUDDIN B. A., WEI H. Y. [2013])[1]. Namely, the HMH theory of isotropic materials was rewritten by Hill (HILL R. [1950]) for orthotropic materials for the case of 3D state of stress as follows:

$$
\begin{aligned}
(G+H)\sigma_{aa}^2 + (F+H)\sigma_{bb}^2 + (F+G)\sigma_{cc}^2 - 2H\sigma_{aa}\sigma_{bb} - 2G\sigma_{aa}\sigma_{cc} + \\
- 2F\sigma_{bb}\sigma_{cc} + 2L\sigma_{bc}^2 + 2M\sigma_{ac}^2 + 2N\sigma_{ab}^2 = 1
\end{aligned}
\tag{4.1}
$$

assuming that 1, 2, 3 are the axes of the material orthotropy. Equation (4.1) is reduced to plane stress, since this is the state of stress of a considered lamina:

$$
(G+H)\sigma_{aa}^2 + (F+H)\sigma_{bb}^2 - 2H\sigma_{aa}\sigma_{bb} + 2N\sigma_{ab}^2 = 1,
\tag{4.2}
$$

The failure strength parameters F, G, H, N can be expressed by means of the X, Y, Z lamina strengths, the same in tension and compression, measured accordingly in the first, second and third direction of orthotropy and S representing in-plane shear strength :

$$
G + H = \frac{1}{X^2},
\tag{4.3}
$$

$$
F + H = \frac{1}{Y^2},
\tag{4.4}
$$

$$
F + G = \frac{1}{Z^2},
\tag{4.5}
$$

$$
2N = \frac{1}{S_l^2},
\tag{4.6}
$$

On the basis of the relations (4.3) - (4.5) it is possible to define:

---

[1] The Huber-Mises-Hencky yield criterion is denoted as HMH criterion mainly in Poland, whereas it is commonly named as v. Mises criterion in other countries.

$$2H = \frac{1}{X^2} + \frac{1}{Y^2} - \frac{1}{Z^2} . \tag{4.7}$$

Some different interpretations of the expression (4.7) are found in the literature. The first one, refer to PRUSTY B. G., SATSANGI S. K., RAY C. [2001] or SATISH KUMAR Y. V., SRIVASTAVA A. [2003] leads to the following failure initiation criterion:

$$\frac{\sigma_{aa}^2}{X^2} + \frac{\sigma_{bb}^2}{Y^2} - \left(\frac{1}{X^2} + \frac{1}{Y^2} \right) \sigma_{aa} \sigma_{bb} + \frac{\sigma_{ab}^2}{S_l^2} = 1 , \tag{4.8}$$

It is assumed in (4.8) that, if plane stress state is considered then the Z strength is neglected. TUTTLE M. E. [2004] states that in the general case of orthotropic material in plane stress the Z strength should be included, as it affects the failure phenomenon. Therefore (4.8) becomes:

$$\frac{\sigma_{aa}^2}{X^2} + \frac{\sigma_{bb}^2}{Y^2} - \left(\frac{1}{X^2} + \frac{1}{Y^2} - \frac{1}{Z^2} \right) \sigma_{aa} \sigma_{bb} + \frac{\sigma_{ab}^2}{S_l^2} = 1 , \tag{4.9}$$

The most common variant of Tsai-Hill criterion was proposed in the work of: TSAI S.W. [1968]: Strength Theories of Filamentary Structures, In: R.T. Schwartz, H.T. Schwartz (eds.) Fundamental Aspects of Fiber Reinforced Plastic Composites, Wiley Interscience, New York, 3-11[2]. It is formulated for unidirectional material, where the strengths in the off−fibre directions are equal ($Y = Z$). In effect (4.7) becomes:

$$2H = \frac{1}{X^2} , \tag{4.10}$$

and the failure initiation (4.9) criterion is expressed as:

$$\frac{\sigma_{aa}^2}{X^2} + \frac{\sigma_{bb}^2}{Y^2} - \frac{\sigma_{aa} \sigma_{bb}}{X^2} + \frac{\sigma_{ab}^2}{S_l^2} = 1 , \tag{4.11}$$

The form of the Tsai-Hill criterion, given by (4.11), is used in many computational works, see e.g. JINGXUAN H., MINGFA R., SHIYONG S., QIZHONG H., XIANNIAN S. [2011], KOLIOS A. J., PROIA S. [2012], YE J., QIU Y., CHEN X., MA J. [2015] for selected recent

---

[2] Unfortunately, this paper is not available to the author of this thesis, however it is cited for instance, among others, in: JONES R. M. [1999], KAW A. K. [2006] or NALI P., CARRERA E. [2012] where Tsai-Hill criterion is described.

applications. It is also implemented in some commercial FEM codes: Autodesk Simulation Composite Design 2014 or ABAQUS 6.14.

Up to this point it was assumed that the strengths *X, Y, Z* are the same in tension and compression, following HILL R. [1950]. However, authors like JONES R. M. [1999], TUTTLE M. E. [2004] argue that it is possible to include standard lamina strengths, which distinguish tension and compression, depending on the sign of the stress acting in the material direction. This adjustment was proposed by Azzi and Tsai (GERMAN J. [2001]). Consequently, when $\sigma_{aa} \geq 0$ then $X = X_t$, whereas $\sigma_{aa} < 0$ imposes $X = X_c$, where X_t and X_c stand for correspondingly absolute value of tensile and compressive strength in the first material direction. Similarly, the sign of σ_{bb} or σ_{cc} influences accordingly Y and Z strengths. Such interpretation of strengths is adopted in e.g. Autodesk Simulation Composite Design 2014 or ABAQUS 6.14. In NX Nastran 7 (NX NASTRAN 7 MANUAL) the sign of X, regarding the interaction term $\dfrac{\sigma_{aa}\sigma_{bb}}{X^2}$ is treated in another way: $X = X_t$ is applied when $\sigma_{aa}\sigma_{bb} > 0$, whereas $X = X_c$ if $\sigma_{aa}\sigma_{bb} < 0$.

A short comment about the name of the Tsai-Hill criterion needs to be made. The name Tsai-Hill is broadly used to describe its 2D plane stress version (4.11), in which different strengths in tension and compression are included. On the other hand CAMANHO P. P. [2002], assumes that the Tsai-Hill criterion refers to the following 3D stress criterion:

$$
\frac{\sigma_{aa}^2}{X^2} + \frac{\sigma_{bb}^2}{Y^2} + \frac{\sigma_{cc}^2}{Z^2} - \sigma_{aa}\sigma_{bb}\left(\frac{1}{X^2} + \frac{1}{Y^2} - \frac{1}{Z^2}\right) - \sigma_{aa}\sigma_{cc}\left(\frac{1}{X^2} - \frac{1}{Y^2} + \frac{1}{Z^2}\right) + \\
- \sigma_{bb}\sigma_{cc}\left(-\frac{1}{X^2} + \frac{1}{Y^2} + \frac{1}{Z^2}\right) + \frac{\sigma_{ab}^2}{S^2} + \frac{\sigma_{ac}^2}{Q^2} + \frac{\sigma_{bc}^2}{R^2} = 1 \tag{4.12}
$$

whereas the 2D plane stress version (4.11) is denoted as Azzi-Tsai-Hill. GERMAN J. [2001] claims that the Azzi-Tsai-Hill and Tsai-Hill names can be used interchangeably for the 2D (4.11) criterion. On the other hand, in ABAQUS the Tsai Hill criterion refer to the (4.11) equation, while Azzi-Tsai-Hill criterion is the one, in which the interactive term is always calculated as an absolute value and consequently becomes:

$$
\frac{\sigma_{aa}^2}{X^2} + \frac{\sigma_{bb}^2}{Y^2} - \frac{|\sigma_{aa}\sigma_{bb}|}{X^2} + \frac{\sigma_{ab}^2}{S_l^2} = 1 , \tag{4.13}
$$

In view of the above, it is not precise which version of the criterion is used when Tsai-Hill name is used. In this work it is assumed that the Tsai-Hill criterion is described by equation (4.11) and enables analysis of an unidirectional lamina, which can have different strengths in tension and compression. Thus, the failure initiation envelopes in σ_{aa} -σ_{bb}, σ_{aa}-σ_{ab}, σ_{bb}-σ_{ab} [3] stress space are shown in Fig. 4.2, Fig. 4.3 and Fig. 4.4 correspondingly for a lamina made of AS4/3501-6 Carbon/Epoxy composite, which has the following elastic and strength properties: $E_{aa} = 127\text{GPa}$, $E_{bb} = 11.5\text{GPa}$, $G_{ab} = G_{ac} = 6.56\text{GPa}$, $G_{bc} = 3.64\text{GPa}$, $v_{ab} = 0.279$, $X_t = 1950\text{MPa}$, $X_c = 1480\text{MPa}$, $Y_t = 48\text{MPa}$, $Y_c = 200\text{MPa}$, $S_l = 79\text{MPa}$.

These are obtained by means of Autodesk Simulation Composite Design 2014 educational version[4].
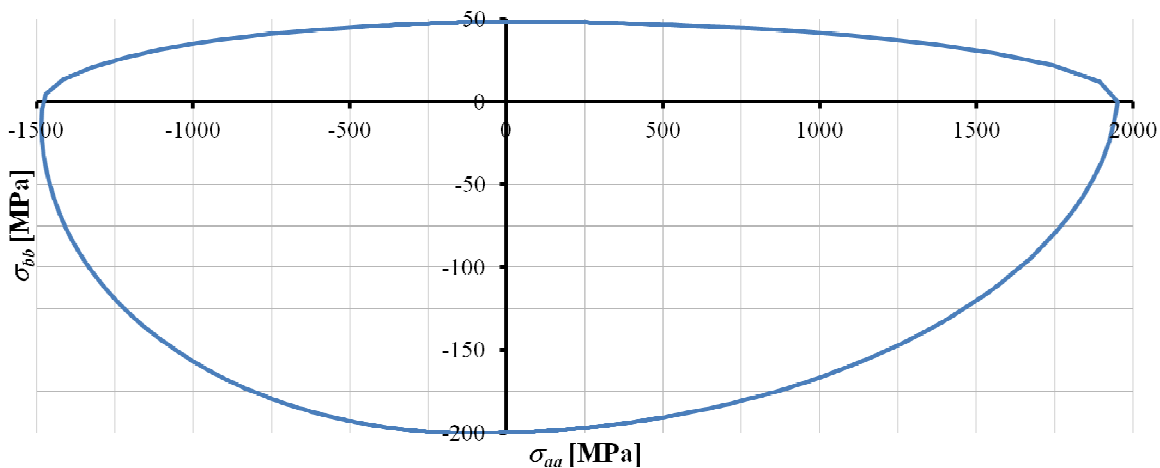
Fig. 4.2 Failure initiation envelope of Tsai-Hill criterion in σ_{aa}-σ_{bb} space.

[3] The direction of in-plane shear stress components does not affect the failure initiation equation. Therefore only the positive values of in-plane shear stress components are shown in the failure envelope plots. This also applies to Tsai-Wu, Hashin and Puck failure envelopes considered later in this work.

[4] All failure envelopes shown in this thesis are created for a lamina made of AS4/3501-6 Carbon/Epoxy composite using the Autodesk Simulation Composite Design 2014 educational version. Therefore the material parameters and this reference will not be repeated, when other criteria are described.
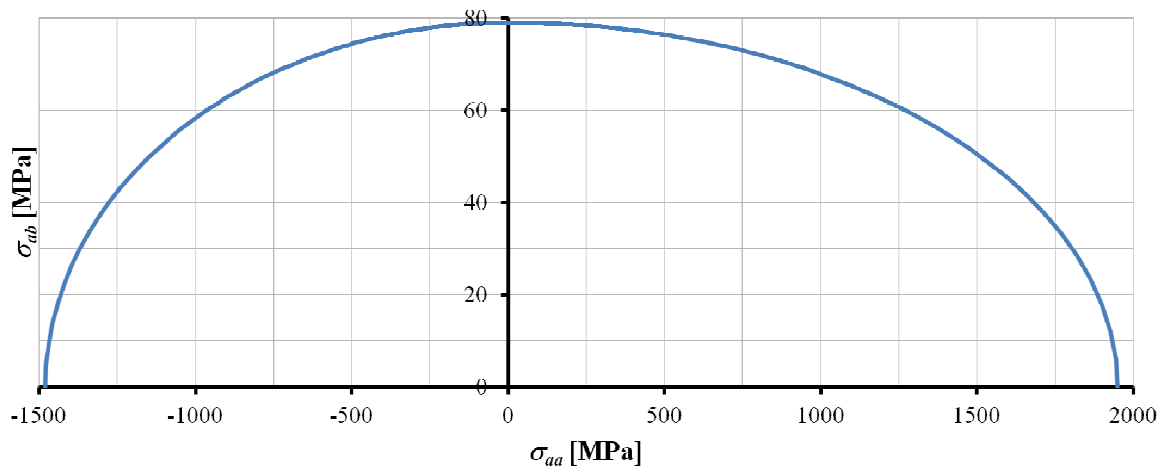
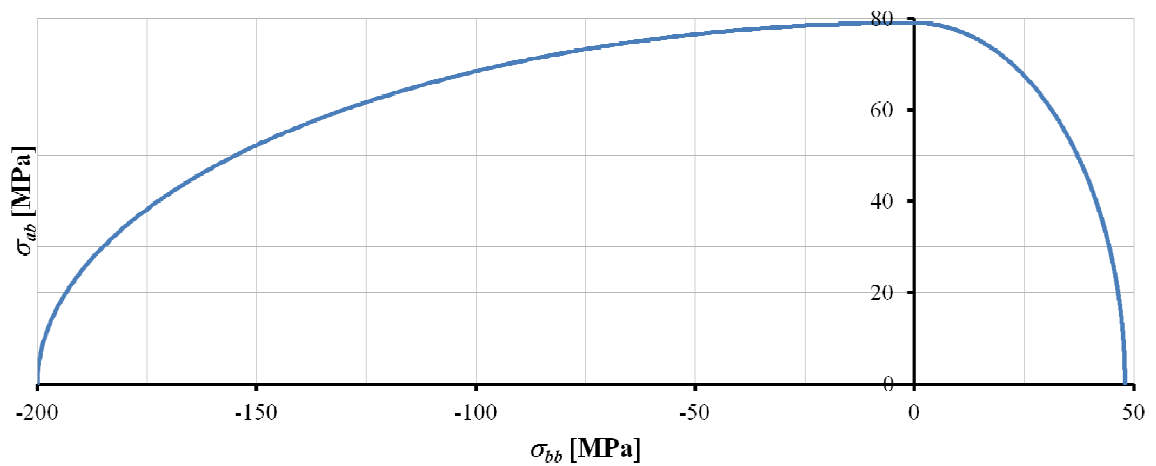Fig. 4.3 Failure initiation envelope of Tsai-Hill criterion in σ_{aa} - σ_{ab} space.

Fig. 4.4 Failure initiation envelope of Tsai-Hill criterion in σ_{bb} - σ_{ab} space.

4.2   Tsai-Wu criterion

The principal assumption leading to the formulation of the Tsai-Wu criterion is the existence of a failure surface in the stress space (TSAI S.W., WU E.M [1971]), which has the following form:

$$f(\sigma_k) = F_i\sigma_i + F_{ij}\sigma_i\sigma_j = 1 \quad i,j,k = 1,2,...,6 . \tag{4.14}$$

The equation (4.14) is written in the so-called contracted notation. The failure surface is described by means of stress components and strength tensors of second F_i and fourth rank F_{ij}. The relation between regular notation and contracted one is given for stress components in Tab. 4.1 and for strength tensors in Tab. 4.2.

Tab. 4.1 Relation between natural and contracted notation for stress components

Natural notation (preferred in this work)	Contracted notation
σ_{aa}	σ_a
σ_{bb}	σ_b
σ_{cc}	σ_c
σ_{bc}	σ_d
σ_{ca}	σ_e
σ_{ab}	σ_f
σ_{cb}	σ_g
σ_{ac}	σ_h
σ_{ba}	σ_i

Tab. 4.2 Relation between natural and contracted notation for 4th rank strength tensors

Natural notation			Contracted notation		
F_{aaaa}	F_{bbbb}	F_{cccc}	F_{aa}	F_{bb}	F_{cc}
F_{bbcc}	F_{ccaa}	F_{aabb}	F_{bc}	F_{ca}	F_{ab}
$2F_{aabc}$	$2F_{aaca}$	$2F_{aaab}$	F_{ad}	F_{ae}	F_{af}
$2F_{bbbc}$	$2F_{bbca}$	$2F_{bbab}$	F_{bd}	F_{be}	F_{bf}
$2F_{ccbc}$	$2F_{ccca}$	$2F_{ccab}$	F_{cd}	F_{ce}	F_{cf}
$4F_{bcbc}$	$4F_{caca}$	$4F_{abab}$	F_{dd}	F_{ee}	F_{ff}
$4F_{bbca}$	$4F_{caab}$	$4F_{abbc}$	F_{de}	F_{ef}	F_{fd}

As a result, the surface equation comprises linear and quadratic terms (TSAI S.W., WU E.M [1971]). Equation (4.14) is general and can be used in the analysis of 3D problems. Although the shape of the failure surface is assumed, no curve fitting (see for instance JONES R. M. [1999]) is performed to adjust the criterion to experimental data. Therefore, as the authors of the criterion claim, such an approach has intrinsic generality and internal consistency (TSAI S.W., WU E.M [1971]). For the purpose of analysis of an orthotropic material under plane stress conditions (4.14) is simplified to the form given in contracted notation:

$$F_a\sigma_a + F_b\sigma_b + F_f\sigma_f + F_{aa}\sigma_a^2 + F_{bb}\sigma_b^2 + F_{ff}\sigma_f^2 + 2F_{ab}\sigma_a\sigma_b = 1 \tag{4.15}$$

All components of the strength tensor are dependent on basic engineering strengths, including absolute values of tensile and compressive strengths in the first material direction X_t and X_c, absolute values of tensile and compressive strengths in the second material

direction Y_t and Y_c and in-plane shear strength S_l. The strength tensor components can be determined on the basis of simple assumptions. If an uniaxial test in the first material direction is analyzed, equation (4.15) can be expressed for tension ($\sigma_1 > 0$) as:

$$F_a X_t + F_{aa} X_t^2 = 1, \tag{4.16}$$

and for compression in the following form:

$$F_a X_c + F_{aa} X_c^2 = 1. \tag{4.17}$$

In effect, on the basis of (4.16) and (4.17), it is possible to define:

$$F_a = \frac{1}{X_t} - \frac{1}{X_c} \tag{4.18}$$

$$F_{aa} = \frac{1}{X_t X_c}. \tag{4.19}$$

The same uniaxial test can be considered in the second material direction, which results in:

$$F_b = \frac{1}{Y_t} - \frac{1}{Y_c}, \tag{4.20}$$

$$F_{bb} = \frac{1}{Y_t Y_c}. \tag{4.21}$$

Then, pure shear test in *a-b* plane of the principal material coordinates is taken into account, regarding (4.15), keeping in mind that shear strength does not depend on the shear stress sign. Consequently, the two following equations can be written:

$$F_f S_l + F_{ff} S_l^2 = 1 \tag{4.22}$$

$$F_f (-S_l) + F_{ff} (-S_l)^2 = 1 \tag{4.23}$$

In effect we get:

$$F_f = 0; \; F_{ff} = \frac{1}{S_l^2} \tag{4.24}$$

The off-diagonal component of strength tensor, namely F_{ab} represents an interaction between normal stresses σ_a and σ_b. Its value must be determined on the basis of a combined stress-state test. For instance, a biaxial tension can be exploited - ($\sigma_a = \sigma_b = \sigma$), which application into (4.15), results in:

$$F_{ab} = \frac{1}{2\sigma^2}\left[1 - \left(F_a + F_b\right)\sigma + \left(F_{aa} + F_{bb}\right)\sigma^2\right] \tag{4.25}$$

Alternatively, when the biaxial strength is not determined, it is possible to calculate F_{ab} (see for instance BAKER A., DUTTON S., KELLY D. [2004]) in the following way:

$$F_{ab} = f^* \sqrt{F_{aa}F_{bb}} \tag{4.26}$$

where f^* can be chosen within the range $-1 \le f^* \le 1$. This enforces the stability of the criterion, i.e. ellipsoid shape of the failure surface won't be open-ended (TSAI S.W., WU E.M [1971]). In many cases $f^* = 0.5$ is used (see for instance KAW A. K. [2006], GERMAN J. [2001], CHRÓŚCIELEWSKI J., KLASZTORNY M., NYCZ D., SOBCZYK B. [2014] and the references cited there). On the other hand there are some works that suggest $f^* = 0$ by default. These are e.g.: BAKER A., DUTTON S., KELLY D. [2004] or ABAQUS 6.14. A different allowable range $-0.5 \le f^* \le 0$ is proposed in Autodesk Simulation Composite Design 2014. In this thesis $f^* = -0.5$ is utilised together with (4.26) formula for the definition of F_{12}. Therefore, the full version of the classical Tsai-Wu criterion is given, using the above assumptions and the notation preferred in this work:

$$\left(\frac{1}{X_t} - \frac{1}{X_c}\right)\sigma_{aa} + \frac{\sigma_{aa}^2}{X_t X_c} + \left(\frac{1}{Y_t} - \frac{1}{Y_c}\right)\sigma_{bb} + \frac{\sigma_{bb}^2}{Y_t Y_c} + \frac{\sigma_{ab}^2}{S_l^2} - \frac{\sigma_{aa}\sigma_{bb}}{\sqrt{X_t X_c Y_t Y_c}} = 1 \tag{4.27}$$

The failure envelopes on σ_{aa}-σ_{bb}, σ_{aa}-σ_{ab}, σ_{bb}-σ_{ab} planes for the surface given by (4.27) are shown in Fig. 4.5, Fig. 4.6 and Fig. 4.7 correspondingly for a lamina made of AS4/3501-6 Carbon/Epoxy composite.
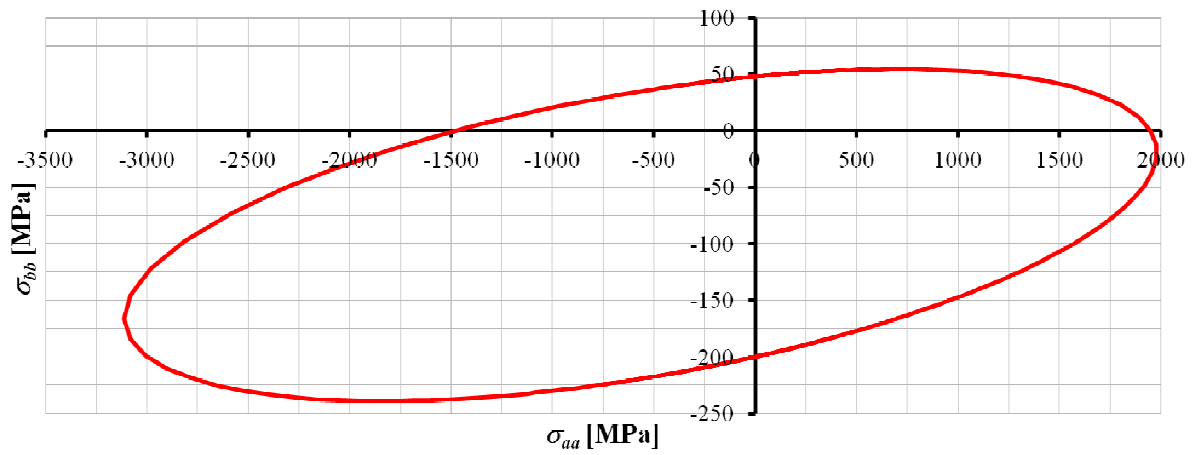
Fig. 4.5 Failure initiation envelope of Tsai-Wu criterion in σ_{aa} - σ_{bb} space, f^*=-0.5.
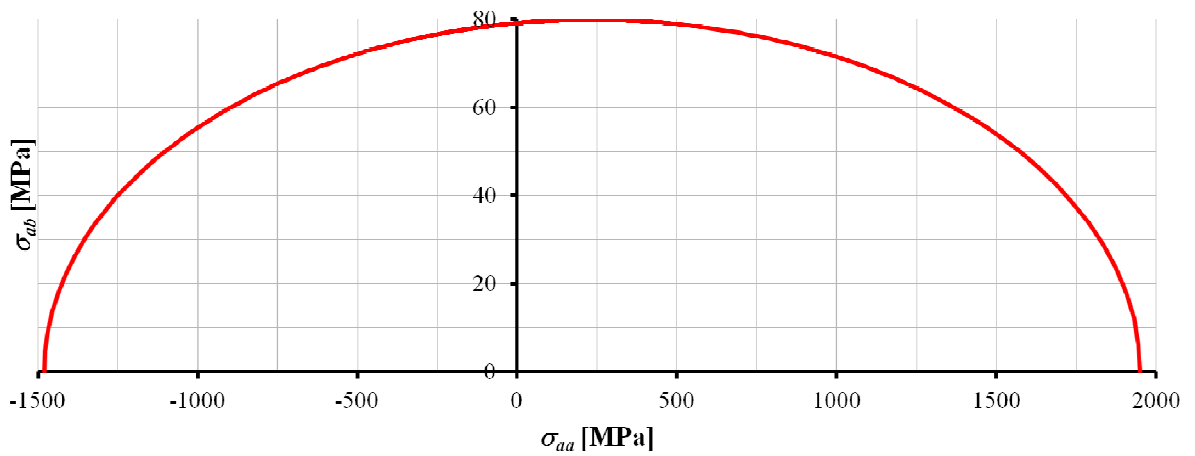

Fig. 4.6 Failure initiation envelope of Tsai-Wu criterion in σ_{aa} - σ_{ab} space, f^*=-0.5.
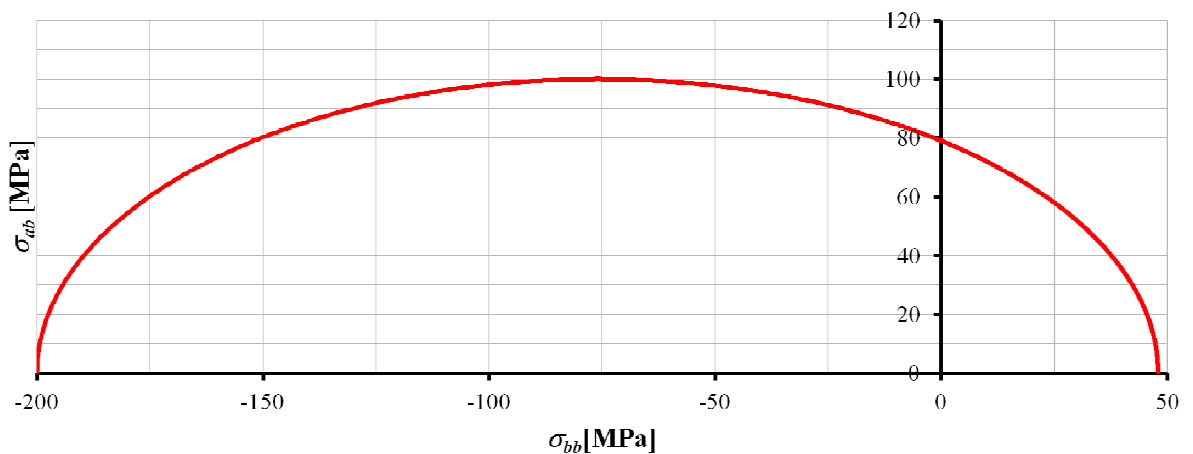

Fig. 4.7 Failure initiation envelope of Tsai-Wu criterion in σ_{bb} - σ_{ab} space, f^*=-0.5.

It should be emphasized that the Tsai-Wu criterion is sensitive to the value of f^*. Three failure envelopes, for $f^* = -0.5$, $f^* = -0.25$ and $f^* = 0$, are printed in the σ_{aa} - σ_{bb} plane for AS4/3501-6 Carbon/Epoxy composite in Fig. 4.8. Two proposed and

recommended values, viz. 0 and 0.5 are quite distinct from each other. This, definitely constitutes a drawback of this criterion.
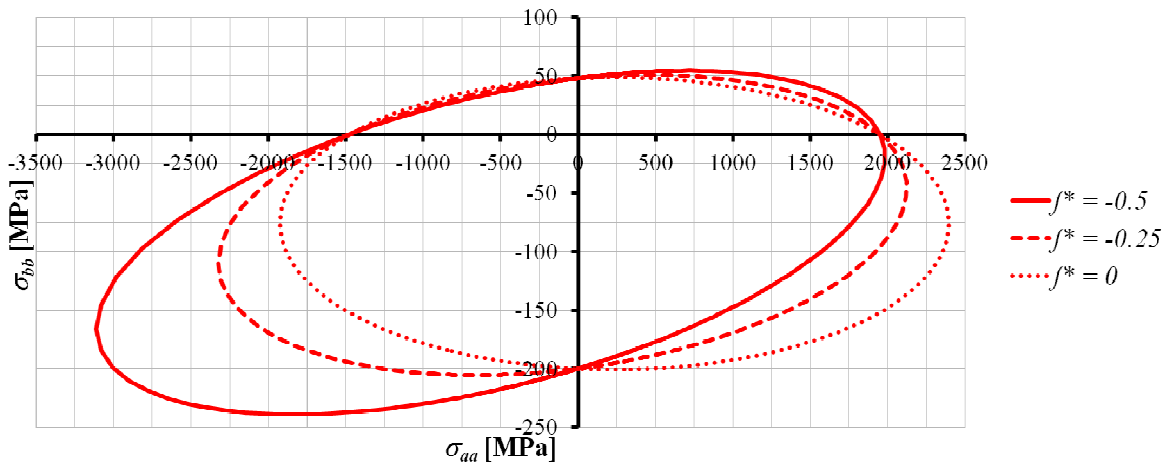
Fig. 4.8 Failure initiation envelope of Tsai-Wu criterion in σ_{bb}-σ_{ab} plane for different values of *f**.

Another issue that may be bothersome in this criterion is associated with some kind of unphysical behaviour. When e.g. biaxial compressive state of stress is applied, the failure index is dependent on tensile strengths (CAMANHO P. P. [2002]). Nevertheless the Tsai-Wu criterion is commonly used and is well established in the field of laminate failure analysis, as it was described in the introduction of this chapter.

4.3   Hashin criterion

The main concept leading to the development of Hashin criterion was connected with the mechanism of failure in laminated composites. Since the composite comprises of resilient matrix and stiff fibres, it may undergo damage in different ways (HASHIN Z. [1980]). No one before Hashin considered this fact in the theoretical descriptions. Only some polynomial criteria were developed, which gave information whether the failure initiates or not.

Hashin limited his considerations to unidirectional layers of fibrous composites, which can be modelled as transversely isotropic material. In such a case the postulated criterion can be represented as a function of the stress invariants of transversely isotropic continuum (HASHIN Z. [1980]). The five invariants described in HASHIN Z. [1980] are:

$$I_1 = \sigma_{aa} \tag{4.28}$$

$$I_2 = \sigma_{bb} + \sigma_{cc} \tag{4.29}$$

$$I_3 = \sigma_{bc}^2 - \sigma_{bb}\sigma_{cc} \text{ or } I_3 = \frac{1}{4}(\sigma_{bb} - \sigma_{cc})^2 + \sigma_{bc}^2 \qquad (4.30)$$

$$I_4 = \sigma_{ab}^2 + \sigma_{ac}^2 \qquad (4.31)$$

$$I_5 = 2\sigma_{ab}\sigma_{bc}\sigma_{ac} - \sigma_{bb}\sigma_{ac}^2 - \sigma_{cc}\sigma_{ab}^2 \qquad (4.32)$$

It is assumed that quadratic approximation of the failure surface shape is utilised, because it generally enables to fit the criterion into the experimental data reasonably well (HASHIN Z. [1980]). Therefore, only the first four invariants are put into the failure surface equation definition, which is expressed as:

$$A_1 I_1 + B_1 I_1^2 + A_2 I_2 + B_2 I_2^2 + C_{12} I_1 I_2 + A_3 I_3 + A_4 I_4 = 1 \qquad (4.33)$$

Two different modes of failure: fibre and matrix mode can be derived from (4.33) through the introduction of failure planes (HASHIN Z. [1980]). Hashin argues that a failure is caused by normal and shear stress components acting on a particular failure plane, which follows from the Mohr theory. If fibre failure occurs, the damage propagates in the plane which normal is parallel to fibre direction. Hence it is caused by σ_{aa}, σ_{ab} and σ_{ac} stress components. The definition of matrix mode failure plane is more complicated. This plane remains parallel to the fibre direction. Different stress components can be determined on this plane, namely, normal component σ_{nn}, shear component in the fibre direction σ_{nl} and shear component perpendicular to σ_{nl}, viz. σ_{nt} (see Fig. 4.9). Additionally, the failure plane inclination angle θ_f (Fig. 4.9) needs to be found.
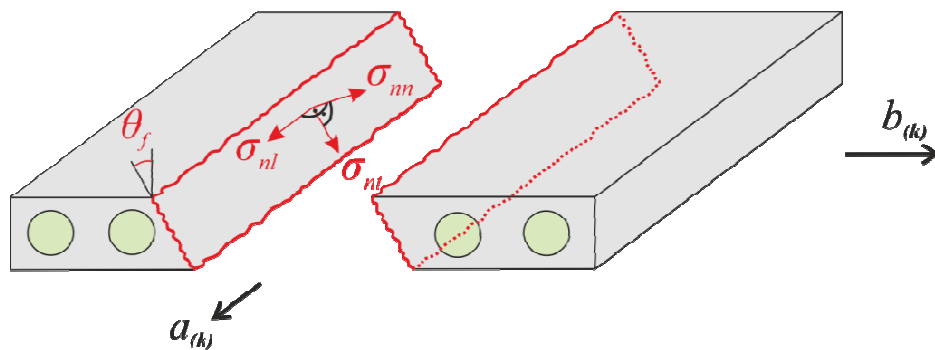

Fig. 4.9 Stress components acting on a possible failure plane.

Hashin discussed some possibilities, where the new stress components σ_{nn}, σ_{nl} and σ_{nt} are described by means of σ_{bb}, σ_{cc}, σ_{ab}, σ_{ac}, σ_{bc} and the inclination angle. However,

such an approach was too complicated at that time and did not allow him to find the inclination angle. Thus, he did not follow this path. He only mentioned that this approach is attractive from the physical point of view, as it would properly describe the failure mechanism and it is similar to the Mohr theory of failure (HASHIN Z. [1980]). Finally, he returned to the equation (4.33) and did not precisely specify the failure plane, but used all stress tensor components in the 3D case, excluding σ_{aa} to define general matrix failure.

Summarising, the following fibre and matrix failure criteria are defined.

Firstly, the pure shear states in *b-c* ($\sigma_{aa} = \sigma_{bb} = \sigma_{cc} = \sigma_{ab} = \sigma_{ac} = 0$; $\sigma_{bc} = S_t$) and *a-b* ($\sigma_{aa} = \sigma_{bb} = \sigma_{cc} = \sigma_{bc} = \sigma_{ac} = 0$; $\sigma_{ab} = S_l$) planes are considered separately with respect to (4.33) equation, including relations (4.28)-(4.31). This allow the definition of:

$$A_3 = S_t^2 \tag{4.34}$$

$$A_4 = S_l^2. \tag{4.35}$$

Consequently, the fibre failure occurs when (σ_{aa}, σ_{ab} and σ_{ac} stress components are considered in (4.28)-(4.31) and applied to (4.33), together with (4.35)):

$$A_f \sigma_{aa} + B_f \sigma_{aa}^2 + \frac{\sigma_{ab}^2 + \sigma_{ac}^2}{S_l^2} = 1 \tag{4.36}$$

while the matrix damage initiates when (σ_{bb}, σ_{ab}, σ_{bc} and σ_{ac} are considered in (4.28)-(4.31) and then included in (4.33) also with (4.34) and (4.35)):

$$A_m (\sigma_{bb} + \sigma_{cc}) + B_m (\sigma_{bb} + \sigma_{cc})^2 + \frac{(\sigma_{bc}^2 - \sigma_{bb}\sigma_{cc})}{S_t^2} + \frac{\sigma_{ab}^2 + \sigma_{ac}^2}{S_l^2} = 1. \tag{4.37}$$

The coefficients A_f, B_f and A_m, B_m, that appear in (4.36) and (4.37) require additional discussion (HASHIN Z. [1980]). This applies also to the determination of the appropriate expressions defining failure under tension and compression.

Firstly, fibre mode under tension is analysed ($\sigma_{aa} > 0$). It is possible to consider uniaxial tension test in view of equation (4.36). However, this results in one equation with two unknowns. Therefore, it is further assumed that the interaction between σ_{aa} and σ_{ab} reduces the resistance to failure and the failure surface should be convex. In effect an

elliptical shape of failure surface is applied for this mode (HASHIN Z. [1980]). Thus, the fibre mode for tension, associating the preceding assumptions with (4.36), becomes for plane stress:

$$\frac{\sigma_{aa}^2}{X_t^2} + \frac{\sigma_{ab}^2}{S_l^2} = 1 \qquad (4.38)$$

Hashin also allows application of the simple maximum stress criterion instead of (4.38) alternatively, namely:

$$\frac{\sigma_{aa}}{X_t} = 1. \qquad (4.39)$$

Also different version of (4.38) is available in e.g. ABAQUS 6.14 and AUTODESK SIMULATION COMPOSITE DESIGN 2014, in which the contribution of in-plane shear in the failure process is controlled by the α parameter ranging from 0 to 1:

$$\frac{\sigma_{aa}^2}{X_t^2} + \alpha \frac{\sigma_{ab}^2}{S_l^2} = 1 \qquad (4.40)$$

According to ABAQUS 6.14 manual it was proposed in the following work: HASHIN Z., AND ROTEM A. [1973]: A Fatigue Criterion for Fiber-Reinforced Materials. *J. Compos. Mater.*, 7, 448–464[5].

In order to define fibre compression mode ($\sigma_{aa} < 0$), it is possible to consider unidirectional test in compression basing on (4.36). However, similarly as in the fibre tension mode, this is not sufficient to establish all the unknown parameters. Since the shear stress influence on the failure resistance under fibre compression was not known to Hashin, he decided to use the maximum stress criterion:

$$\frac{-\sigma_{aa}}{X_c} = 1. \qquad (4.41)$$

The maximum stress criterion for fibre compression case is used for instance in: SANTIUSTE C. SÁNCHEZ-SÁEZ S., BARBERO E. [2010] or WARREN K. C., LOPEZ-ANIDO R. A., S. S. VEL, BAYRAKTAR H. H. [2016]. However, in e.g. FAN X. L., WANG T. J., SUN Q.

---

[5] Unfortunately, this paper is not available to the author of this thesis.

[2011], ABAQUS 6.14, AUTODESK SIMULATION COMPOSITE DESIGN 2014 it is represented in quadratic form:

$$\frac{\sigma_{aa}^2}{X_c^2} = 1 \tag{4.42}$$

In this work the expressions (4.38) and (4.42) are used as the fibre mode criterion.

Matrix damage in tension is analyzed from (4.37). If the state of uniaxial tension in the 2nd material direction b is considered and the assumptions analogous to that leading to the formulation of fibre mode in tension are incorporated, it is possible to define the matrix tension failure criterion (HASHIN Z. [1980]), which in plane stress becomes:

$$\frac{\sigma_{bb}^2}{Y_t^2} + \frac{\sigma_{ab}^2}{S_l^2} = 1 \tag{4.43}$$

Following the concept of inclined failure plane, which is parallel to the fibre direction (see Fig. 4.9), the matrix tension occurs when the normal stress component on this plane - σ_{nn} is greater than 0. The component σ_{nn} can be described by means of σ_{bb}, σ_{cc} and trigonometric functions of the inclination angle θ_f. The analysis of the dependency between the sign of σ_{nn} and the signs of σ_{bb} and σ_{cc} led Hashin to the conclusion that for general 3D case matrix tension occurs when $\sigma_{bb} + \sigma_{cc}$ is greater than 0. This deduction is not completely correct from the physical point of view, since it implies that the matrix failure may occur only for inclination angle equal to $\pm 45^\circ$ (HASHIN Z. [1980]). This is a consequence of the quadratic approximation which was chosen to develop the criterion. Nevertheless, it is used. Hence, in the case of plane stress the matrix tension is defined when $\sigma_{bb} > 0$. Similarly, for $\sigma_{bb} < 0$ matrix failure in compression occurs. A set of equation should be constructed from (4.37) to obtain the expression for the matrix damage in compression. In order to create the first equation, the state of uniaxial compression is assumed. The second equation is built assuming that transversely isotropic pressure is applied, namely $\sigma_{bb} = \sigma_{cc} = \sigma$, which is significantly greater than unidirectional strength ($\sigma \gg Y_c$), since it is predicted that the strength resistance will be much higher in this case (HASHIN Z. [1980]). In effect we get:

$$
\begin{cases}
-A_m Y_c + B_m Y_c^2 = 1 \\
-2\sigma A_m + 4\sigma^2 B_m - \dfrac{\sigma^2}{S_t^2} = 1
\end{cases}
\tag{4.44}
$$

Constants A_m and B_m are determined from (4.44) assuming that $\dfrac{Y_c}{\sigma} \sim 0$ ($\sigma_{bb} = \sigma_{cc} = \sigma$ and $\sigma \gg Y_c$). Finally, the matrix failure in compression occurs when (HASHIN Z. [1980]):

$$
\left(\frac{\sigma_{bb}}{2S_t} \right)^2 + \left[\left(\frac{Y_c}{2S_t} \right)^2 - 1 \right] \frac{\sigma_{bb}}{Y_c} + \left(\frac{\sigma_{ab}}{S_l} \right)^2 = 1
\tag{4.45}
$$

As it is reported in HASHIN Z. [1980] it may be problematic to determine S_t strength by means of experiments. Therefore some simplified methods are proposed to estimate its value. According to the first one (see for instance DAVILA C. G., CAMANHO P. P., ROSE C. A. [2005] or ABAQUS 6.14) $S_t \approx 0.5 Y_C$. On the other hand it may be assumed that: $S_t \approx 0.5\sqrt{Y_c Y_t}$. The second proposal is utilised in AUTODESK SIMULATION COMPOSITE DESIGN 2014. In this work the first method is used to calculate transverse shear strength of a lamina.

To sum up, the failure envelopes on σ_{aa} - σ_{bb}, σ_{aa} - σ_{ab}, σ_{bb} - σ_{ab} planes are shown in Fig. 4.10, Fig. 4.11 and Fig. 4.12. These are given for the most unfavourable combination of expressions (4.38), (4.42), (4.43), (4.45) and are shown for a lamina made of AS4/3501-6 Carbon/Epoxy composite (assuming that $S_t = 0.5 Y_C$).
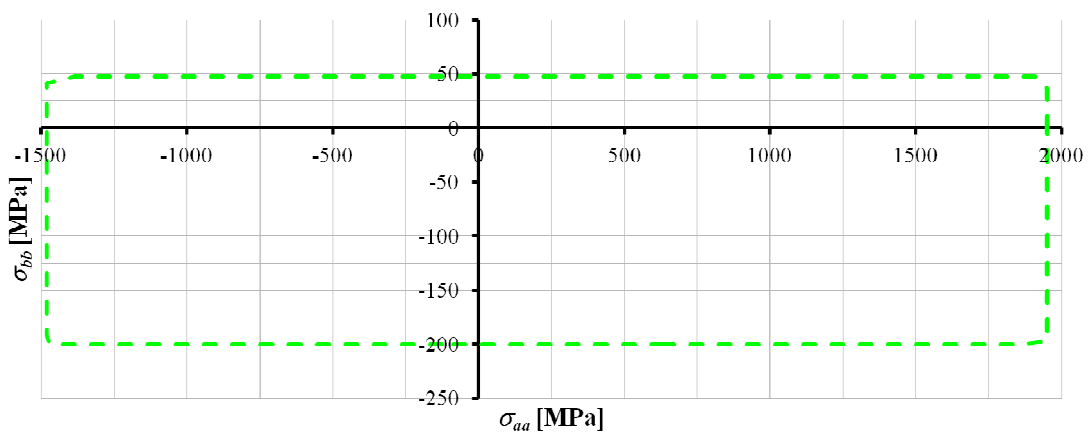
Fig. 4.10 Failure initiation envelope of Hashin criterion in σ_{aa} - σ_{bb} space.
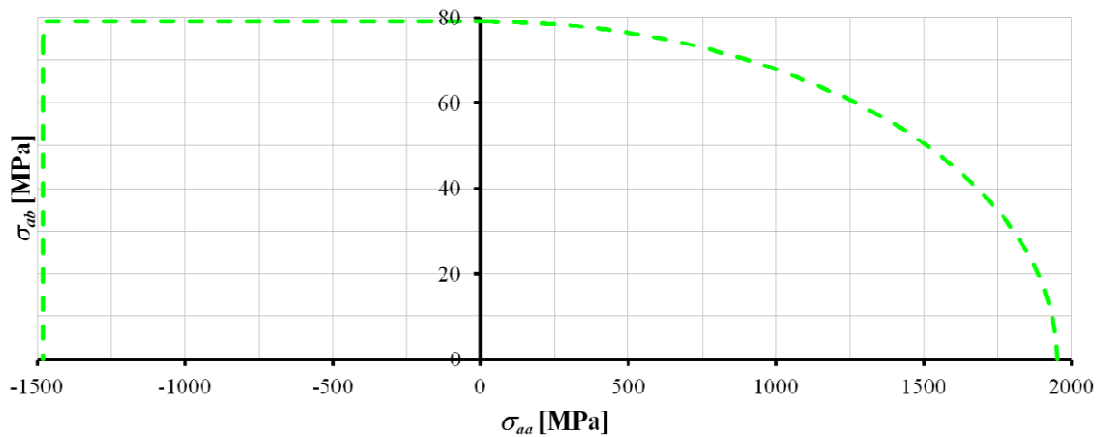
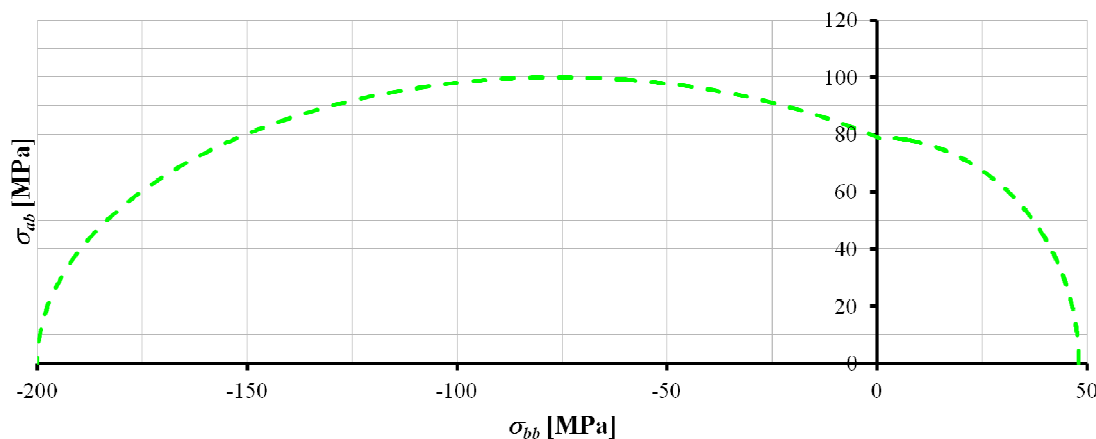Fig. 4.11 Failure initiation envelope of Hashin criterion in σ_{aa} - σ_{ab} space.

Fig. 4.12 Failure initiation envelope of Hahsin criterion in σ_{bb} - σ_{ab} space.

4.4 Puck criterion

The Puck criterion is the most sophisticated one discussed in this work. It can be applied in the analysis of unidirectional layers of FRP made of glass or carbon fibres. The modes of fibre failure (FF) and matrix failure, named by Puck as inter fibre failure (IFF) are distinguished. From the designer's point of view the FF modes are of great importance, because their occurrence causes a rapid loss of load capacity of a structure. However, the IFF, which is observed at lower load levels, may lead to some local internal damage with possible significant decrease of strength of the construction, as some discontinuities in the structure of the material emerge (PUCK A., SCHÜRMANN H. [1998]). Nevertheless, formulation of FF conditions is less complicated than of IFF ones. Therefore the Puck criterion is mainly focused on a proper and detailed definition of the latter one.

Initially, PUCK A., SCHÜRMANN H. [1998] proposed to define the FF surface in terms of strains with respect to the failure of fibres, instead of limiting it only to the failure of

unidirectional layer in the direction parallel to fibres. Since, generally, a lamina may be subjected to combined stress of state, additional material effort is included. This is a consequence of the action of normal transverse stress components, that leads to additional strain in the fibre direction through Poisson's ratio. Therefore, in the case of fibre tension the failure initiates when the following condition is met:

$$f_{E,FF} = \frac{1}{\varepsilon_{aaT}}\left(\varepsilon_{aa} + \frac{v_{fab}}{E_{faa}}m_{\sigma f}\sigma_{bb}\right) = 1,\qquad(4.46)$$

which is valid for; $\left(\varepsilon_{aa} + \frac{v_{fab}}{E_{faa}}m_{\sigma f}\sigma_{bb}\right) > 0$. The properties of fibres in (4.46) are described by additional constants: fibre strain at tensile failure ε_{aaT}, fibre elastic modulus E_{faa} and fibre Poisson's ratio v_{fab}. Because the distribution of stress in a lamina is not uniform (the fibres repossess higher stress in their direction than the matrix) the stress in fibres (see (4.46)) is increased via magnification factor, which is assumed $m_{\sigma f} \approx 1.3$ for glass fibres and $m_{\sigma f} \approx 1.1$ for carbon ones (PUCK A., SCHÜRMANN H. [1998]).

According to the observations of Puck and Schürmann, the action of in-plane shear reduce the load capacity of fibres in compression. Thus, in the case of $\left(\varepsilon_{aa} + \frac{v_{fab}}{E_{faa}}m_{\sigma f}\sigma_{bb}\right) < 0$, additional correction is introduced on the right hand side of $f_{E,FF}$ definition, which results in (PUCK A., SCHÜRMANN H. [1998]):

$$f_{E,FF} = \frac{1}{\varepsilon_{aaC}}\left(\varepsilon_{aa} + \frac{v_{fab}}{E_{faa}}m_{\sigma f}\sigma_{bb}\right) = 1 - \left(10\gamma_{ba}\right)^2.\qquad(4.47)$$

where ε_{aaC} denotes the fibre compression failure strain. Nonetheless, the difference between the predictions of fibre FPF calculated by means of (4.46) and (4.47) in comparison with maximum stress or maximum strain criterion is negligible and the derivation of (4.46) and (4.47) is assessed later by the authors of the criterion as "academic exercise" (PUCK A., SCHÜRMANN H). [2002]). Therefore it is concluded in PUCK A., SCHÜRMANN H). [2002] that the use of the maximum stress criterion instead of (4.46) and (4.47) for the FF is fully acceptable. Consequently, in this thesis maximum stress criterion will be used for FF estimations, which is expressed as:

$$f_{E,FF} = \begin{cases} \dfrac{\sigma_{aa}}{X_t} = 1 & \text{for } \sigma_{aa} \geq 0 \\[2mm] \dfrac{-\sigma_{aa}}{X_c} = 1 & \text{for } \sigma_{aa} < 0 \end{cases}. \tag{4.48}$$

It was observed in some experiments (PUCK A., SCHÜRMANN H. [1998]) that unidirectional layers of laminated fibrous composites fail because of brittle matrix cracking[6]. This mechanism of failure is the starting point of IFF criterion development as done by Puck and Schürmann. A general analytical description of brittle damage was proposed by Mohr. First attempt of its utilization, regarding failure in FRP, was described by HASHIN Z. [1980]. However, such a criterion was not developed in 1980, because the numerical effort required to find fracture plane was too high. Nevertheless, it was successfully done in the work of PUCK A., SCHÜRMANN H. [1998].

Hence, following Mohr, it is assumed that IFF is caused by stress, which arises on a particular failure plane. In this case the plane is parallel to fibre direction, but may be variously inclined. Its inclination is measured by θ angle (see also Fig. 4.9). Thus, it is possible to distinguish three stress components on the plane: normal σ_{nn}, shear in the fibre direction (transverse-longitudinal shear) σ_{nl} and shear perpendicular to σ_{nl}, viz. σ_{nt} (transverse-transverse shear) (PUCK A., SCHÜRMANN H. [1998]).

If $\sigma_{nn} > 0$, then all three components contribute to the IFF process. Therefore, the damage onset is observed when:

$$f_{E,IFF0} = \left(\frac{\sigma_n}{R_{\perp}^{(+)\mathrm{A}}} \right)^2 + \left(\frac{\tau_{nt}}{R_{\perp\perp}^{\mathrm{A}}} \right)^2 + \left(\frac{\tau_{nl}}{R_{\perp\parallel}^{\mathrm{A}}} \right)^2 = 1. \tag{4.49}$$

It should be emphasized, that in (4.49) and in subsequent equations, that describe the failure surface in stress space, the stress components are referred to the corresponding strengths of the failure plane e.g. $R_{\perp}^{(+)\mathrm{A}}$ denote the strength of the failure plane against the action of normal stress component σ_n. These strengths, in general, are different than the

---

[6] It is worth to mention that in the light of the experimental research, mentioned in this paragraph, the criteria which follow from the analysis of ductile materials, as e.g. Tsai-Hill, seem to be questionable (PUCK A., SCHÜRMANN H. [1998])

standard ones given in material coordinate system and should not be mistaken (PUCK A., SCHÜRMANN H. [1998]). Nevertheless, it is possible to express strengths of failure planes by means of the standard ones in order to provide a simple and consistent description of the final form of the criterion, which will be shown later.

When $\sigma_{nn} < 0$ different IFF mechanism is observed. In this case only shear components increase the risk of failure, while the normal compressive stress component prevents IFF development. In effect, the failure initiates when the following condition is satisfied:

$$f_{E,IFF0} = \left(\frac{\tau_{nt}}{R_{\perp\perp}^A - p_{\perp\perp}^{(-)}\sigma_n} \right)^2 + \left(\frac{\tau_{nl}}{R_{\perp\parallel}^A - p_{\perp\parallel}^{(-)}\sigma_n} \right)^2 = 1, \qquad (4.50)$$

The parameters $p_{\perp\parallel}^{(-)}$ and $p_{\perp\perp}^{(-)}$ define, correspondingly, the slope of σ_n-τ_{nl} fracture plane at $\sigma_{nn} = 0$ and (σ_n, τ_{nt}) at $\sigma_{nn} = 0$ for $\sigma_{nn} < 0$ (see e.g. Fig. 9 of PUCK A., SCHÜRMANN H. [2002]). Their values have to be carefully defined (PUCK A., SCHÜRMANN H). [2002]) and will be described later.

To simplify the IFF consideration it is assumed (PUCK A., SCHÜRMANN H. [1998]) that there exists a coupling between the slope parameters and strengths of the failure plane, resulting in:

$$\frac{p_{\perp\perp}^{(-)}}{R_{\perp\perp}^A} = \frac{p_{\perp\parallel}^{(-)}}{R_{\perp\parallel}^A} = \frac{p}{R} = \text{const.}. \qquad (4.51)$$

In order to improve the accuracy of damage prediction, regarding the experimental results, the equations (4.49) and (4.50) are modified, correspondingly, in the following way:

$$f_{E,IFF0} = c_2 \left(\frac{\sigma_n}{R_\perp^{(+)A}} \right)^2 + c_1 \frac{\sigma_n}{R_\perp^{(+)A}} + \left(\frac{\tau_{nt}}{R_{\perp\perp}^A} \right)^2 + \left(\frac{\tau_{nl}}{R_{\perp\parallel}^A} \right)^2 = 1 \quad \text{for } \sigma_n \geq 0, \qquad (4.52)$$

$$f_{E,IFF0} = \frac{\tau_{nt}^2}{\left(R_{\perp\perp}^A \right)^2 - 2 p_{\perp\perp}^{(-)}\sigma_n} + \frac{\tau_{nl}^2}{\left(R_{\perp\parallel}^A \right)^2 - 2 p_{\perp\parallel}^{(-)}\sigma_n} = 1 \quad \text{for } \sigma_n < 0, \qquad (4.53)$$

Equations (4.52) and (4.53) are treated as the base form of Puck's IFF criteria (PUCK A., SCHÜRMANN H. [1998]) and are the starting point for further considerations.

The final form of IFF criterion is obtained after some extensive derivations, which are moved to the Appendix. In effect the following three criteria for failure initiation (without inclusion of additional weakening due to high stress in fibres) become:

mode A ($\theta_f = 0°$) for $\sigma_{bb} \geq 0$:

$$f_{E,IFF0,A} = \sqrt{\left(1 - p_{\perp\parallel}^{(+)}\frac{Y_T}{S_l}\right)^2 \left(\frac{\sigma_{bb}}{Y_T}\right)^2 + \left(\frac{\sigma_{ba}}{S_l}\right)^2} + \frac{p_{\perp\parallel}^{(+)}}{S_l}\sigma_{bb} = 1, \qquad (4.54)$$

mode B ($\theta_f = 0°$) for $\sigma_{bb} < 0$ and $0 \leq \dfrac{\left|\sigma_{ba,crit}\right|}{R_{\perp\perp}^{A}} \leq \left|\dfrac{\sigma_{ba}}{\sigma_{bb}}\right|$:

$$f_{E,IFF0,B} = \frac{1}{S_l}\left(\sqrt{\sigma_{ba}^2 + \left(p_{\perp\parallel}^{(-)}\sigma_{bb}\right)^2} + p_{\perp\parallel}^{(-)}\sigma_{bb}\right) = 1, \qquad (4.55)$$

mode C ($\theta_f \neq 0°$; $\theta_f = \arccos\sqrt{\dfrac{1}{2\left(1+p_{\perp\perp}^{(-)}\right)}\left[\left(\dfrac{\sigma_{ba}}{\sigma_{bb}}\right)^2\left(\dfrac{R_{\perp\perp}^{A}}{S_l}\right)^2 + 1\right]}$) for $\sigma_{bb} < 0$

and $0 \leq \left|\dfrac{\sigma_{ba}}{\sigma_{bb}}\right| \leq \dfrac{\left|\sigma_{ba,crit}\right|}{R_{\perp\perp}^{A}}$:

$$f_{E,IFF0,C} = \left[\left(\frac{\sigma_{ba}}{2\left(1+p_{\perp\perp}^{(-)}\right)S_l}\right)^2 + \left(\frac{\sigma_{bb}}{Y_c}\right)^2\right]\frac{Y_c}{\left(-\sigma_{bb}\right)} = 1. \qquad (4.56)$$

The sketches of A, B and C failure modes are shown in Fig. 4.13 and are associated with the corresponding parts of the IFF envelope created on $\sigma_{bb} - \sigma_{ba}$ stress plane for AS4/3501-6 Carbon/Epoxy UD lamina.
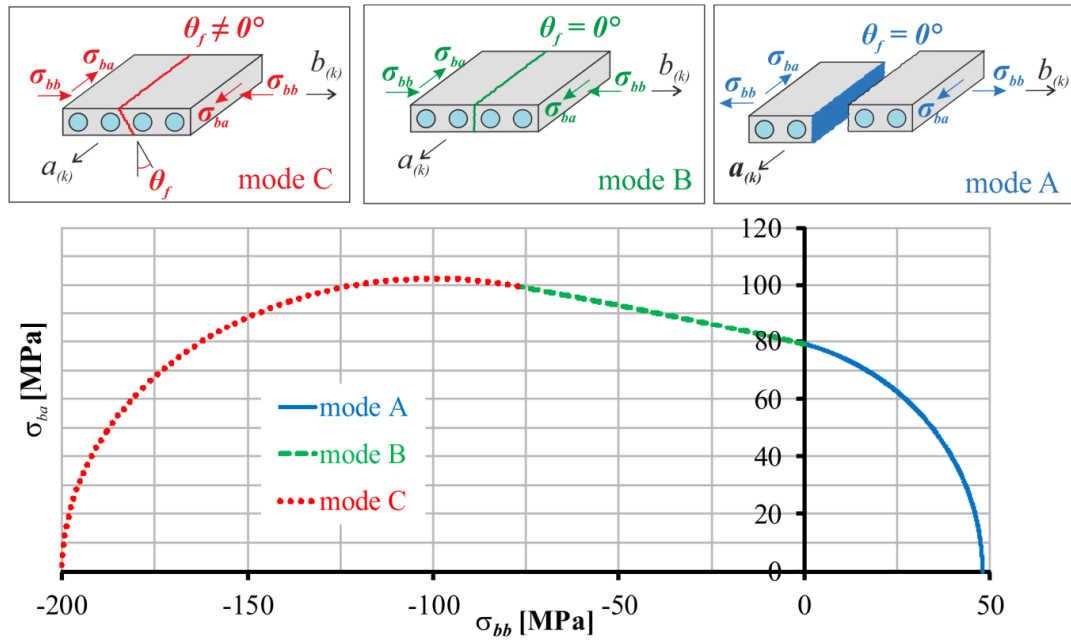
Fig. 4.13 Sketches of IFF A, B, C failure associated with the IFF envelope in σ_{bb} - σ_{ba} space

The $R_{\perp\perp}^{A}$ resistance, which is used to determine the range of validity of mode B and C IFF criterion cannot be expressed by a standard strength, as it was done in the case of $R_{\perp}^{(+)A}$, $R_{\perp}^{(-)A}$, $R_{\perp\parallel}^{A}$ (PUCK A., SCHÜRMANN H. [1998]). Since there is no experimental method to measure this strength, it is calculated on the basis of the following relation proposed by PUCK A., SCHÜRMANN H. [1998]:

$$R_{\perp\perp}^{A} = \frac{Y_c}{2\left(1+p_{\perp\parallel}^{(-)}\right)} = \frac{S_l}{2p_{\perp\parallel}^{(-)}}\left(\sqrt{1+2p_{\perp\parallel}^{(-)}\frac{Y_c}{S_l}}-1\right). \tag{4.57}$$

The inclination parameters $p_{\perp\parallel}^{(+)}$, $p_{\perp\parallel}^{(-)}$, $p_{\perp\perp}^{(-)}$ which are required in (4.54), (4.55), (4.56) and (4.57), define the inclination of the Puck criterion failure envelope at $\sigma_n = 0$ (PUCK A., KOPP J., KNOPS M. [2002]). They are determined on the basis of some considerations for typical composites made of epoxide matrix and glass or carbon fibres (GFRP and CFRP correspondingly). The values of $p_{\perp\parallel}^{(-)}$ and $p_{\perp\parallel}^{(+)}$ can be determined from experimental data (see e.g. PUCK A., KOPP J., KNOPS M. [2002], KNOPS M. [2008]). It is not possible to determine $p_{\perp\perp}^{(-)}$, $p_{\perp\perp}^{(+)}$ by means of experimental validation. However $p_{\perp\perp}^{(-)}$ can be estimated in the following way (PUCK A., SCHÜRMANN H. [1998]):

$$p_{\perp\perp}^{(-)} = p_{\perp\parallel}^{(-)}\frac{R_{\perp\perp}^{A}}{S_l}. \tag{4.58}$$

In the case of $p_{\perp\perp}^{(+)}$ it is reasonable to assume that $p_{\perp\perp}^{(+)} = p_{\perp\perp}^{(-)}$ (PUCK A., KOPP J., KNOPS M. [2002]). The recommended values of the aforementioned parameters are summarized in Tab. 4.3.

Tab. 4.3 Recommended values of the inclination parameters (PUCK A., KOPP J., KNOPS M. [2002]).

Composite type (fibre volume fraction - 60%)	$p_{\perp\parallel}^{(+)}$ [-]	$p_{\perp\parallel}^{(-)}$ [-]	$p_{\perp\perp}^{(+)}$ [-]	$p_{\perp\perp}^{(-)}$ [-]
GFRP/Epoxy	0.3	0.25	0.2-0.25	0.2-0.25
CFRP/Epoxy	0.35	0.3	0.25-0.3	0.25-0.3

According to the Mohr theory, only the stress components that act on the failure plane lead to the failure. However, as it was mentioned earlier, it was observed in experiments that high stressing in fibres (when $\sigma_{aa} >\sim 0.7X_T$) facilitate the process of IFF. Some of the fibres may break before their strength is attained. In effect, some microcracks and debondings at fibre-matrix interface develop and reduce the IFF resistance (PUCK A., SCHÜRMANN H. [1998]). Similar situation may be observed for high compressive σ_{aa} stress. Some fibres may start to kink before their failure strength is achieved, which can cause local damage in matrix (KNOPS M. [2008]). To include these effects, a weakening factor $\eta_{w1} \in \langle 0:1 \rangle$ is introduced. Consequently, all fracture resistances considered in the criterion, namely Y_t, Y_c, S_l, $R_{\perp\perp}^A$ in (4.54), (4.55), (4.56) and (4.57) are multiplied by η_{w1}, which by assumption is the same for all of them. Thus, the derivation of the fracture plane inclination angle do not have to be re-established (PUCK A., KOPP J., KNOPS M. [2002]). In effect the new condition for failure, including existence of high σ_{aa} stress, for each mode, is expressed as:

$$f_{E,IFF} = \frac{f_{E,IFF0}}{\eta_{w1}} = 1 \tag{4.59}$$

A proposal for η_{w1} estimation is given in PUCK A., SCHÜRMANN H. [1998]:

$$\eta_{w1} = 1 - \left(\frac{\sigma_{aa}}{\sigma_{aa,d}} \right)^n \tag{4.60}$$

where $\sigma_{aa,d} = \begin{cases} 1.1X_t & \text{for } \sigma_{aa} \geq 0 \\ -1.1X_c & \text{for } \sigma_{aa} < 0 \end{cases}$. The exponent n is an experimentally estimated value, that define the degradation effect. For matrices with low failure strain $n = 6$, while for matrices with high strain at failure $n = 8$ is proposed. If the calculations of the failure surface require iterative calculations, (4.60) is replaced by:

$$\eta_{w1} = 1 - \frac{\sigma_{aa}}{\sigma_{aa,D}} \qquad (4.61)$$

to keep the failure conditions homogenous and of first degree (PUCK A., SCHÜRMANN H. [1998]), where $\sigma_{aa,D} = \dfrac{\sigma_{aa}}{\left(\dfrac{\sigma_{aa}}{\sigma_{aa,d}}\right)^n}$.

Another possibility of η_{w1} definition is described in details e.g. in KNOPS M. [2008] or DEUSCHLE H. M. [2010]. A closed form solution was found for η_{w1}, thus the iterative calculations are not required. Its final form is written below:

$$\eta_{w1} = \frac{c\left(\sqrt{c^2 + 12} + 3\right)}{2\left(c^2 + 3\right)} \qquad (4.62)$$

where c is the ratio of IFF and FF failure indices ($c = \dfrac{f_{E,IFF0}}{f_{E,FF}}$ and

$f_{E,IFF0} = \max\left(f_{E,IFF0,A}; f_{E,IFF0,B}; f_{E,IFF0,C}\right)$) The range of η_{w1} validity is $0.5 \leq c \leq 2$. If $c > 2$, then there is no decrease of IFF resistance, thus $\eta_{w1} = 1$, whereas for $c < 0.5$ no IFF occurs and it does not have to be checked (DEUSCHLE H. M. [2010]). This version of η_{w1} estimation is adapted for calculations in this work.

The Puck's criterion failure initiation conditions, which are used in this work are summarized in Tab. 4.4.

The failure envelopes on σ_{aa}-σ_{bb}, σ_{aa}-σ_{ab}, σ_{bb}-σ_{ab} planes of Puck criterion are depicted for a lamina made of AS4/3501-6 Carbon/Epoxy composite in Fig. 4.14, Fig. 4.15 and Fig. 4.16.

Tab. 4.4 Puck's criterion summary.

Failure type	Failure mode	Failure condition	Validity condition
FF	Tensile / Compressive	$$f_{E,FF} = \begin{cases} \dfrac{\sigma_{aa}}{X_t} = 1 \\[2mm] \dfrac{\sigma_{aa}}{-X_c} = 1 \end{cases}$$	$\sigma_{aa} \geq 0$ $\sigma_{aa} < 0$
IFF	Mode A ($\theta = 0°$)	$$f_{E,IFF,A} = \frac{f_{E,IFF0,A}}{\eta_{w1}} = 1$$ $$f_{E,IFF0,A} = \sqrt{\left(1 - p_{\perp\parallel}^{(+)}\frac{Y_T}{S_l}\right)^2\left(\frac{\sigma_{bb}}{Y_T}\right)^2 + \left(\frac{\sigma_{ba}}{S_l}\right)^2} + \frac{p_{\perp\parallel}^{(+)}}{S_l}\sigma_{bb}$$	$\sigma_{bb} > 0$ η_{w1} - see (4.62)
	Mode B ($\theta = 0°$)	$$f_{E,IFF,B} = \frac{f_{E,IFF0,B}}{\eta_{w1}} = 1$$ $$f_{E,IFF0,B} = \frac{1}{S_l}\left(\sqrt{\sigma_{ba}^2 + \left(p_{\perp\parallel}^{(-)}\sigma_{bb}\right)^2} + p_{\perp\parallel}^{(-)}\sigma_{bb}\right)$$	$\sigma_{bb} < 0$ and $0 \leq \dfrac{\left|\sigma_{ba,crit}\right|}{R_{\perp\perp}^A} \leq \left|\dfrac{\sigma_{ba}}{\sigma_{bb}}\right|$ η_{w1} - see (4.62)
	Mode C ($\theta \neq 0°$)	$$f_{E,IFF,C} = \frac{f_{E,IFF0,C}}{\eta_{w1}} = 1$$ $$f_{E,IFF0,C} = \left[\left(\frac{\sigma_{ba}}{2\left(1 + p_{\perp\perp}^{(-)}\right)S_l}\right)^2 + \left(\frac{\sigma_{bb}}{Y_c}\right)^2\right]\frac{Y_c}{(-\sigma_{bb})} = 1$$	$\sigma_{bb} < 0$ and $0 \leq \left|\dfrac{\sigma_{ba}}{\sigma_{bb}}\right| \leq \dfrac{\left|\sigma_{ba,crit}\right|}{R_{\perp\perp}^A}$ η_{w1} - see (4.62)
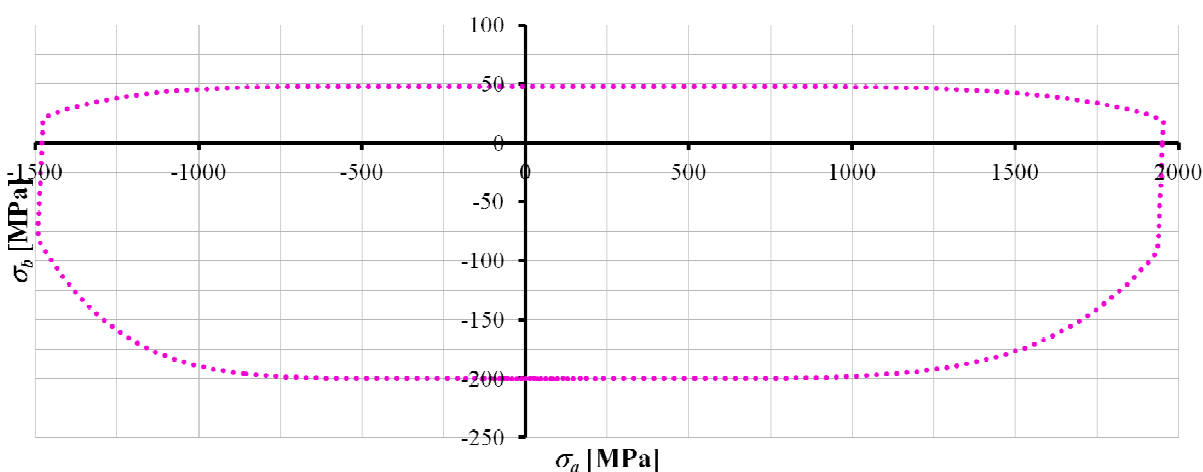
Fig. 4.14 Failure initiation envelope of Puck criterion in σ_a - σ_b space.
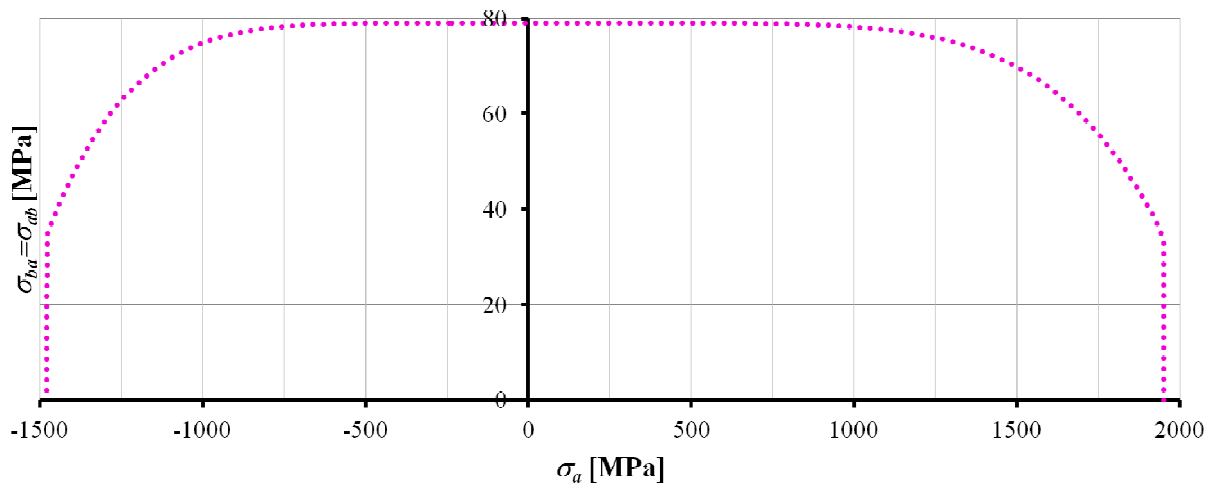
Fig. 4.15 Failure initiation envelope of Puck criterion in σ_a - σ_{ba} space.
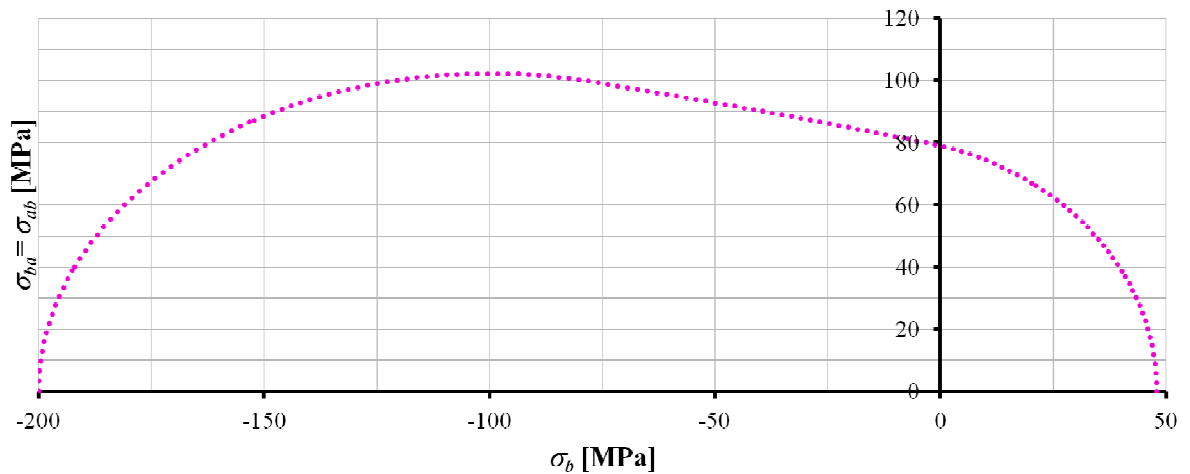
Fig. 4.16 Failure initiation envelope of Puck criterion in σ_b - σ_{ba} space.

Concluding, the Puck criterion is a sophisticated formulation, giving a thorough description of IFF failure. The mechanisms of IFF is described by two different types of cracks: straight ($\theta = 0°$, modes A and B) and oblique ($\theta \neq 0°$, mode C). Generally, mode A failure is treated as not dangerous and mode C as a serious effect (PUCK A., SCHÜRMANN H. [2002]). It is also noticeable that despite the fact that the in-plane shear is assumed to be symmetric $\sigma_{ab} = \sigma_{ba}$ only σ_{ba} component is used to define IFF. This gives an opportunity of straightforward application of the Puck criterion to the theories which incorporate asymmetric in-plane shear components.

4.5 Comparison of discussed failure criteria

This paragraph intends to present summary of all the considered failure envelopes.

The Tsai-Hill failure surface is created on the basis of Huber Mises Hencky theory of failure, established for ductile materials. The considerations for isotropic materials are converted to orthotropic ones. This seems not to be an appropriate approach, because laminated composites are rather brittle materials. The Tsai-Wu criterion is developed assuming that the failure surface for laminates is of quadratic type and all stress tensor components interact and contribute in one failure expression. The Hashin criterion is historically the first one to distinguish modes of failure. Therefore, some piecewise equations are introduced. Hashin expressed his criterion by means of the stress tensor components that, as he claimed, contribute to the failure process. He tried to describe the mechanism of failure of and UD lamina in a more sophisticated way, by incorporation of Mohr theory of failure, however did not manage to do it because of extensive numerical effort which was required. Nevertheless the Hashin cirterion was a big step forward in the analysis of FRP's, because it paved the way for further considerations. Finally, the Puck criterion tends to be rather a theory than an assumed criterion. It is in a way a continuation of Hashin's concept, because the Mohr theory constitutes its foundations. In effect some sophisticated failure initiation expressions, which are additionally adjusted to the experimental data are formulated for an UD lamina.

Fig. 4.17 - Fig. 4.19 portray failure envelopes of Tsai-Hill, Tsai-Wu, Hashin and Puck criteria correspondingly in σ_{aa}-σ_{bb}, σ_{aa}-σ_{ab} and σ_{bb}-σ_{ab} stress space for a lamina made of AS4/3501-6 Carbon/Epoxy composite.
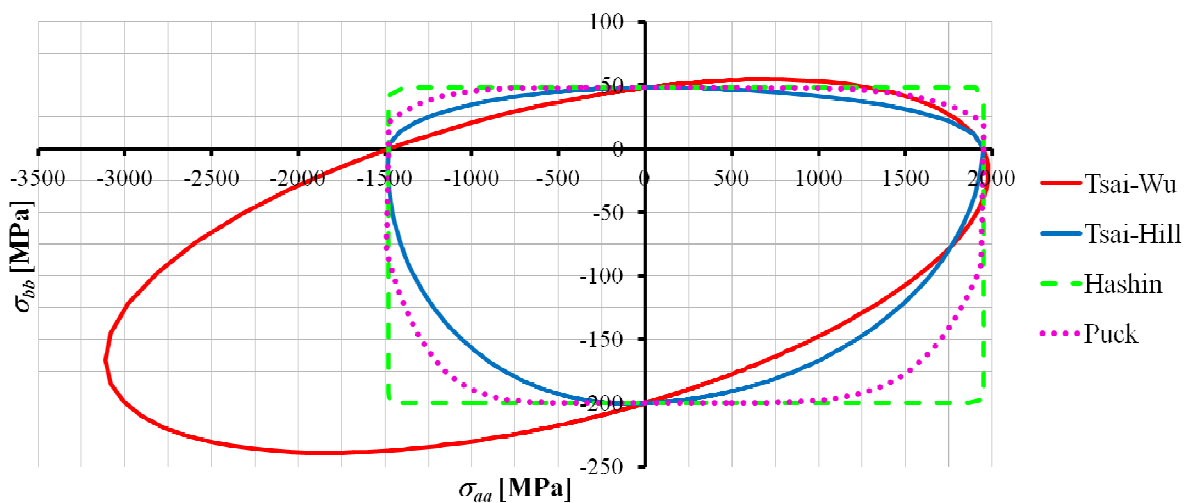
Fig. 4.17 Failure initiation envelopes of Tsai-Hill, Tsai-Wu, Hashin and Puck criteria in σ_{aa}-σ_{bb} space.
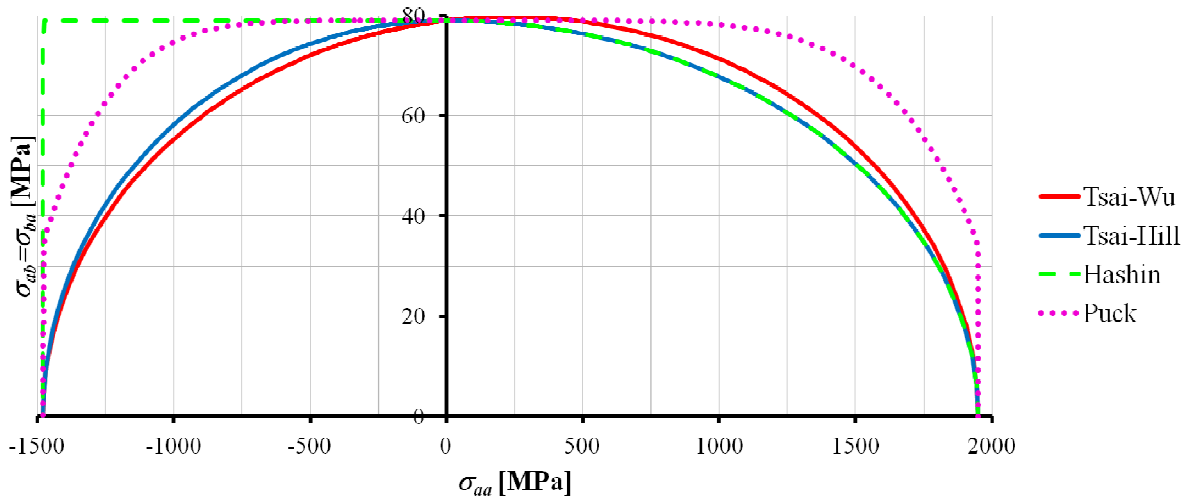
Fig. 4.18 Failure initiation envelopes of Tsai-Hill, Tsai-Wu, Hashin and Puck criteria in σ_{aa} - σ_{ab}
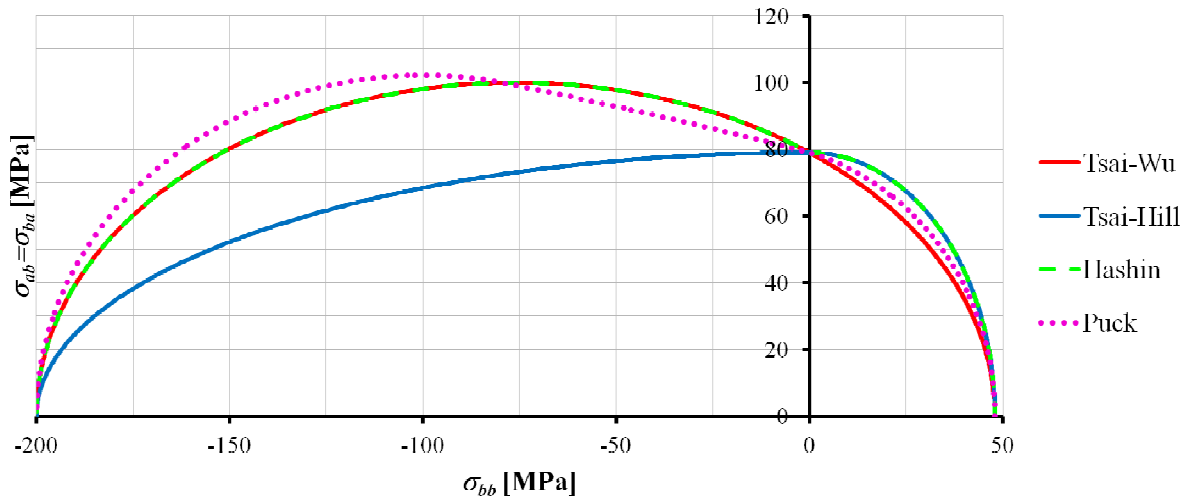
space.

Fig. 4.19 Failure initiation envelopes of Tsai-Hill, Tsai-Wu, Hashin and Puck criteria in σ_{bb} - σ_{ab}

space.

5. FAILURE CRITERIA MODIFICATIONS

In this chapter modifications of the failure initiation criteria, that were described in chapter 4, are proposed. The modified criteria are associated with the 6p theory with asymmetric in-plane shear stress.

The failure initiation criteria, considered in chapter 4 are formulated, assuming the classical symmetry of stress measures. The 6p theory and the material law discussed in chapter 3 are formulated with asymmetric measures. Therefore, it is not possible to use the classical criteria versions in 6p theory directly and some modifications need to be introduced. The proposed modifications are original Author's achievement.

It needs also to be mentioned that the used material law does not involve drilling couple stresses and thus they are not introduced into the failure initiation equations. Nevertheless, formulation of a constitutive relation with this stresses is planned in further research, as well, as consequent modifications of failure initiation criteria that meet the requirements of the planned law.

In order to make the modifications easy to follow the τ_{ab} symbol is used in the case when symmetric in-plane shear components is discussed. The asymmetric components of the 6p theory are in contrary denoted as σ_{ab} and σ_{ba}.

5.1 Modified Tsai-Hill criterion

The Tsai-Hill criterion derivation is repeated to formulate the modification.

The 3D failure condition, according to HMH hypothesis, assuming that there is no shear stress symmetry holds:

$$\left[\left(\sigma_{aa} - \sigma_{bb} \right)^2 + \left(\sigma_{bb} - \sigma_{cc} \right)^2 + \left(\sigma_{cc} - \sigma_{aa} \right)^2 + \right.$$
$$\left. + 3 \left(\sigma_{ab}^2 + \sigma_{ba}^2 + \sigma_{bc}^2 + \sigma_{cb}^2 + \sigma_{ac}^2 + \sigma_{ca}^2 \right) \right] = 2\sigma_0^2 \qquad (5.1)$$

The equation (5.1) is rewritten to enable analysis of orthotropic materials, as proposed in HILL R. [1950]:

$$H \left(\sigma_{aa} - \sigma_{bb} \right)^2 + F \left(\sigma_{bb} - \sigma_{cc} \right)^2 + G \left(\sigma_{cc} - \sigma_{aa} \right)^2 +$$
$$+ N \left(\sigma_{ab}^2 + \sigma_{ba}^2 \right) + L \left(\sigma_{bc}^2 + \sigma_{cb}^2 \right) + \left(\sigma_{ac}^2 + \sigma_{ca}^2 \right) = 1 \qquad (5.2)$$

In the case of plane stress, which is used in this work by initial assumption, (5.2) becomes:

$$\left(G+H\right)\sigma_{aa}^2 + \left(F+H\right)\sigma_{bb}^2 - 2H\sigma_{aa}\sigma_{bb} + N\left(\sigma_{ab}^2 + \sigma_{ba}^2\right) = 1. \qquad (5.3)$$

The failure strength parameters $\left(G+H\right)$, $2H$, $\left(F+H\right)$ can be determined similarly as it was shown in subchapter 4.1. In order to establish a new value of N, a pure in-plane shear test ($\sigma_{ab} = \sigma_{ba} = S_l$) is considered in (5.3), which results in the following relation:

$$N\left(S^2 + S^2\right) = 1 \qquad (5.4)$$

and N is determined:

$$N = \frac{1}{2S^2}. \qquad (5.5)$$

It will be shown later in subchapter 6.2, that equal in-plane shear stress components are obtained in such a test for the 6p theory and the associated material law when pure in-plane shear state occurs. Hence the assumption that $\sigma_{ab} = \sigma_{ba} = S_l$ is valid.

Consequently, the Author's modified Tsai-Hill criterion (5.3), including the newly derived failure strength parameter N, becomes:

$$\frac{\sigma_{aa}^2}{X^2} + \frac{\sigma_{bb}^2}{Y^2} - \frac{\sigma_{aa}\sigma_{bb}}{X^2} + \frac{\left(\sigma_{ab}^2 + \sigma_{ba}^2\right)}{2S_l^2} = 1. \qquad (5.6)$$

Equation (4.11) is an effect of the application of the theoretical considerations, that underlie original criterion. While equation (4.11) seems to be straightforward modification of Tsai-Hill criterion, it is not used, from the following reasons.

It may be argued that when one in-plane shear component is greater than the other one, it will lead to failure, since interaction of all stress tensor components is considered in one equation. According to this assumption the final form of modified Tsai-Hill criterion is postulated as:

$$\frac{\sigma_{aa}^2}{X^2} + \frac{\sigma_{bb}^2}{Y^2} - \frac{\sigma_{aa}\sigma_{bb}}{X^2} + \frac{\left[\max\left(|\sigma_{ab}|; |\sigma_{ba}|\right)\right]^2}{S_l^2} = 1, \qquad (5.7)$$

because:

$$\left[\max\left(\left|\sigma_{ab}\right|;\left|\sigma_{ba}\right|\right)\right]^2 \geq \frac{1}{2}\left(\sigma_{ab}^2 + \sigma_{ba}^2\right). \tag{5.8}$$

In effect two failure initiation envelopes are analyzed. One dependent on σ_{ab} and the second one dependant on σ_{ba}. The least favourable case is chosen for the estimation of the initial failure, which is the safest one from the designer's point of view.

Concluding, the classical and modified version of Tsai-Hill criterion are summarized in Tab.5.1

Tab.5.1 Comparison of terms, that define the failure surface in classical and modified Tsai-Hill criterion

The considered term	Classical criterion	Modified criterion
quadratic normal term in *a* direction	$\dfrac{\sigma_{aa}^2}{X^2}$	
quadratic normal term in *b* direction	$\dfrac{\sigma_{bb}^2}{Y^2}$	
Interactive term	$-\dfrac{\sigma_{aa}\sigma_{bb}}{X^2}$	
In-plane shear effects	$\dfrac{\tau_{ab}^2}{S_l^2}$	$\dfrac{\left[\max\left(\left|\sigma_{ab}\right|;\left|\sigma_{ba}\right|\right)\right]^2}{S_l^2}$

5.2 Modified Tsai-Wu criterion

The modified criterion is established from the failure surface proposed in TSAI S.W., WU E.M [1971], assuming that the in-plane shear components are treated as asymmetric, similarly as in the case of Tsai-Hill criterion. In order to keep the derivation clear, it will be conducted in the natural notation instead of the contracted one (see chapter 4.2).

The failure surface of Tsai-Wu criterion in the natural notation is expressed as:

$$F_{ij}\sigma_{ij} + F_{ijkl}\sigma_{ij}\sigma_{kl} = 1 \quad i,j,k,l = 1,2,3. \tag{5.9}$$

It is possible to list 9 linear and 81 quadratic terms of the strength tensor components from (4.14), when $\sigma_{ij} \neq \sigma_{ji}$. Then, according to (TSAI S.W., WU E.M [1971]) some terms are excluded from the failure surface definition (4.14) i.e.:

- all linear terms containing in-plane shear components

- all terms containing interaction of normal and in-plane shear components

- all terms where in-plane shear components are coupled.

In TSAI S.W., WU E.M [1971] it is assumed that $\sigma_{ab} = \sigma_{ba}$, thus the terms representing coupling between shear components that act in the same plane e.g. σ_{ab} and σ_{ba} are retained. Additionally, the terms which are not associated with the plane state of stress are also removed from considerations. In effect the equation for damage onset becomes:

$$F_{aa}\sigma_{aa} + F_{bb}\sigma_{bb} + F_{aaaa}\sigma_{aa}^2 + F_{bbbb}\sigma_{bb}^2 + 2F_{aabb}\sigma_{aa}\sigma_{bb} + $$
$$+ F_{abba}\sigma_{ab}\sigma_{ba} + F_{baab}\sigma_{ba}\sigma_{ab} + F_{abab}\sigma_{ab}^2 + F_{baba}\sigma_{ba}^2 = 1 \tag{5.10}$$

The determination of terms F_{aa}, F_{bb}, F_{aaaa}, F_{bbbb}, F_{aabb} was described in subchapter 4.2 and is also valid here. It is crucial, however, to establish F_{abba}, F_{baab}, F_{abab}, F_{baba}. It can be done basing on (5.10) by the consideration of the pure in-plane shear test similarly as in the modified Tsai-Hill criterion: $\sigma_{ab} = \sigma_{ba} = S_l$. This results in one equation with four unknown parameters:

$$F_{abba}S_l^2 + F_{baab}S_l^2 + F_{abab}S_l^2 + F_{baba}S_l^2 = 1. \tag{5.11}$$

Since it is assumed in the analysis of laminated composites that in-plane shear strengths $S_{12} = S_{21} = S_l$ (see e.g. PUCK A., SCHÜRMANN H. [1998]), it can be assumed that the strength tensor components in (5.11) should also be equal, namely that $F_{1221} = F_{2112} = F_{1212} = F_{2121} = F_l$, hence (by analogy to the minor and major symmetry utilised in some constitutive equations, refer to BELYTSCHKO T., LIU K. W., MORAN B. [2003]):

$$F_l S_l^2 + F_l S_l^2 + F_l S_l^2 + F_l S_l^2 = 1 \quad \Rightarrow \quad F_l = \frac{1}{4S_l^2}. \tag{5.12}$$

Therefore the modified Tsai-Wu criterion (5.10) after some basic manipulation takes the following form:

$$\left(\frac{1}{X_t}-\frac{1}{X_c}\right)\sigma_{aa}+\frac{\sigma_{aa}^2}{X_tX_c}+\left(\frac{1}{Y_t}-\frac{1}{Y_c}\right)\sigma_{bb}+\frac{\sigma_{bb}^2}{Y_tY_c}-\frac{\sigma_{aa}\sigma_{bb}}{\sqrt{X_tX_cY_tY_c}}+$$

$$+\frac{1}{S_l^2}\left(\frac{\sigma_{ab}+\sigma_{ba}}{2}\right)^2=1 \qquad (5.13)$$

Although the equation (5.13) seems to be a natural modification of the Tsai-Wu criterion, it is not exploited further in this work. The version of Tsai-Wu criterion used in the analysis of laminated composites carried out with aid of the 6p theory is:

$$\left(\frac{1}{X_t}-\frac{1}{X_c}\right)\sigma_{aa}+\frac{\sigma_{aa}^2}{X_tX_c}+\left(\frac{1}{Y_t}-\frac{1}{Y_c}\right)\sigma_{bb}+\frac{\sigma_{bb}^2}{Y_tY_c}-\frac{\sigma_{aa}\sigma_{bb}}{\sqrt{X_tX_cY_tY_c}}+$$

$$+\frac{\left[\max\left(|\sigma_{ab}|;|\sigma_{ba}|\right)\right]^2}{S_l^2}=1 \qquad (5.14)$$

The (5.14) modification is chosen instead of (5.13) from the same reasons given in case of (5.7) and (4.11) for the modified Tsai-Hill criterion.

To sum up, the classical and modified version of Tsai-Wu criterion are summarized in Tab.5.2.

Tab.5.2 Comparison of terms, that define the failure surface in classical and modified Tsai-Wu criterion

The considered term	Classical criterion	Modified criterion
Linear normal term in a direction	$\left(\frac{1}{X_t}-\frac{1}{X_c}\right)\sigma_{aa}$	
Linear normal term in b direction	$\left(\frac{1}{Y_t}-\frac{1}{Y_c}\right)\sigma_{bb}$	
quadratic normal term in a direction	$\frac{1}{X_tX_c}\sigma_{aa}^2$	
quadratic normal term in b direction	$\frac{1}{Y_tY_c}\sigma_{bb}^2$	
Interactive term	$-\frac{1}{\sqrt{X_tX_cY_tY_c}}\sigma_{aa}\sigma_{bb}$	
In-plane shear effects	$\frac{\tau_{ab}^2}{S_l^2}$	$\frac{\left[\max\left(|\sigma_{ab}|;|\sigma_{ba}|\right)\right]^2}{S_l^2}$

For the completeness of this consideration the works are referenced, in which the modifications of the Tsai-Wu criterion are also considered: SOBCZYK B. [2015]; CHRÓŚCIELEWSKI J., WITKOWSKI W., SOBCZYK B., SABIK A. [2015], CHRÓŚCIELEWSKI J., SABIK A., SOBCZYK B., WITKOWSKI W. [2016].

5.3 Modified Hashin criterion

The proposed modification of Hashin criterion, results from the adaptation of the failure mechanism which is described in HASHIN Z. [1980].

The fibre tension failure is initiated by stress tensor components that act on a failure plane, which by assumption remains perpendicular to fibres (HASHIN Z. [1980]). In the case of fibre tension, according to the material law used in this work (see chapter 3), the components σ_{aa} and σ_{ab} influence the plane of failure. Thus, this mode is described by the following equation:

$$\frac{\sigma_{aa}^2}{X_t^2} + \frac{\sigma_{ab}^2}{S_l^2} = 1 \quad \text{for } \sigma_{aa} \geq 0 \,. \tag{5.15}$$

Since there is no in-plane shear influence on the failure initiation for fibre compression, according to HASHIN Z. [1980], this mode does not have to be modified and it remains the same as the classical one, viz.:

$$\frac{\sigma_{aa}^2}{X_c^2} = 1 \qquad \text{for } \sigma_{aa} < 0 \,. \tag{5.16}$$

HASHIN Z. [1980] assumes, that the criterion for matrix failure modes is developed basing on the concepts of failure planes and stress invariants (see chapter 4.3 for details). In effect all available stress tensor components, excluding σ_{aa}, are collected into quadratic criterion. Thus, in the case of the plane stress and within the material law considered in this work σ_{bb}, σ_{ba}, σ_{ab} can be used in the description of matrix damage in tension and compression. However, the σ_{ab} in-plane shear component (refer to Fig. 3.5) does not act on the possible matrix failure plane. It may produce cracks which are perpendicular to fibres and therefore is associated with the fibre failure plane. Hence, only σ_{bb} and σ_{ba} stress tensor components are used to define matrix failure surface in the modified criterion. Owing to the findings given above, the symmetric in-plane shear τ_{ab} in the classical

criterion is replaced by the asymmetric σ_{ba} one. Therefore, the modified Hashin criterion becomes as follows:

$$\frac{\sigma_{bb}^2}{Y_t^2} + \frac{\sigma_{ba}^2}{S_l^2} = 1 \qquad \text{for } \sigma_{bb} \geq 0, \tag{5.17}$$

$$\left(\frac{\sigma_{bb}}{2S_t}\right)^2 + \left[\left(\frac{Y_c}{2S_t}\right)^2 - 1\right]\frac{\sigma_{bb}}{Y_c} + \left(\frac{\sigma_{ba}}{S_l}\right)^2 = 1 \qquad \text{for } \sigma_{bb} < 0. \tag{5.18}$$

Finally, the differences between classical and modified Hashin criteria are collected in Tab.5.3.

Tab.5.3 The differences between classical and modified Hashin criterion

Mode of failure	Standard criterion	Modified criterion
Fibre tension $\sigma_{aa} \geq 0$	$\left(\dfrac{\sigma_{aa}}{X_t}\right)^2 + \left(\dfrac{\tau_{ab}}{S_l}\right)^2$	$\left(\dfrac{\sigma_{aa}}{X_t}\right)^2 + \left(\dfrac{\sigma_{ab}}{S_l}\right)^2$
Fibre compression $\sigma_{aa} < 0$	$\left(\dfrac{\sigma_{aa}}{X_c}\right)^2$	
Matrix tension $\sigma_{bb} \geq 0$	$\left(\dfrac{\sigma_{bb}}{Y_t}\right)^2 + \left(\dfrac{\tau_{ab}}{S_l}\right)^2$	$\left(\dfrac{\sigma_{bb}}{Y_t}\right)^2 + \left(\dfrac{\sigma_{ba}}{S_l}\right)^2$
Matrix compression $\sigma_{bb} < 0$	$\left(\dfrac{\sigma_{bb}}{2S_t}\right)^2 + \left[\left(\dfrac{Y_c}{2S_t}\right)^2 - 1\right]\dfrac{\sigma_{bb}}{Y_c} + \left(\dfrac{\tau_{ab}}{S_l}\right)^2$	$\left(\dfrac{\sigma_{bb}}{2S_t}\right)^2 + \left[\left(\dfrac{Y_c}{2S_t}\right)^2 - 1\right]\dfrac{\sigma_{bb}}{Y_c} + \left(\dfrac{\sigma_{ba}}{S_l}\right)^2$

The modifications of the Hashin criterion are also used in: SOBCZYK B. [2015] and CHRÓŚCIELEWSKI J., SABIK A., SOBCZYK B., WITKOWSKI W. [2016].

5.4 Modified Puck criterion

The Puck criterion in its classical variant is the only one in which the in-plane shear stress components are distinguished, despite their assumed symmetry. In effect, the failure surface equations describing classical plane stress IFF criteria contain in fact $\sigma_{ba} = \tau_{ab}$

component. This results from the mechanics of IFF phenomenon. The σ_{ba} component (not σ_{ab}) acts on the plane, which is parallel to fibres and can initiate development of IFF.

Therefore, additional modifications of Puck criterion regarding 6p theory are not formally required. However, it needs to be emphasized that the application of the Puck criterion in 6p theory may lead to different IFF predictions, because the asymmetric in-plane shear component σ_{ba}, may differ, as compared with the symmetric τ_{ab} one. This may also affect the predicted mode of failure, because the range of validity of B and C modes is dependent on the value of in-plane shear. Therefore it is appropriate to speak about modified Puck criterion, regarding application to 6p theory. This difference is shown in Tab.5.4.

Tab.5.4 The differences between classical and modified Puck criterion

IFF	Standard criterion	Modified criterion
IFF, A	$\dfrac{1}{\eta_{w1}}\left(\sqrt{\left(1-p_{\perp\parallel}^{(+)}\dfrac{Y_T}{S_l}\right)^2\left(\dfrac{\sigma_{bb}}{Y_T}\right)^2+\left(\dfrac{\tau_{ab}}{S_l}\right)^2} + \dfrac{p_{\perp\parallel}^{(+)}}{S_l}\sigma_{bb}\right)=1$	$\dfrac{1}{\eta_{w1}}\left(\sqrt{\left(1-p_{\perp\parallel}^{(+)}\dfrac{Y_T}{S_l}\right)^2\left(\dfrac{\sigma_{bb}}{Y_T}\right)^2+\left(\dfrac{\sigma_{ba}}{S_l}\right)^2} + \dfrac{p_{\perp\parallel}^{(+)}}{S_l}\sigma_{bb}\right)=1$
IFF, B	$\dfrac{1}{\eta_{w1}}\dfrac{1}{S_l}\left(\sqrt{\tau_{ab}^2+\left(p_{\perp\parallel}^{(-)}\sigma_{bb}\right)^2}+p_{\perp\parallel}^{(-)}\sigma_{bb}\right)=1$	$\dfrac{1}{\eta_{w1}}\dfrac{1}{S_l}\left(\sqrt{\sigma_{ba}^2+\left(p_{\perp\parallel}^{(-)}\sigma_{bb}\right)^2}+p_{\perp\parallel}^{(-)}\sigma_{bb}\right)=1$
IFF, C	$\dfrac{1}{\eta_{w1}}\left[\left(\dfrac{\tau_{ab}}{2\left(1+p_{\perp\perp}^{(-)}\right)S_l}\right)^2+\left(\dfrac{\sigma_{bb}}{Y_c}\right)^2\right]\dfrac{Y_c}{\left(-\sigma_{bb}\right)}=1$	$\dfrac{1}{\eta_{w1}}\left[\left(\dfrac{\sigma_{ba}}{2\left(1+p_{\perp\perp}^{(-)}\right)S_l}\right)^2+\left(\dfrac{\sigma_{bb}}{Y_c}\right)^2\right]\dfrac{Y_c}{\left(-\sigma_{bb}\right)}=1$

6. NUMERICAL EXAMPLES

In this chapter selected numerical examples of FPF analyzes are presented. The obtained results are used to justify whether the modified failure initiation criteria, presented in chapter 5, give different damage onset predictions, as compared with the classical ones, described in chapter 4. The calculations are performed with the use of FEM in CAM code and in Abaqus 6.14. The CAM code is operating under the theory and assumptions given in chapter 3. Since the strain and stress measures are asymmetric in CAM, the modified versions of failure initiation criteria are utilised in this code. The FPF estimations determined by modified criteria are compared with the ones resulting from the classical approach. The latter ones are calculated with aid of Abaqus, in which the assumptions of in-plane shear stress symmetry is utilised.

Firstly a case of simply supported plate is investigated in the field of the obtained states of displacement and stress, in order to validate the Author's stress estimation procedure. Then FPF analyzes of plates and shells with and without intersections are performed.

The following finite elements are used in Abaqus calculations: S4, S4R, S8R (see ABAQUS 6.14 manual for details). The S4 shell element has 4 nodes, linear shape functions, full 2×2 Gauss-Legendre in-plane integral rule and some additional procedures preventing against locking effect. The S4R element has also 4 nodes and linear shape functions, however, as opposed to S4, reduced integration with hourglass control is used. The S8R shell element has 8 nodes, quadratic shape functions and the reduced integration rule associated with the in-plane numerical integrals.

Finite elements implemented in CAM are named as CAMen (see CHRÓŚCIELEWSKI J., MAKOWSKI J., STUMPF H. [1992]), where the natural number n indicates the total number of element nodes, namely 4 (2×2), 9 (3×3) or 16 (4×4). The Gauss-Legendre rule with uniformly reduced (URI) or full (FI) integration is used for the purpose of numerical integration in these elements.

All the finite element meshes, which were created for the purpose of FPF analyzes in this chapter, were checked in the field of results convergence. Therefore discussion about this problem is omitted within the text.

6.1 Stress analysis of simply supported plate

The CAM code in the version presented in the work CHRÓŚCIELEWSKI J., KREJA I., SABIK A., WITKOWSKI W. [2011] does not support the analysis of stress state in each lamina. This feature was added in this PhD thesis by the Author in order to make FPF calculations possible. Since it is a new routine of the CAM code a short analysis of a simply supported plate is performed to check the stress predictions. The stress tensor components, which are used in failure initiation criteria equations, are examined along the plate diagonal in external fibres of the plate. Over-the-thickness stress distributions in the corner and centre of the plate are verified as well.

The analytical linear Navier solution of laminated simply supported, rectangular, symmetric, cross-ply plates subjected to uniformly distributed vertical load is implemented in Scilab following REDDY J. N. [2004] and consequently two different plates are analyzed.

The first one, [0/90/0] plate, is presented in Fig. 6.1. The reference values of such an analysis available in REDDY J. N. [2004] are compared with the analytical Author's Scilab procedure and the Author's FEM calculations.
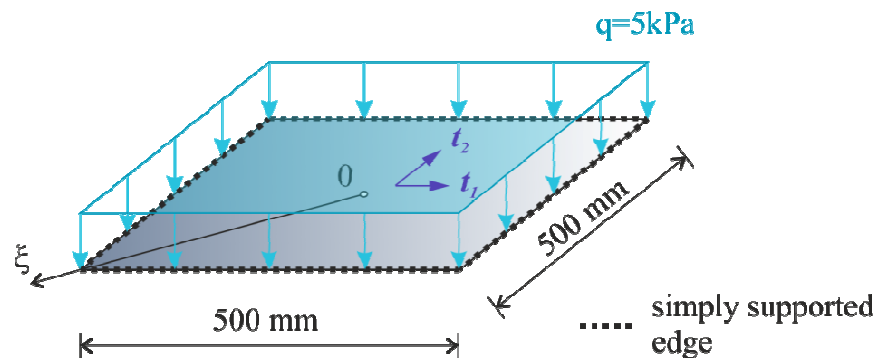
Fig. 6.1 Properties of the [0/90/0] laminated plate

Each lamina of the plate is 1.667mm thick and has the following material properties: $E_a = 25\text{GPa}$, $E_b = 1\text{GPa}$, $G_{ab} = G_{ac} = 0.5\text{GPa}$, $G_{bc} = 0.2\text{GPa}$, $v_{ab} = 0.25$.

The numerical calculations in CAM are performed with aid of CAMe16FI shell elements, whereas S4 shell element is utilised in ABAQUS. A structured (regular) mesh of finite elements is generated and comprises of 225 nodes in both cases. The considered stress results are monitored in each layer in three points with respect to the thickness coordinate, namely in external and middle locations.

The results of maximal displacements and stresses[7] are compared in Tab. 6.1.

Tab. 6.1 Comparison of results of extreme displacements and stresses

Variable and its location	REDDY J. N. [2004] analytical	Author's present		
		analytical	CAM	ABAQUS
Vertical displacement in the plate centre [mm]	16.741	16.742	16.774	16.776
σ_{aa} stress in the bottom layer in the plate centre [MPa]	40.358	40.352	40.350	40.322
In-plane shear stress in the bottom layer in the plate corner [MPa]	$\tau_{ab} = 2.130$	$\tau_{ab} = 2.130$	$\sigma_{ab} = 2.147$ $\sigma_{ba} = 2.118$	$\tau_{ab} = 2.117$

All the results are in good correspondence. The analytical Author's solutions are positively verified in the plate centre and corner with the available reference REDDY J. N. [2004] results. The reference REDDY J. N. [2004] solution is given only for a limited number of points. Therefore, in order to extensively verify the state of stress, which is crucial for the failure initiation criteria predictions, the Author's Scilab procedure is used to analyze the state of stress, occurring along the plate diagonal.

A chart of σ_{aa} stress in the top layer obtained along the plate diagonal ξ (see Fig. 6.1) is shown in Fig. 6.2. Similar graph is created for σ_{bb} and in-plane shear stress components. These are shown correspondingly in Fig. 6.3 and Fig. 6.4. The values of stresses from Abaqus are read in nodes, while the corresponding CAM values are checked in the finite element surface integration points.

---

[7] It is recalled here that the symmetric in-plane shear component is denoted with τ_{ab} while the asymmetric ones are expressed by σ_{ab} and σ_{ba} symbols. This convention is introduced in chapter 5 to make classical and modified criteria results easier to distinct.
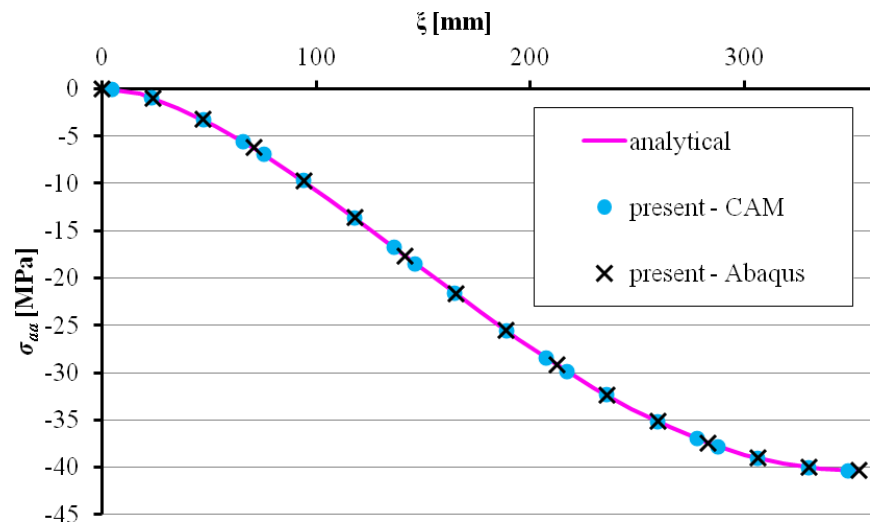
Fig. 6.2 σ_{aa} stress distributions in the top layer obtained on the plate diagonal
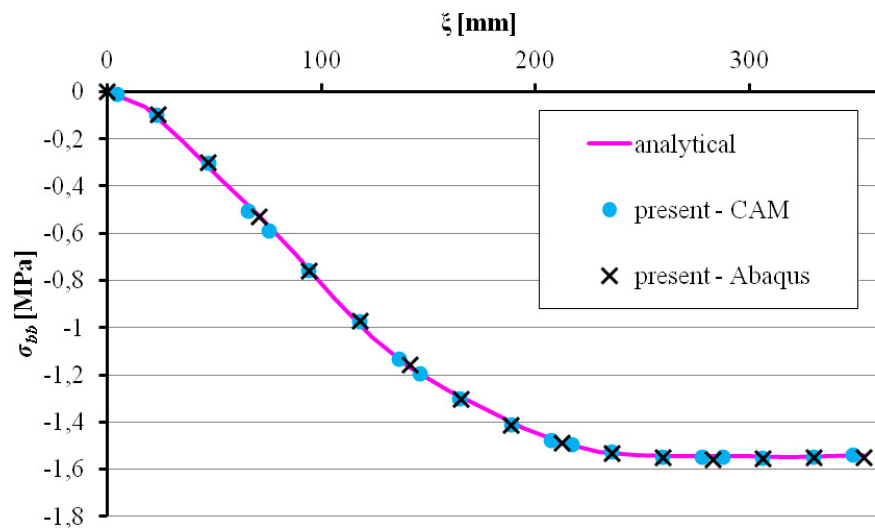
Fig. 6.3 σ_{bb} stress distributions in the top layer obtained on the plate diagonal
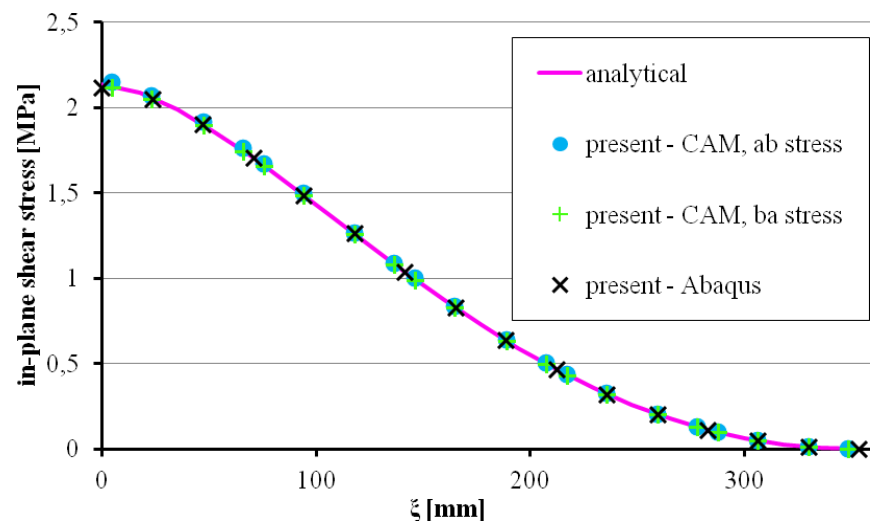
Fig. 6.4 In-plane shear stress distributions in the top layer obtained on the plate diagonal

The state of stress predicted by CAM is nearly the same as the Author's analytical solution and the numerical Abaqus one as well.

The over-the-thickness stress distributions, including the Author's analytical and numerical calculations, are examined for the second simply supported plate, having [0/90/0/90/0] lamination scheme, which is shown in Fig. 6.5.
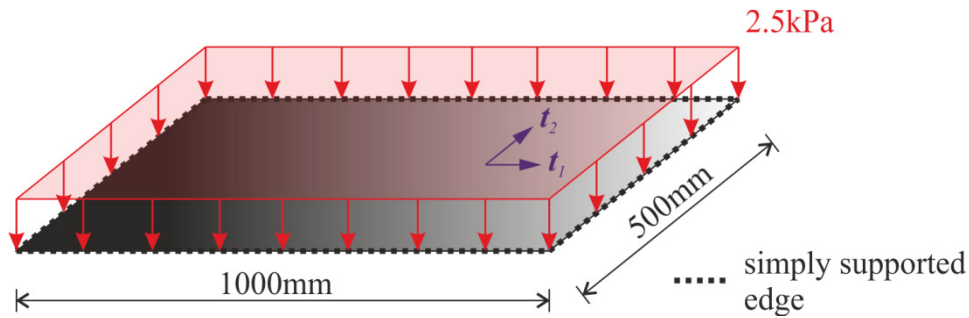
Fig. 6.5 Properties of the [0/90/0/90/0] laminated plate

Each lamina of the plate is 1mm thick, while its elastic properties are the same as in the analysis of the first plate.

The FEM models utilize the same types of finite elements as in the previous analysis. A regular mesh is created, that contains 496 nodes in both cases.

The stress σ_{aa} and σ_{bb} values obtained in numerical calculations are probed in the shell surface integration points adjacent to the plate centre, while the analytical values are read precisely in the plate centre. The numerical in-plane shear stress values are checked in the shell surface integration points adjacent to the plate corner, whereas the analytical ones are read exactly in the plate corner. A plot of the thickness coordinate versus σ_{aa} stress in the middle of the plate is shown in Fig. 6.6. A chart of thickness coordinate versus σ_{bb} stress in the middle of the plate is shown in Fig. 6.7. Thickness coordinate versus in-plane shear stress relation calculated in the plate corner is shown in Fig. 6.8.

It is emphasized here, that the transverse shear stress distribution are not presented here, because these components are not the subject of the analysis in this work, since they are not included in the failure initiation criteria considered in the thesis.

All the over the thickness stress distributions are in very good agreement.
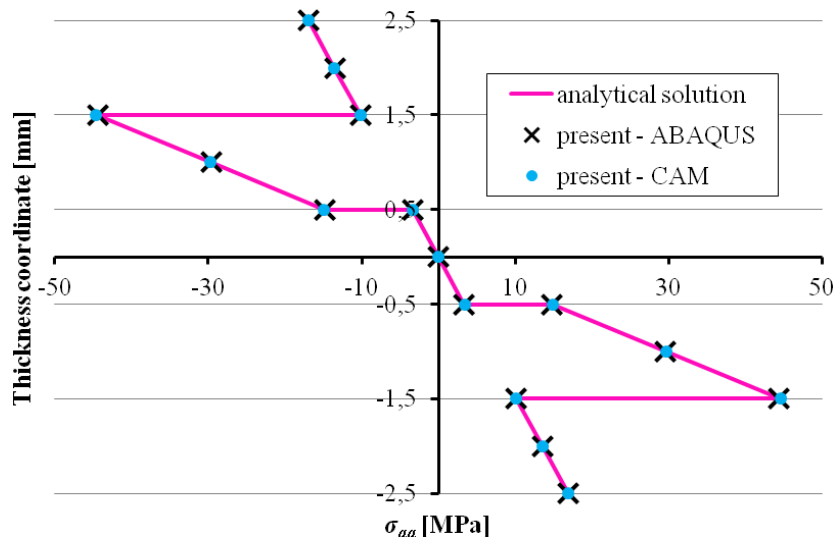
Fig. 6.6 Thickness coordinate versus σ_{aa} stress checked in the middle of the plate
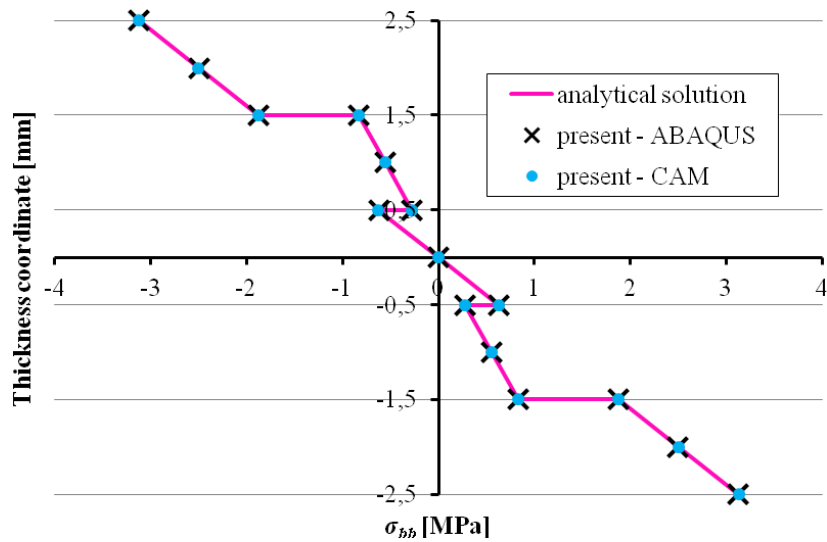
Fig. 6.7 Thickness coordinate versus σ_{bb} stress checked in the middle of the plate
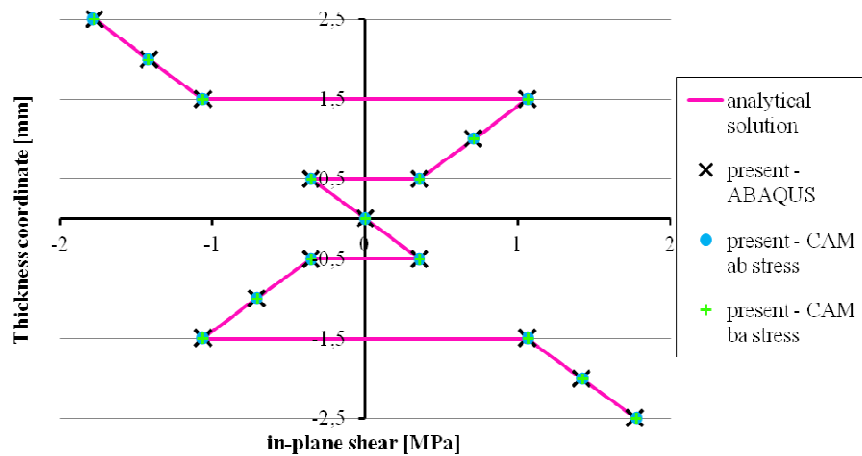
Fig. 6.8 Thickness coordinate versus in-plane shear stress checked in the plate corner

6.2 Pure shear test

The problem discussed here intends to verify if it is possible to obtain symmetric in-plane shear stress components under pure shear, when 6p theory is used. If it is true it means that the $\sigma_{ab} = \sigma_{ba} = S_l$ assumption, made during the Tsai-Hill and Tsai-Wu criteria modifications in chapters 5.1 and 5.2, is valid. What is more, this would suggest that the modified and classical criteria will give very similar damage onset prediction for the states which are close to the pure in-plane shear. This original example was proposed and analyzed in CHRÓŚCIELEWSKI J., SABIK A., SOBCZYK B., WITKOWSKI W. [2016].

Linear static calculations of a 2D, one-layer, square plate simulating membrane behaviour are performed. The dimensions, surface coordinate system (t_1-t_2), loads and boundary conditions (BCs) of the membrane are shown in Fig. 6.9.
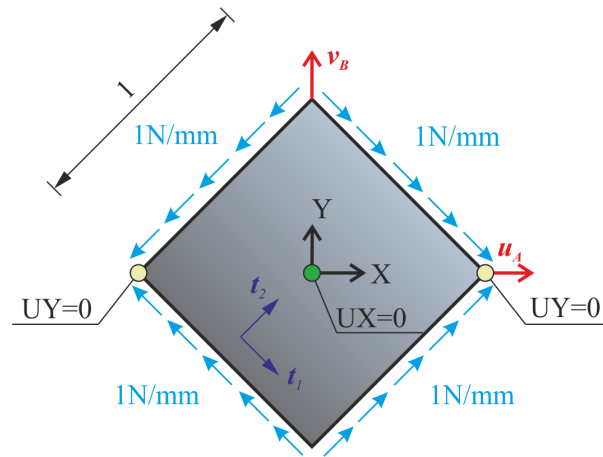
Fig. 6.9 Geometry, surface coordinate system, loads and BCs of the plate

The lamina material properties are: $E_a = 45.0$ GPa, $E_b = 12.5$ GPa, $G_{ab} = G_{ac} = 5.5$ GPa, $G_{bc} = 3.6$ GPa, $v_{ab} = 0.28$. The membrane is 0.01mm thick and has [0] stacking sequence.

The numerical model, pertaining to geometry presented in Fig. 6.9, is constructed with CAMe4FI or S4 elements. The 12×12 structured mesh is used in both cases. Additionally, higher order elements, namely CAMe9FI (6×6 mesh) and CAMe16FI (4×4 mesh) are also used in this study in CAM calculations. This is because low order Lagrange finite elements may be susceptible to the locking effect.

The state of pure shear is successfully recreated in the course of the analysis in all the considered cases. None of the numerical model revealed any sign of the locking effect. The following values of displacements (see Fig. 6.9) were obtained during all FEA:

$u_A = 6.428 \cdot 10^{-3}\,\text{mm}$ $v_B = -6.428 \cdot 10^{-3}\,\text{mm}$. The comparison of displacement magnitudes obtained in S4 and CAMe4FI computations is portrayed in Fig. 6.10.
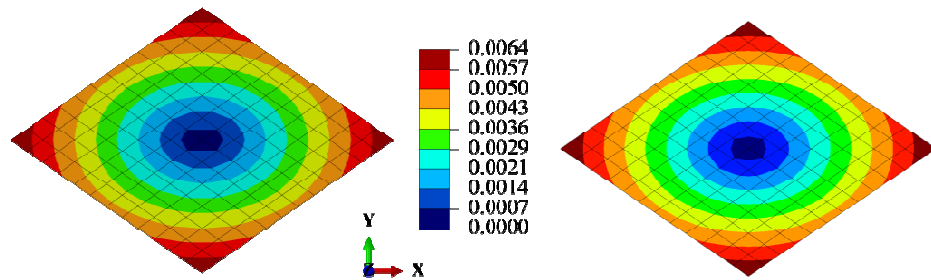
Fig. 6.10. Displacement magnitudes contours (scaled 20 times): S4 (left) and CAMe4FI (right)

As far as the stress state is concerned, the normal components are zeros in both codes for all finite elements under consideration. The drilling couples, available in the 6p theory in CAM are zeros as well and the in-plane shear components obtained in Abaqus and CAM are: $\tau_{ab} = \sigma_{ab} = \sigma_{ba} = -100\,\text{MPa}$. Such a numerical prediction corresponds perfectly with the analytical value.

Therefore it is found that the initial assumption is true and that the damage onset predictions for classical and modified criteria will be similar, when the pure shear occurs.

6.3   Cylindrical panels

Cylindrical panels subjected to uniformly distributed vertical load, with geometry defined via R/b ratio, as shown in Fig. 6.11, are analyzed in order to find load intensity q_{FPF} leading to the onset of damage.
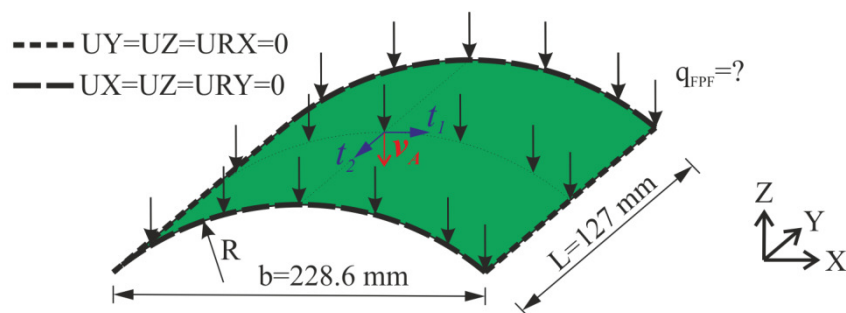
Fig. 6.11. The cylindrical panel - geometry, surface coordinate system, loads and BCs

Each panel is built of laminas, which are endowed with the following elastic and strength parameters: $E_a = 132.4\,\text{GPa}$, $E_b = 10.7\,\text{GPa}$, $G_{ab} = G_{ac} = 5.6\,\text{GPa}$, $G_{bc} = 3.4\,\text{GPa}$,

$v_{ab} = 0.24$, $\quad X_t = 1514$ MPa, $\quad X_c = 1696.7$ MPa, $\quad Y_t = 43.8$ MPa, $\quad Y_c = 43.8$ MPa, $S_l = 87$ MPa. The ply thickness is 0.127 mm.

This example is motivated by the static linear analysis of the plate, described in REDDY J. N., PANDEY A. K. [1987], which was extended by others. For instance PRUSTY B. G., SATSANGI S. K., RAY C. [2001] determined FPF loads of the panel for chosen R/b ratios and stacking sequences, using shell elements. Similar analyses were performed by RATTANAWANGCHAROEN N. [2005], however for numerical models built of solid finite elements. CHRÓŚCIELEWSKI J., SABIK A., SOBCZYK B., WITKOWSKI W. [2016] compared FPF loads obtained with aid of standard and Tsai-Wu modified criterion for shell panels with [0/90]$_s$ layup.

In this work, at first, the results from PRUSTY B. G., SATSANGI S. K., RAY C. [2001] and RATTANAWANGCHAROEN N. [2005] are examined for [45/−45/0/90/45/0/−45/90]$_s$ lamination sequence and geometries with R/b equal to 100, 1000 and plate ($R = \infty$). Linear static calculations are performed, following PRUSTY B. G., SATSANGI S. K., RAY C. [2001], in CAM and ABAQUS in order to estimate initial failure for the modified and classical Tsai-Hill and Tsai-Wu criteria.

Numerical models built here are similar to the one presented in PRUSTY B. G., SATSANGI S. K., RAY C. [2001]. A 8×8 mesh is created and shell elements are utilised: S8R in Abaqus and CAMe9FI in CAM. The failure indices are checked in points, which location results from the applied in-plane integration rule and top middle and bottom location within each layer in shell thickness direction[8], as it is shown in Fig. 6.12.
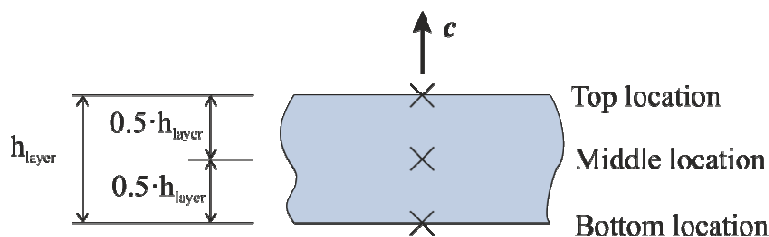
Fig. 6.12. Location of results points in the thickness direction in each lamina.

The q$_{FPF}$ loads calculated with aid of Tsai-Wu criterion are collected in Tab. 6.2. According to the Author's numerical calculations FPF occurs in external layers (top for R/b=1000 and plate, bottom for R/b=100) in the Gauss point lying closest to the panel

---

[8] Such an approach is used in all subsequent FEA, whenever element results are compared.

corner in both codes (CAM and ABAQUS). The location of FPF is neither given in PRUSTY B. G., SATSANGI S. K., RAY C. [2001] nor in RATTANAWANGCHAROEN N. [2005]. The failure indices obtained for the Author's classical and modified Tsai-Wu criterion are shown in Fig. 6.13 for R/b=100. Almost the same patterns are observed for the remaining R/b ratios under consideration.

Tab. 6.2 q_{FPF} loads [kPa] calculated with aid of Tsai-Wu criterion

R/b	PRUSTY B. G., ET AL. [2001] - classical criterion	RATTANAWANGCHAROEN N. [2005] - classical criterion	Abaqus - classical criterion	CAM - modified criterion
100	147.5	136.2	134.0	127.4
1000	146.6	136.9	134.6	127.8
plate R = ∞	146.2	136.8	133.9	127.3

a)   b)
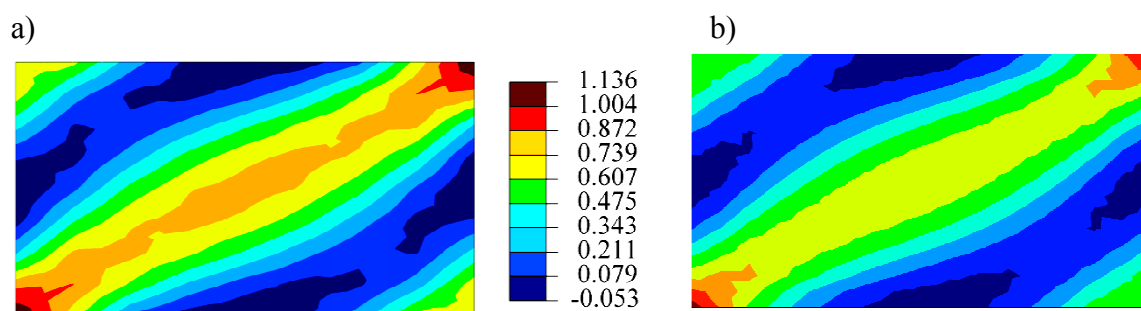
Fig. 6.13. Tsai-Wu failure indices for the cylindrical panel, R/b=100, bottom layer, classical criterion - Abaqus (a), modified criterion - CAM (b)

The difference between the Tsai-Wu failure loads for the Abaqus and CAM results is caused by the location in which the failure indices are read. Since FI scheme is used in CAM, the in-plane integration point lies closer to the panel corner as compared with the one resulting from reduced integration rule in Abaqus. Thus, some small discrepancies between the stress states are observed. The contours of all the stress tensor components included in the classical and modified failure initiation equations are shown in Fig. 6.14÷Fig. 6.17.

The failure is driven mainly by σ_{bb} component, because of low Y strength values. Therefore, the failure indices are sensitive to even small changes of σ_{bb}. It should be also mentioned that the asymmetry of in-plane shear observed for the 6p theory (CAM code) is minor.
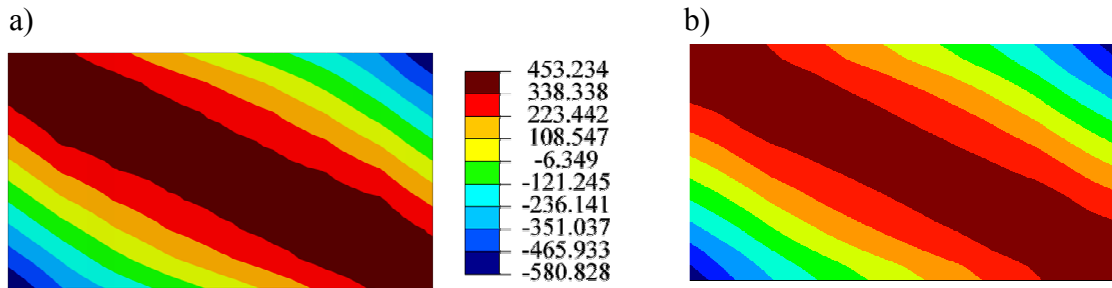
a)   b)

Fig. 6.14. Contours of σ_{aa} stresses, R/b=100, the bottom layer, Abaqus (a), CAM (b)

a)   b)
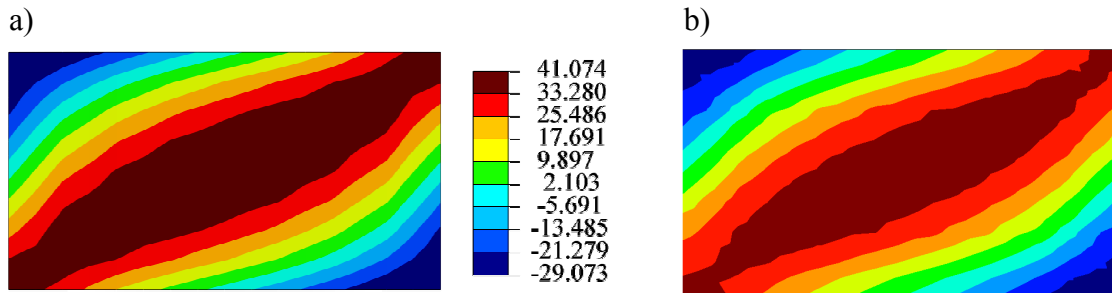

Fig. 6.15. Contours of σ_{bb} stresses, R/b=100, the bottom layer, Abaqus (a), CAM (b)
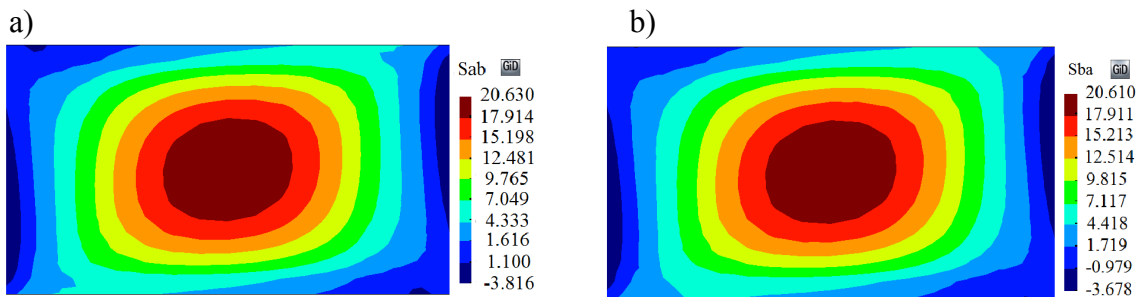
a)   b)

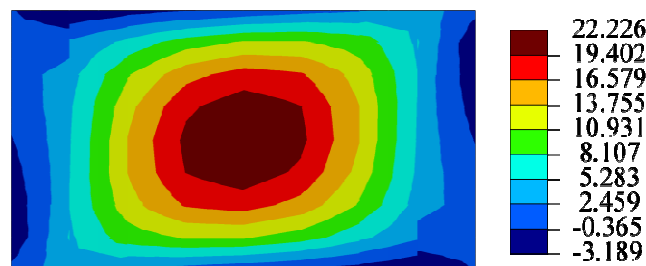Fig. 6.16. Contours of in-plane shear stresses, 6p theory (CAM), R/b=100, the bottom layer, σ_{ab} (a),

σ_{ba} (b)

Fig. 6.17. Contours of τ_{ab} in-plane shear stresses, 5p theory (Abaqus), R/b=100, the bottom layer.

The Author's Abaqus and CAM results, gathered in Tab. 6.2, are comparable with the solution obtained by RATTANAWANGCHAROEN N. [2005]. The Author's and RATTANAWANGCHAROEN N. [2005] failure loads are lower than the ones published in PRUSTY B. G., SATSANGI S. K., RAY C. [2001]. This can be attributed to the fact that the failure indices in Author's calculations (Abaqus and CAM codes) are checked in three

points within each layer (top, middle and bottom location - Fig. 6.**12**). RATTANAWANGCHAROEN N. [2005] used solid finite elements, hence he also could check the indices in the top and bottom location of a lamina, therefore the results are similar. The q_{FPF} loads published by PRUSTY B. G., SATSANGI S. K., RAY C. [2001] seem to be read only in the middle of the layer, as it is made by REDDY J. N., PANDEY A. K. [1987]. Comparable values were obtained by the Author, when the top and bottom location results were omitted. Similar conclusions are raised in CHRÓŚCIELEWSKI J., SABIK A., SOBCZYK B., WITKOWSKI W. [2016].

The FPF analysis using Tsai-Hill criterion led to the q_{FPF} loads presented in Tab. 6.3.

Tab. 6.3 q_{FPF} loads [kPa] calculated with aid of Tsai-Hill criterion

R/b	PRUSTY B. G., ET AL. [2001] - classical criterion	RATTANAWANGCHAROEN N. [2005] - classical criterion	Abaqus - classical criterion	CAM - modified criterion
100	50.0	131.8	129.8	130.1
1000	51.3	134.2	132.2	131.9
plate R = ∞	51.5	133.9	131.8	131.6

The Author's CAM and Abaqus Tsai-Hill FPF loads (Tab. 6.3) are almost identical. The damage initiation is observed in the external layers (top for R/b=1000 and 100, bottom for R/b=plate) in the middle of the panel in both codes (see Fig. 6.18). The indices contours for the remaining R/b ratios under consideration look nearly the same. The failure initiation location is not described in the reference works.
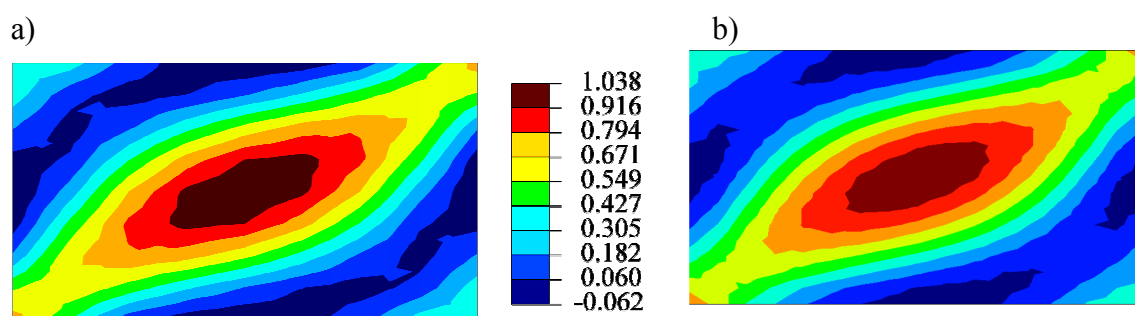
a)   b)

Fig. 6.18. Tsai-Wu failure indices for the cylindrical panel, R/b=100, bottom layer, classical criterion - Abaqus (a), modified criterion - CAM (b)

The stress states predicted by the 5p theory and the 6p one are pretty much the same in the area of damage initiation (e.g. refer to the contours presented in Fig. 6.14 ÷ Fig.

6.17), with negligible asymmetry of in-plane shear components according to the 6p theory. The Author's Abaqus and CAM results are very close to the reference RATTANAWANGCHAROEN N. [2005] solution. This shows that the ESL approach, used here, is sufficient enough to recreate behaviour of the panel and predict failure initiation and application of more precise modelling, e.g. 3D formulation can be avoided.

The difference between the aforementioned results and the PRUSTY B. G., SATSANGI S. K., RAY C. [2001] solution is attributed to the different form of Tsai-Hill failure equation used in the reference work. The Tsai-Hill equation utilised by PRUSTY B. G., SATSANGI S. K., RAY C. [2001] is not commonly used and seems not to be appropriate in view of the information given in TUTTLE M. E. [2004]. This problem was described in details in chapter (4.8). Therefore FPF predictions given by PRUSTY B. G., SATSANGI S. K., RAY C. [2001] are not treated as the reference ones to formulate any further conclusions about Tsai-Hill criterion.

The research conducted up to this point was motivated by the works PRUSTY B. G., SATSANGI S. K., RAY C. [2001] AND RATTANAWANGCHAROEN N. [2005], where linear calculations were carried out. Nevertheless, the Author's nonlinear calculations revealed that the response of the cylindrical panels under consideration is geometrically nonlinear, which may affect FPF predictions.

Therefore, some new results are presented here. Geometrically nonlinear calculations are performed for the R/b=100 panel with aid of numerical models with fine meshes, having 589 nodes in both codes. They comprise of: 30×18 S4 elements in Abaqus and 10×6 CAMe16FI elements in CAM. Only one panel is considered, since the response of the two remaining ones turned out to be similar in the field of the shape of equilibrium paths and failure indices distribution patterns. In the case of nonlinear calculations classical and modified versions of Tsai-Hill, Tsai-Wu, Hashin and Puck criteria are used to estimate the onset of damage.

The relation between vertical load intensity and v_A displacement (see Fig. 6.11) for the R/b=100 panel is shown in Fig. 6.19. The calculated responses of the shell are almost equal.
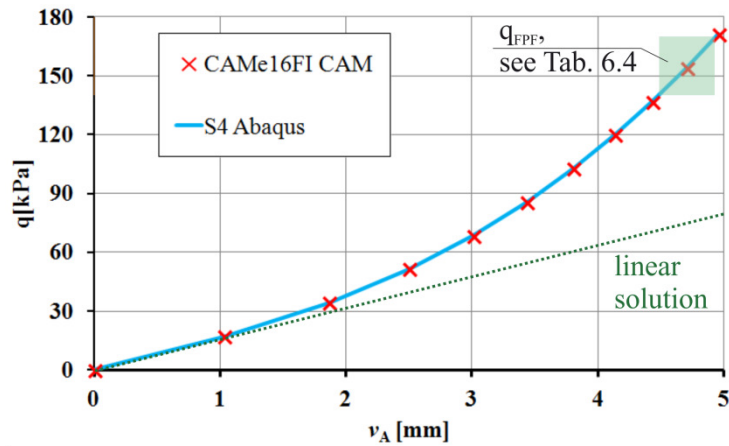
Fig. 6.19. Vertical load intensity vs. v_A displacement for the R/b=100 cylindrical panel

The q_{FPF} loads obtained by means of Tsai-Wu, Tsai-Hill, Hashin and Puck classical and modified criteria are collected in Tab. 6.4. The locations of initial damage that occurred for the considered criteria are shown in Fig. 6.20.

Tab. 6.4 Uniformly distributed vertical q_{FPF} loads [kPa] calculated by means of Tsai-Wu, Tsai-Hill, Hashin and Puck classical and modified criteria in the case of nonlinear calculations

Criterion type	TSAI-WU	TSAI-HILL	Hashin	Puck
Classical (Abaqus)	145.7	166.5	171.4	171.4
Modified (CAM)	139.4	165.5	171.0	171.0

cl. - classical criterion   mod. - modified criterion
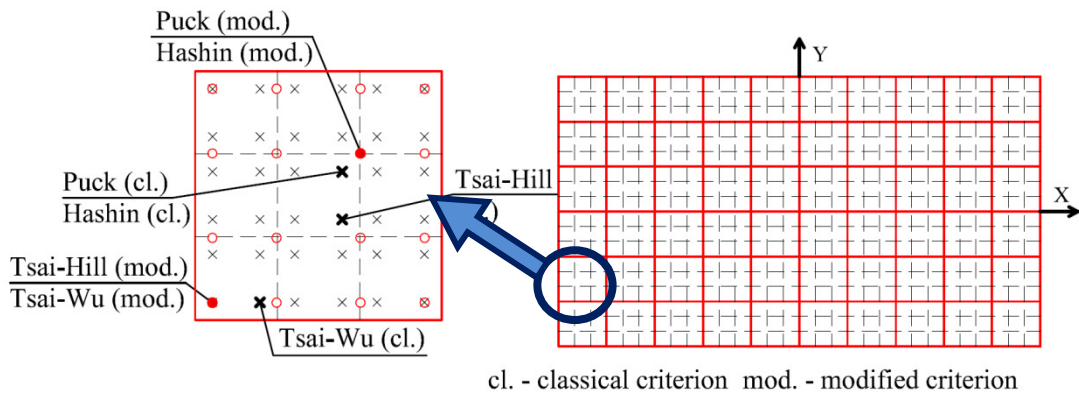
Fig. 6.20. Location of initial damage (in-plane integration points: red circles CAM, black x-marks Abaqus) and the mesh of finite elements: red lines CAMe16FI, black dashed lines S4 Abaqus.

Small discrepancies between the classical and modified Tsai-Wu and Tsai-Hill predictions are observed. These are attributed to slightly different location of FPF. In effect the failure loads are sensitive to small changes of σ_{bb}, as it was described in the case of linear calculations earlier in this chapter. Since the classical and modified Hashin and Puck criteria estimations appear in approximately the same point the differences between them are minor. Nevertheless, it can be said that the q_{FPF} loads are in good agreement. The in-

plane shear stress asymmetry in 6p theory for the modified criteria is low and did not affect damage onset predictions.

To sum up it can be concluded that for the cylindrical panel analyzed by means of linear and nonlinear calculations the FPF loads calculated with either 5 parameter (Abaqus) or 6 parameter shell theory (CAM) are similar. A minor level of in-plane shell asymmetry is observed when 6 parameter shell theory is utilised, which does not affect initial failure estimations.

6.4   Flat rectangular panel subjected to compression

Behaviour of a flat rectangular panel subjected to compression, named in the literature as the C4 panel (see for example REDDY J. N. [2004]), is investigated. Its geometry and properties are shown in Fig. 6.21.
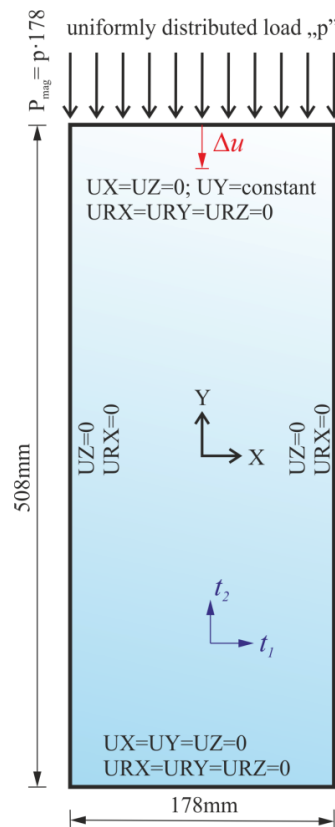
Fig. 6.21. The C4 panel - geometry, surface coordinate system, loads and BCs

It is made of unidirectional plies, each 0.132 mm thick, combined into the sequence [45/−45/90/90/45/−45/90/90/45/−45/90/0]$_s$, having the following elastic and strength characteristics (adapted from KNIGHT JR. N. F., RANKIN C. C., BROGAN F. A. [2002]): $E_a = 131.0$ GPa , $E_b = 13.031$ GPa , $G_{ab} = G_{ac} = 6.205$ GPa , $G_{bc} = 3.447$ GPa , $v_{ab} = 0.38$,

$X_t = 1400$ MPa , $\quad X_c = 1138$ MPa , $\quad Y_t = 80.9$ MPa , $\quad Y_c = 189$ MPa , $\quad S_l = 62.05$ MPa ,

$S_t = 31.03$ MPa .

Response of such a panel was originally experimentally determined by: STARNES J. H., ROUSE M. [1981]: Postbuckling and Failure Characteristics of Selected Flat Rectangular Graphite-Epoxy Plates Loaded in Compression. *AIAA J. Compos. Mater.*, **81**, 423–434. This paper is not available to the Author. Nevertheless, the experiment was studied by other researches, who made FPF and LPF calculations using selected classical failure initiation criteria, see e.g. inter alia, ENGELSTAD S. P., REDDY J. N., KNIGHT JR. N.F. [1992], SLEIGHT D. W. [1999], KNIGHT JR. N. F., RANKIN C. C., BROGAN F. A. [2002]. They also gave information about the geometry and elastic properties of the panel.

Thus, it is possible for the Author of this thesis to perform own analyzes of the C4 panel. The postbuckling response and FPF loads, resulting from the classical and modified criteria considered in chapters 4 and 5, are studied here by means of geometrically nonlinear calculations in CAM and Abaqus. Tsai-Wu and Hashin criteria were used, correspondingly, in ENGELSTAD S. P., REDDY J. N., KNIGHT JR. N.F. [1992] and SLEIGHT D. W. [1999] to estimate FPF, hence this results will be also compared with the Author's ones.

Numerical models, created according to Fig. 6.21, contain 24×48 mesh of S4 elements in Abaqus and 8×16 mesh of CAMe16FI in CAM (1225 nodes in both cases). The $P_{mag} - \Delta u$ equilibrium path of the panel, obtained during the analyzes, is shown in Fig. 6.22.
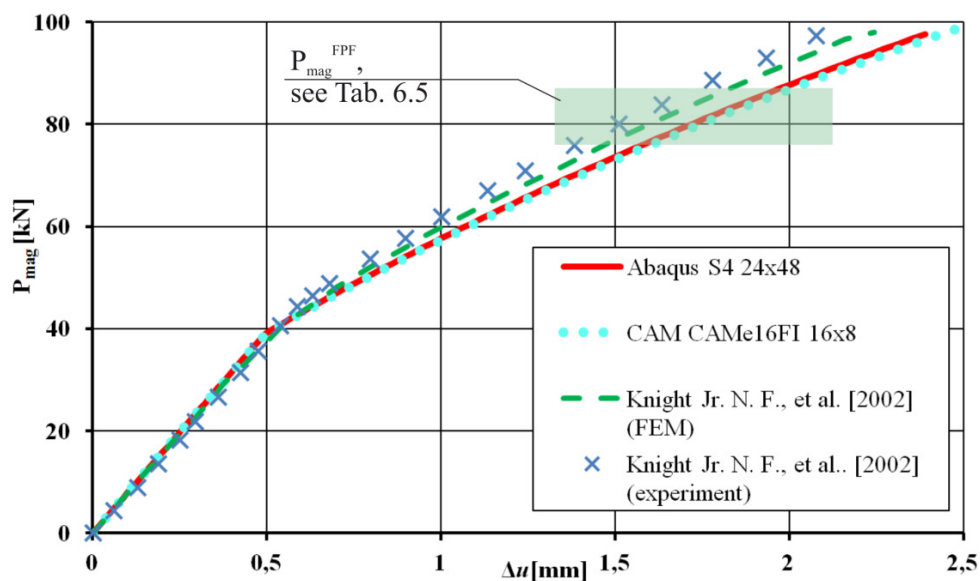

Fig. 6.22. The $P_{mag} - \Delta u$ response of the panel, obtained during the analyzes

The panel buckles into two half-waves along the Y direction and one in the X direction. The buckling loads are: ~39.1kN Abaqus, ~39.0kN CAM. The FPF loads (denoted as P_{mag}^{FPF}) with additional information about the failed layer obtained in the current calculations by means of the classical and modified criteria are shown in Tab. 6.5. Fig. 6.23 depicts the in-plane integration points in which the damage onset is observed.

Tab. 6.5 P_{mag}^{FPF} loads [kN] calculated by means of Tsai-Wu, Tsai-Hill, Hashin and Puck classical and modified criteria for the C4 panel.

Criterion type	Classical criterion (Abaqus)		Modified criterion (Cam)	
	P_{mag}^{FPF}	location	P_{mag}^{FPF}	location
Tsai-Wu	77.15	1 (bottom)	76.2	1 (bottom)
Tsai-Hill	83.0	3 (bottom)	82.0	3 (bottom)
Hashin	86.95	3 (bottom)	85.5	3 (bottom)
Puck	81.5	1 (bottom)	80.5	1 (bottom)
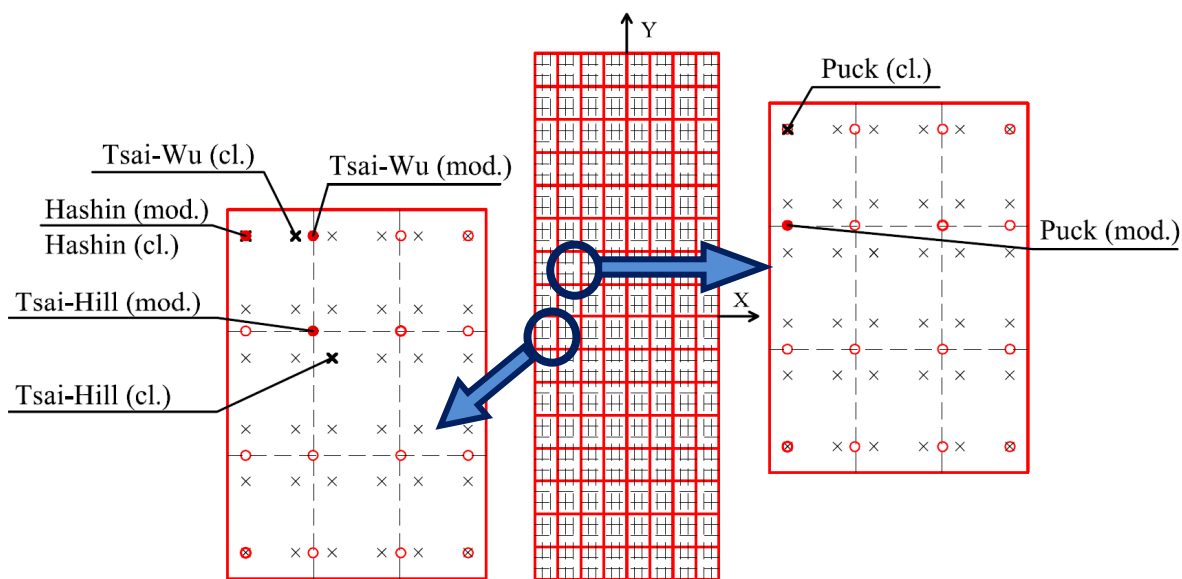
cl. - classical criterion mod. - modified criterion

Fig. 6.23. Location of initial damage (in-plane integration points: red circles CAM, black x-marks Abaqus) and the mesh of finite elements: red lines CAMe16FI, black dashed lines S4 Abaqus.

The failure index contours of Tsai-Wu, Tsai-Hill, Hashin and Puck criteria (classical and modified ones) at the moment of damage onset are shown, accordingly in Fig. 6.24÷Fig. 6.27.
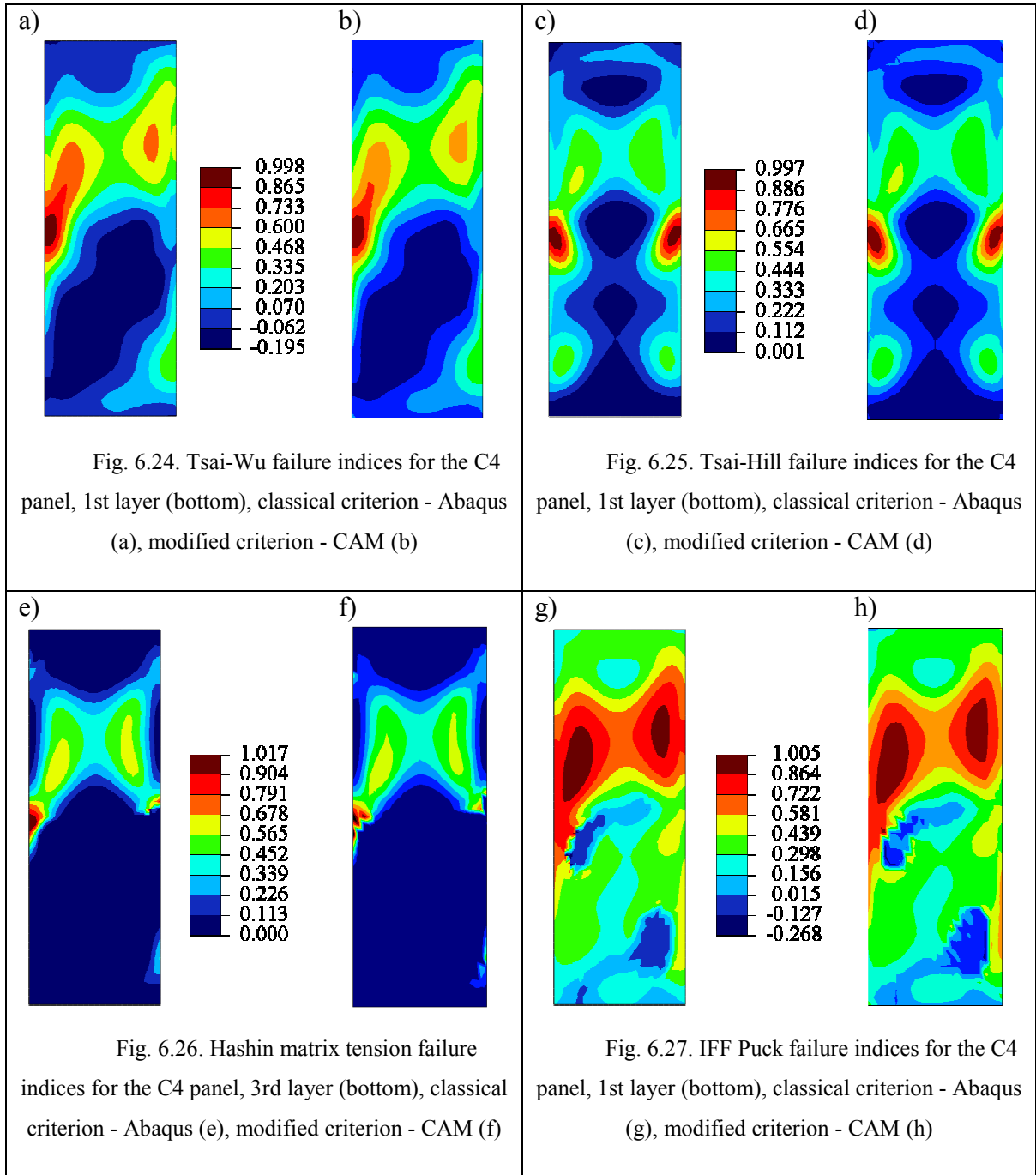
Fig. 6.24. Tsai-Wu failure indices for the C4 panel, 1st layer (bottom), classical criterion - Abaqus (a), modified criterion - CAM (b)

Fig. 6.25. Tsai-Hill failure indices for the C4 panel, 1st layer (bottom), classical criterion - Abaqus (c), modified criterion - CAM (d)

Fig. 6.26. Hashin matrix tension failure indices for the C4 panel, 3rd layer (bottom), classical criterion - Abaqus (e), modified criterion - CAM (f)

Fig. 6.27. IFF Puck failure indices for the C4 panel, 1st layer (bottom), classical criterion - Abaqus (g), modified criterion - CAM (h)

All the results presented above show that there is no big difference between FPF estimations for the C4 panel resulting from the classical and modified criteria. The failure loads, location of initial failure and contours of failure indices are almost the same in all codes. Very low in-plane shear stress asymmetry is observed in CAM (6p theory).

The CAM and Abaqus results are compared with the reference ones. ENGELSTAD S. P., REDDY J. N., KNIGHT JR. N.F. [1992] gave the load value for Tsai-Wu FPF, normalized by the buckling load. It yields ~1.97. The actual predictions are: Abaqus ~1.97, CAM

~1.95 and correspond well with the published value. SLEIGHT D. W. [1999] predicted that the damage initiates, according to Hashin criterion, when $P_{mag}^{FPF} = 96.87kN$. This value is higher than the Author's estimations (classical Abaqus - 86.95kN, modified CAM - 85.5kN). This is a consequence of slightly different strength parameters and properties of the lamina. SLEIGHT D. W. [1999] uses 68.95MPa for the in-plane shear strength and 0.136mm as the ply thickness. If the aforesaid properties proposed by SLEIGHT D. W. [1999] are applied to the current numerical models, then similar failure loads can be obtained.

6.5 Blade-stiffened, partially clamped panel

Almost no significant differences are found in the FPF analyzes of regular shells carried out with aid of the classical and modified criteria proposed in this work. It is expected that some distinctions will appear, when shells with branches or intersections are studied. This is the area to which the 6p theory is especially dedicated (see e.g. CHRÓŚCIELEWSKI J., MAKOWSKI J., PIETRASZKIEWICZ W. [2000]).

Therefore, original study of blade-stiffened, partially clamped panel is conducted. However, the geometry and material parameters are somehow motivated by the work KONG C. W., LEE I. C., KIM C. G., HONG C. S. [1998]. They are modified in order to make the numerical description of the panel easier. The newly proposed geometry, boundary and loading conditions enforce torsion of the blade-stiffener and quite complex deformation of the full panel, which lead to asymmetry of in-plane shear stress components in laminas, which was not observed for the ones described by KONG C. W., LEE I. C., KIM C. G., HONG C. S. [1998]. What is more the new conditions does not cause high hourglassing, when finite elements with ultimate reduced integration are used, which was observed for the KONG C. W., LEE I. C., KIM C. G., HONG C. S. [1998] panel.

The geometry, loads, BCs and surface coordinate systems of the panel are shown in Fig. 6.28.

The lamination scheme of the panel is [0/90/±45]$_s$. It is given with respect to t_1-t_2 system. Each layer (0.131mm thick) has the following elastic and strength properties:

$E_a = 130\,\text{GPa}$, $E_b = 10\,\text{GPa}$, $G_{ab} = G_{ac} = 4.85\,\text{GPa}$, $G_{bc} = 3.62\,\text{GPa}$, $v_{ab} = 0.31$,

$X_t = 1933\,\text{MPa}$, $X_c = 1051\,\text{MPa}$, $Y_t = 51\,\text{MPa}$, $Y_c = 141\,\text{MPa}$, $S_l = 61\,\text{MPa}$,
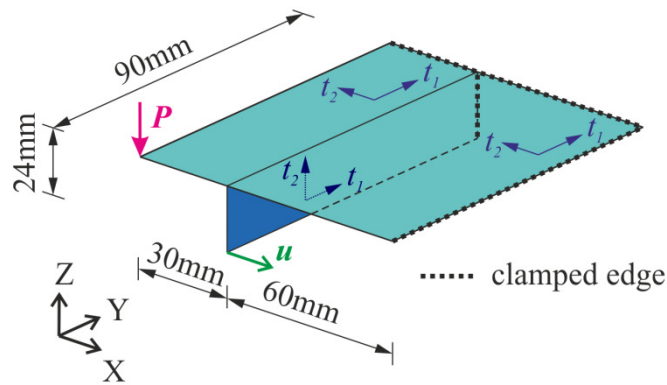
$S_t = 31.03\,\text{MPa}$.

Fig. 6.28. The blade-stiffened, partially clamped panel - geometry, surface coordinate system, loads and BCs

Geometrically nonlinear calculations are performed. It is shown at first that some asymmetry of in-plane shear may arise in the course of nonlinear calculations. Additionally, it is elucidated why only higher order elements with full integration are used in CAM. Finally, the damage onset estimation of the panel is performed.

The same analysis of the panel was carried out in CHRÓŚCIELEWSKI J., SABIK A., SOBCZYK B., WITKOWSKI W. [2016].

The panel is discretized with finite elements, by edge divisions. In Abaqus S4 or S4R elements are used: 15 elements are created across the narrower part of the plate, 12 elements across the stiffener, 30 elements across the wider part of the plate and 45 elements along the panel [this division is denoted as $(15 + 12 + 30) \times 45$]. In CAM either CAMe4URI elements are used with the same divisions as in Abaqus or CAMe16FI elements with $(5 + 4 + 10) \times 15$ mesh. Structured meshes comprising of 2668 nodes are created in all considered mesh variants.

It is intended to check whether it is possible to use similar 4−node elements with reduced integration in Abaqus and CAM, because in such a case interpretation of FPF results would be easier (e.g. the location of in-plane integration points is the same). The CAMe4URI element does not have hourglass control, while the S4R element has. In order to minimize the effect of the hourglass control in S4R, the membrane and bending hourglass stiffness is set to the value of $\gamma = 10^{-9}$, which is the smallest one acceptable in Abaqus. Since results of reduced integration finite elements are susceptible to hourglass modes, they are compared with full integration elements analyzes.

Firstly, the response of the panel is investigated for all mesh variants. The corresponding force - displacement $P-u$ paths are shown in Fig. 6.29. They are in very good agreement.
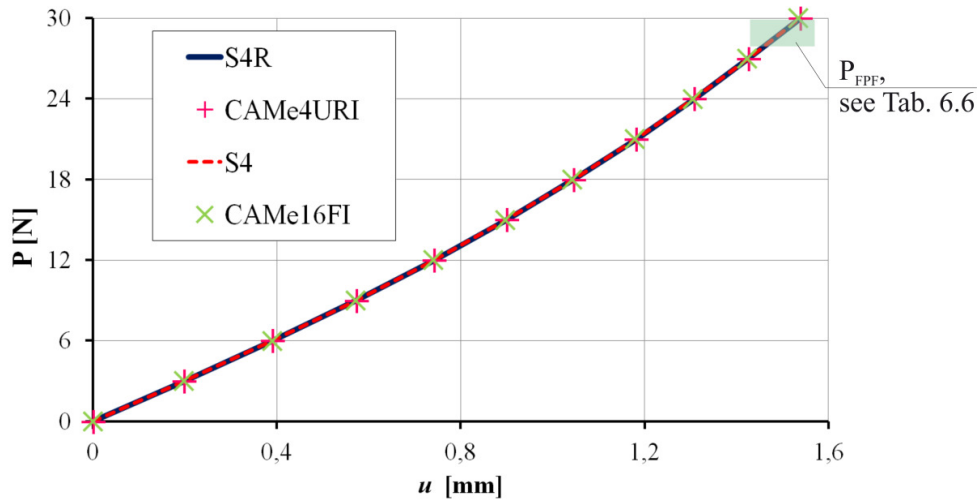

Fig. 6.29. $P-u$ paths of the blade-stiffened, partially clamped panel

Consequently, a chart of in-plane shear stress vs. x coordinate is shown in Fig. 6.30 for all the considered elements in the top layer of the plate in the section marked with red, dashed line, shown in Fig. 6.30 as well. This particular cross section is chosen, because it contains location of FPF, that occurs in subsequent calculations.
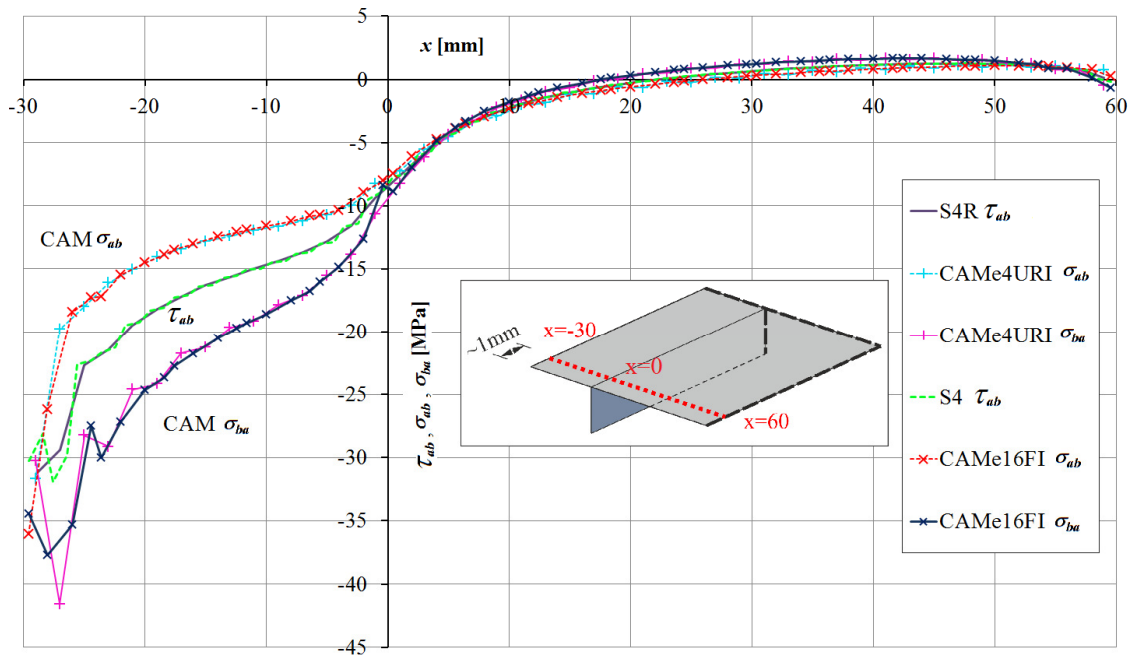
Fig. 6.30. The change of in-plane shear stress in the top layer of the blade-stiffened panel in the presented location (red dashed line)

Additionally two parts of the chart shown in Fig. 6.30 ranging from $x \in [-30; 0]$ and $x \in [15; 60]$ are illustrated in more details, accordingly, in Fig. 6.31 and Fig. 6.32.
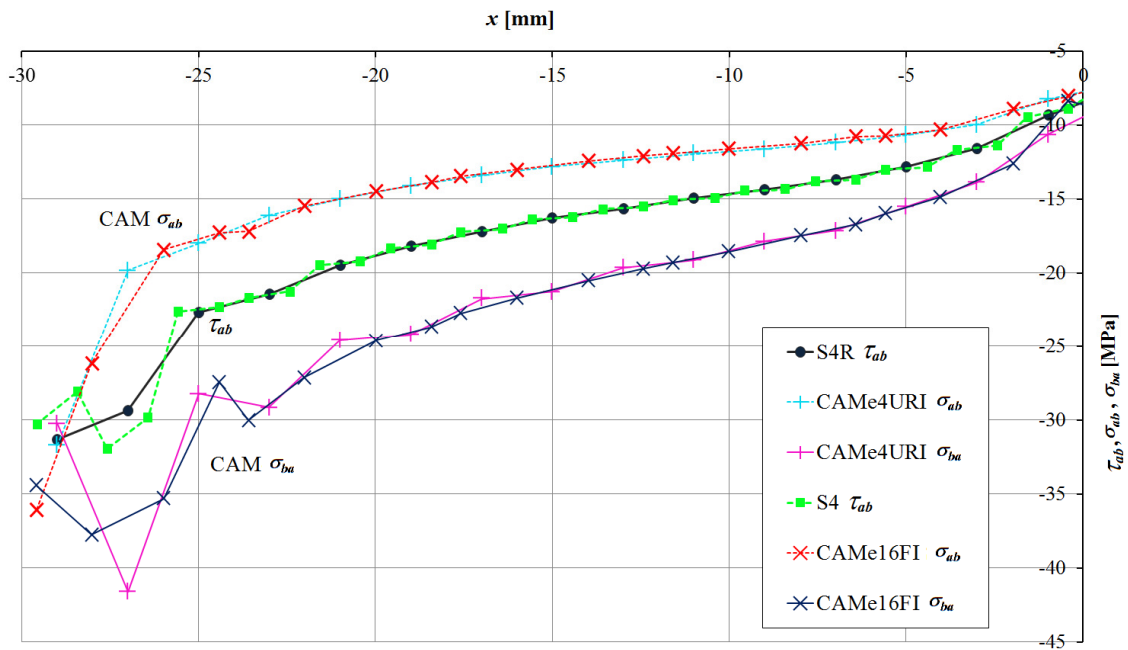

Fig. 6.31. The change of in-plane shear stress in the top layer of the blade-stiffened panel $x \in [-30; 0]$
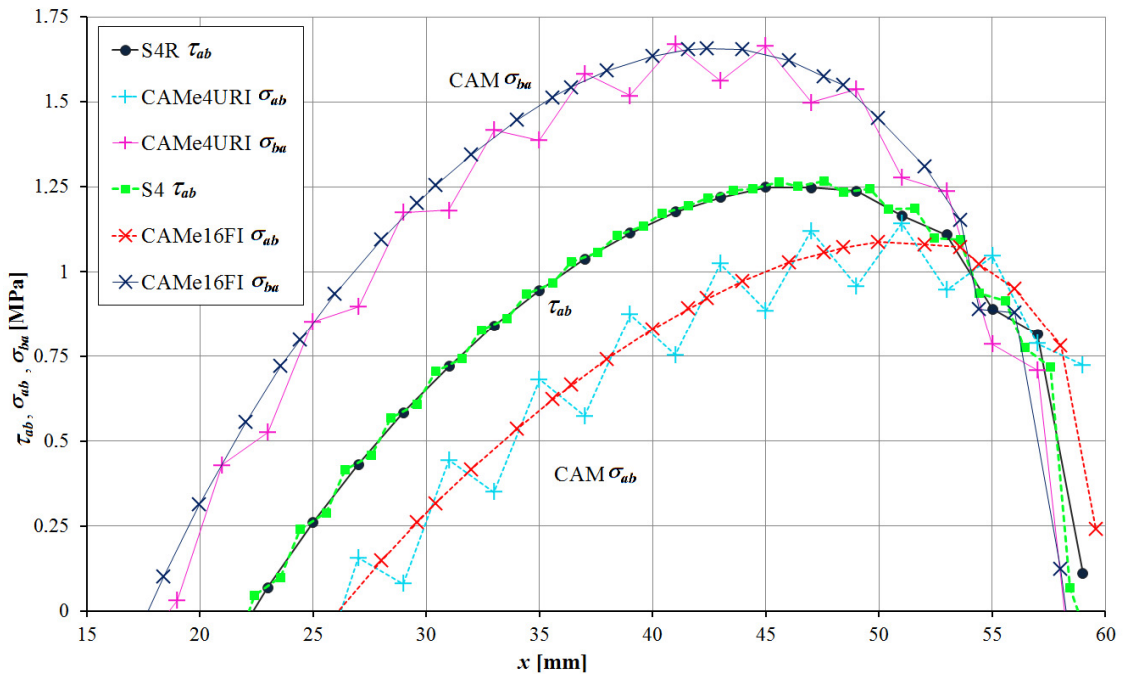

Fig. 6.32. The change of in-plane shear stress in the top layer of the blade-stiffened panel $x \in [15; 60]$

On the basis of Fig. 6.30÷Fig. 6.32 it can be concluded that some in-plane shear asymmetry appears in 6 p theory calculations. What is more, the shape of in-plane shear stress distribution is similar in Abaqus and CAM. This shows clearly that the differences

between the results coming from the considered codes is attributed to the use of 5 parameter (Abaqus) and 6 parameter theory (CAM) and not to the formulation underlying the used finite elements. The CAMe4URI results exhibited spurious zero-energy effect, which is visible especially in Fig. 6.32. From this reason only higher order CAMe16FI elements are used in further 6p theory FEM calculations.

Hence, the FPF analysis is performed with aid of S4 and CAMe16FI models. The damage onset loads, estimated with Tsai-Hill, Tsai-Wu, Hashin and Puck classical and modified criteria are presented in Tab. 6.6.

Tab. 6.6 P_{FPF} loads [N] calculated with aid of the considered failure criteria

Criterion	Abaqus - classical criterion	CAM - modified criterion
Tsai-Hill	29.91	28.59
Tsai-Wu	29.02	27.86
Hashin (matrix tension)	29.96	28.63
Puck (IFF mode A)	29.81	28.52

The damage is observed in top location of top layer in all cases and in the vicinity of plate stiffener connection, as it is shown in Fig. 6.33. Comparisons of the corresponding contours of failure indices are shown in Fig. 6.34÷Fig. 6.37.
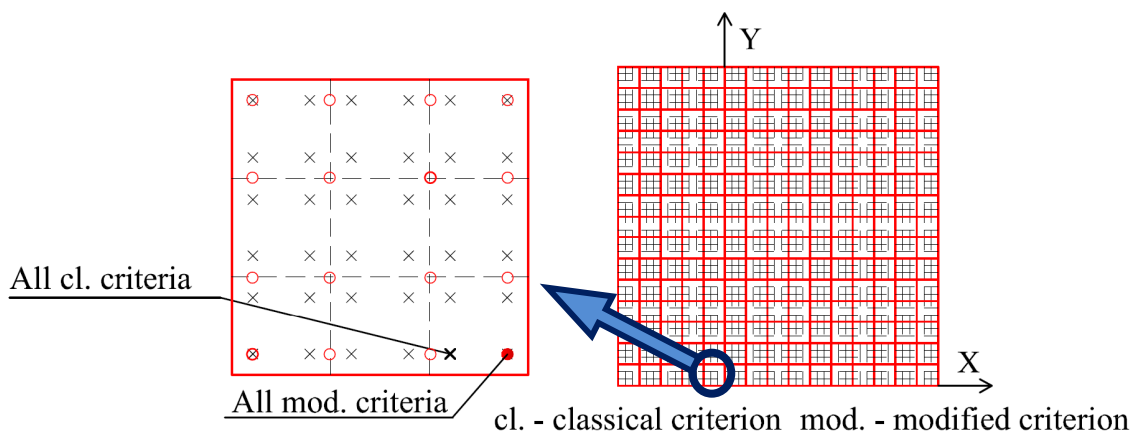

Fig. 6.33. Location of initial damage (in-plane integration points: red circles CAM, black x-marks Abaqus) and the mesh of finite elements: red lines CAMe16FI, black dashed lines S4 Abaqus.
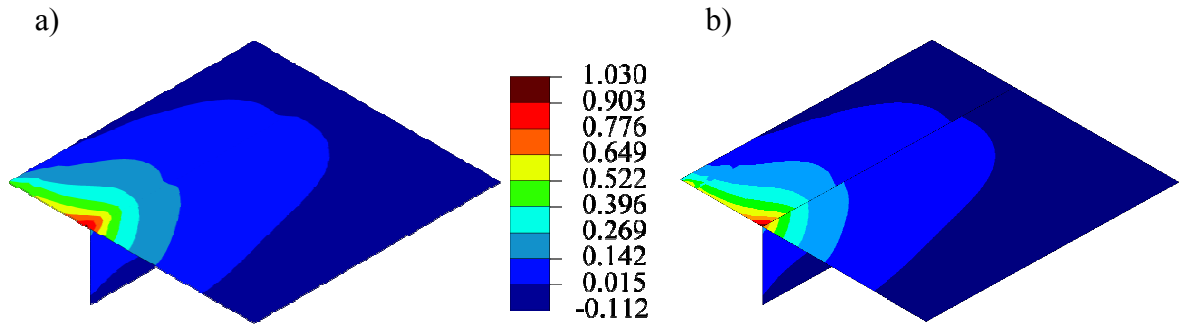
a)   b)

Fig. 6.34. Tsai-Wu failure indices for the blade-stiffened panel, 8th layer (top), classical criterion - Abaqus (a), modified criterion - CAM (b)
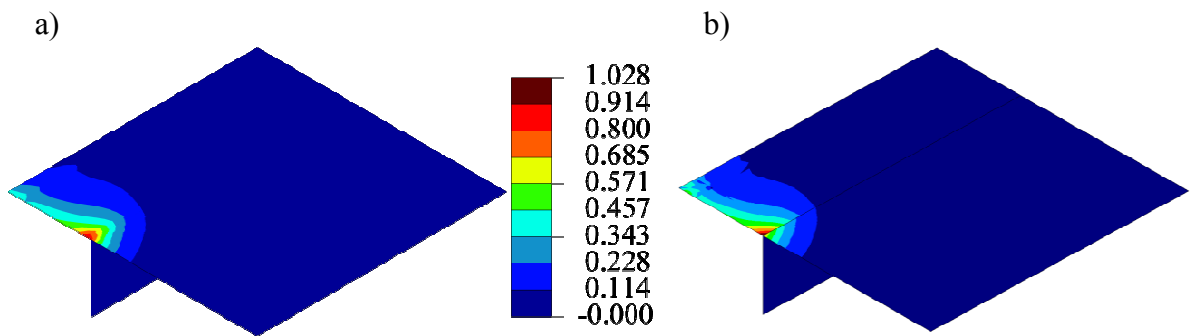
a)   b)

Fig. 6.35. Tsai-Hill failure indices for the blade-stiffened panel, 8th layer (top), classical criterion - Abaqus (a), modified criterion - CAM (b)
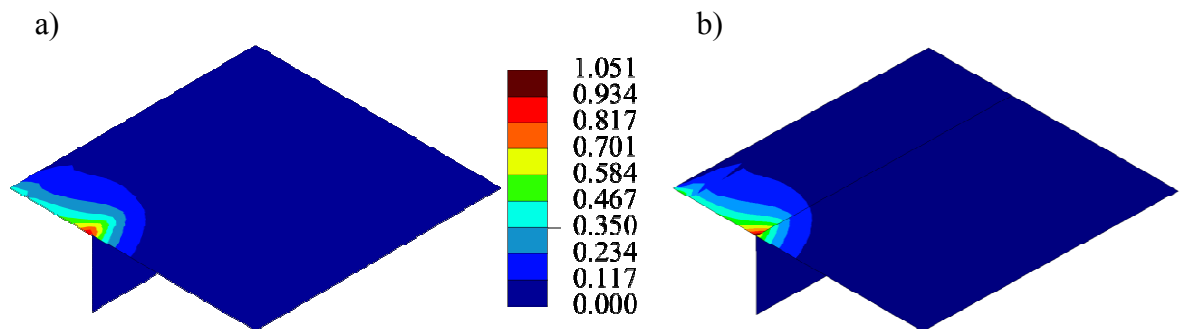
a)   b)

Fig. 6.36. Hashin matrix tension failure indices for the blade-stiffened panel, 8th layer (top), classical criterion - Abaqus (a), modified criterion - CAM (b)

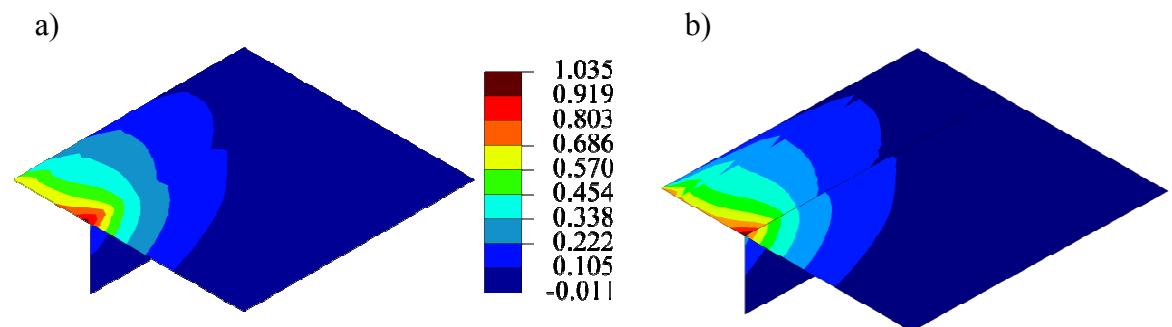a)   b)

Fig. 6.37. Puck IFF failure indices for the blade-stiffened panel, 8th layer (top), classical criterion - Abaqus (a), modified criterion - CAM (b)

The FPF results shown above indicates that some quantitative differences between the classical and modified criteria predictions appear, with similar failure indices patterns. The relative error[9] of P_{FPF} ranges from 4.16%÷4.65%. It is worth to mention that in the analysis of regular shells e.g. C4 panel, such an error ranges from 1.22%÷1.70%. Small in-plane shear stress asymmetry is observed in 6p theory in the failure location, for example $\sigma_{ab} = -7.708\text{MPa}$, $\sigma_{ab} = -8.010\text{MPa}$ for the Hashin criterion (relative error 3.92%).

To sum up, the first type of difference between damage onset predictions, resulting from the classical and modified criteria application is found in this example. The values of FPF loads are different, as a consequence of different estimations of stress state with small in-plane shear stress asymmetry in 6p theory. Since there are no large differences between in-plane shear stress components in 6p theory, the contours of failure indices calculated with aid of modified criteria are similar to those determined by the classical ones.

6.6 Compressed U-shaped column

The second example of FPF analysis of shells with intersections is a compressed U-shaped column. The geometry and properties required to build numerical models of the structure are given in Fig. 6.38.
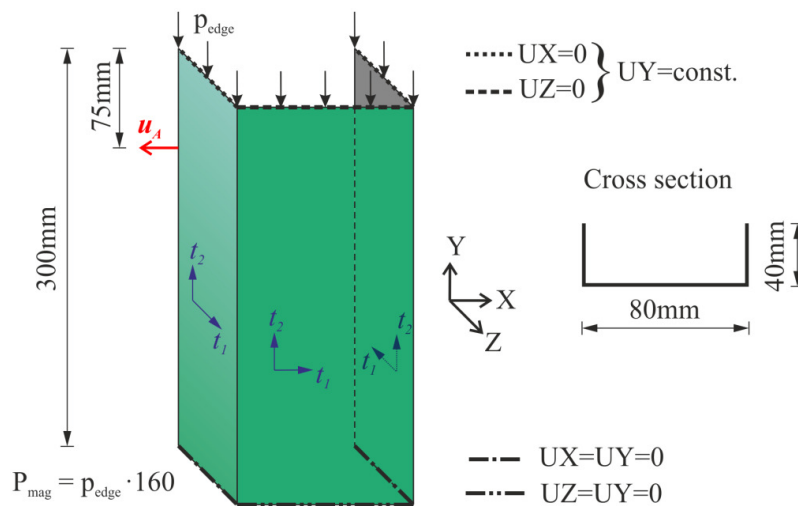

Fig. 6.38. The compressed U-shaped column - geometry, surface coordinate system, loads and BCs

---

[9] The relative error is calculated as follows: $\dfrac{\left| P_{classical}^{FPF} - P_{modified}^{FPF} \right|}{P_{modified}^{FPF}} \cdot 100\%$, where $P_{classical}^{FPF}$ denotes the classical criterion failure load and $P_{modified}^{FPF}$ refers to the modified criterion FPF load. Such a definition is used in all subsequent error estimations.

The column has the following layer stacking sequence [90/45/−45/0]$_s$. The single ply thickness is 0.131mm. The elastic and strength properties of the lamina are given below:

$E_a = 130.71\,\text{GPa}$, $\quad E_b = 6.36\,\text{GPa}$, $\quad G_{ab} = G_{ac} = 4.18\,\text{GPa}$, $\quad G_{bc} = 1.0\,\text{GPa}$, $\quad v_{ab} = 0.3$,

$X_t = 1867.2\,\text{MPa}$, $\quad X_c = 1531\,\text{MPa}$, $\quad Y_t = 25.97\,\text{MPa}$, $\quad Y_c = 214\,\text{MPa}$, $\quad S_l = 100.15\,\text{MPa}$,

$S_t = 50.0\,\text{MPa}$.

The results of stability and FPF analysis, carried out with classical Tsai-Wu criterion, of such a column were firstly presented in DĘBSKI H. [2013]. Similar analysis was also performed in CHRÓŚCIELEWSKI J., SABIK A., SOBCZYK B., WITKOWSKI W. [2016], where the damage onset was predicted with aid of modified Tsai-Wu and Hashin criterion. Analysis of a column with the same geometry, other lamination schemes and some changed boundary conditions was recently described in DĘBSKI H., TETER A., KUBIAK T., SAMBORSKI S. [2016], where experimental and numerical results according to the classical Tsai-Wu failure initiation criteria were shown. Analysis of another U-shaped column, made in this case from GFRP and fibre metal laminate (FML) is described in KUBIAK T., MANIA R. J. [2016]. In BANAT D., KOŁAKOWSKI Z., MANIA R. J. [2016] FML U-shaped and Z-shaped columns are investigated under axial compression. Therefore the problem of load capacity and postbuckling response determination of composite U-shaped columns is quite actual.

In this work geometrically nonlinear calculations are performed to recreate the loss of stability of the column similarly as in DĘBSKI H. [2013]. FPF loads are estimated, using classical and modified Tsai-Wu, Tsai-Hill, Hashin and Puck criteria. It is expected here, on the basis of the previous example, that some differences between the estimations will occur, because of the presence of intersections.

The following numerical discretizations of the structure are created by edge divisions to predict its behaviour, applying 5p or 6p shell theories. In Abaqus S4 elements are utilised: 12 elements are created across each flange, 24 elements across the web and 92 elements along the column. Hence, the division is named as: $(12 + 24 + 12) \times 92$. In CAM $(4 + 8 + 4) \times 30$ mesh of CAMe16FI elements is built.

The equilibrium paths $P_{mag} - u_A$ of the current numerical models and the reference ones, given in DĘBSKI H. [2013], are portrayed in Fig. 6.39.
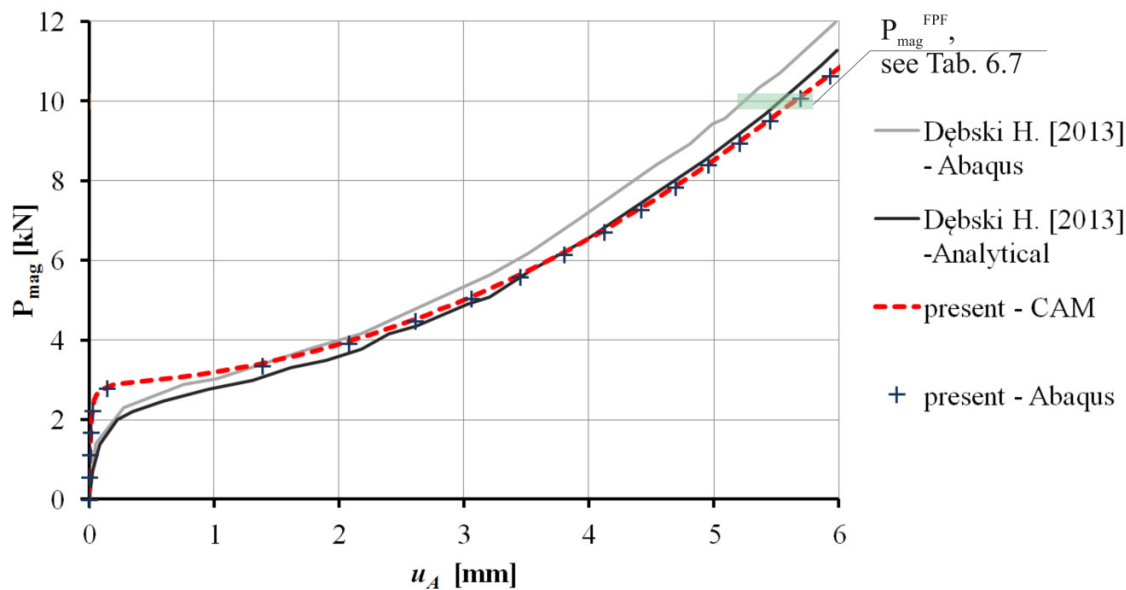
Fig. 6.39. $P_{mag} - u_A$ equilibrium paths of the U-shaped compressed column

The CAM and Abaqus global response predictions are similar to the reference analytical solution in the postbuckling range. It is not clear to the Author of this thesis why the reference Abaqus results differ from the actual ones, as the numerical model and analysis properties were adapted directly from DĘBSKI H. [2013].

The FPF P_{mag} loads, obtained during actual analyzes, are collected in Tab. 6.7. The estimations are similar (relative error for each criterion ranges from 0.94%÷1.63%). DĘBSKI H. [2013] calculated the initial failure force by means of classical Tsai-Wu criterion, which is equal to 10.123kN. The difference between this reference value and the actual one calculated with classical criterion (Abaqus) is devoted to slightly different predictions of the column response (see Fig. 6.39).

Tab. 6.7 P_{mag}^{FPF} loads [kN] calculated with aid of the considered failure criteria

Criterion	Abaqus - classical criterion	CAM - modified criterion
Tsai-Wu	9.979	9.819
Tsai-Hill	10.098	10.177
Hashin (matrix tension)	10.099	10.195
Puck (IFF mode A)	10.094	10.194

The precise locations of FPF for all the considered classical and modified criteria are shown in Fig. 6.40.
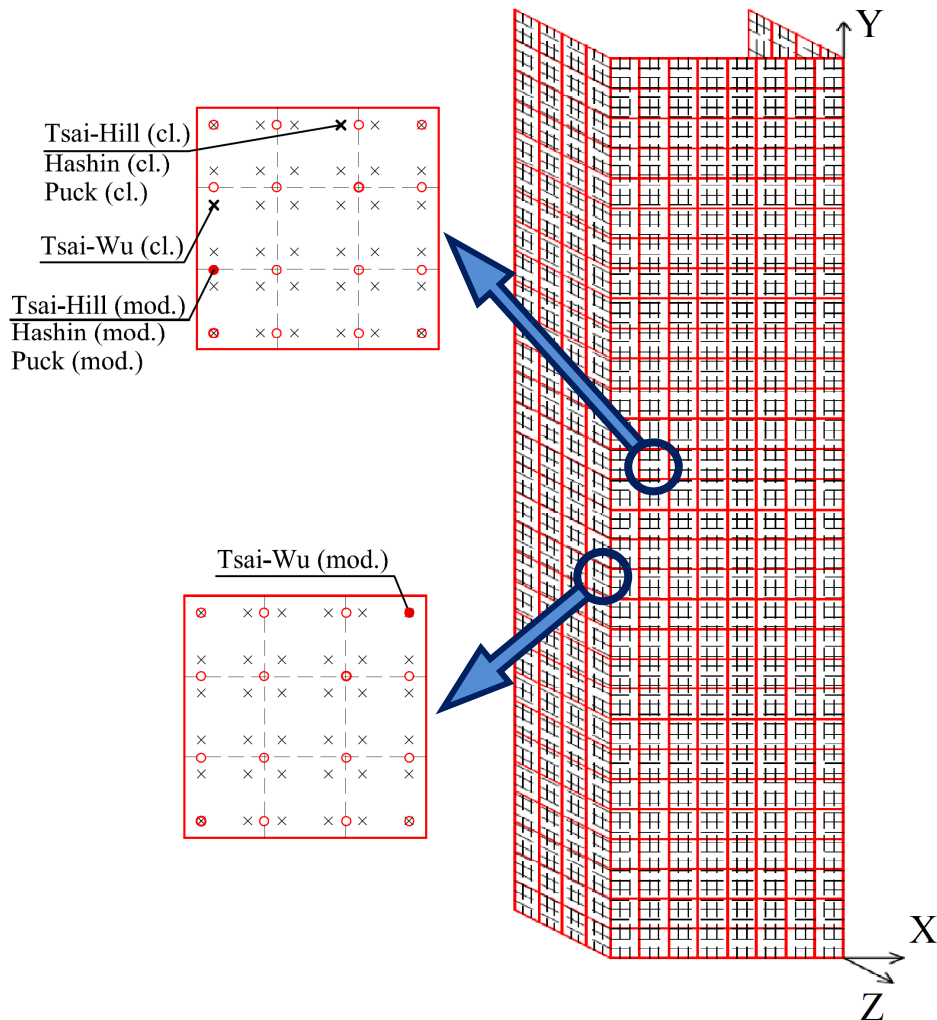

Fig. 6.40 Location of initial damage (in-plane integration points: red circles CAM, black x-marks Abaqus) and the mesh of finite elements: red lines CAMe16FI, black dashed lines S4 Abaqus.

Differences are observed between the classical and modified contours of Tsai-Wu, Tsai-Hill, Hashin and Puck failure indices, which are shown accordingly in Fig. 6.41÷Fig. 6.44. These differences are marked with pink ellipses and are observed in the vicinities of flange-web intersections. The differences are a consequence of arising in-plane shear asymmetry.
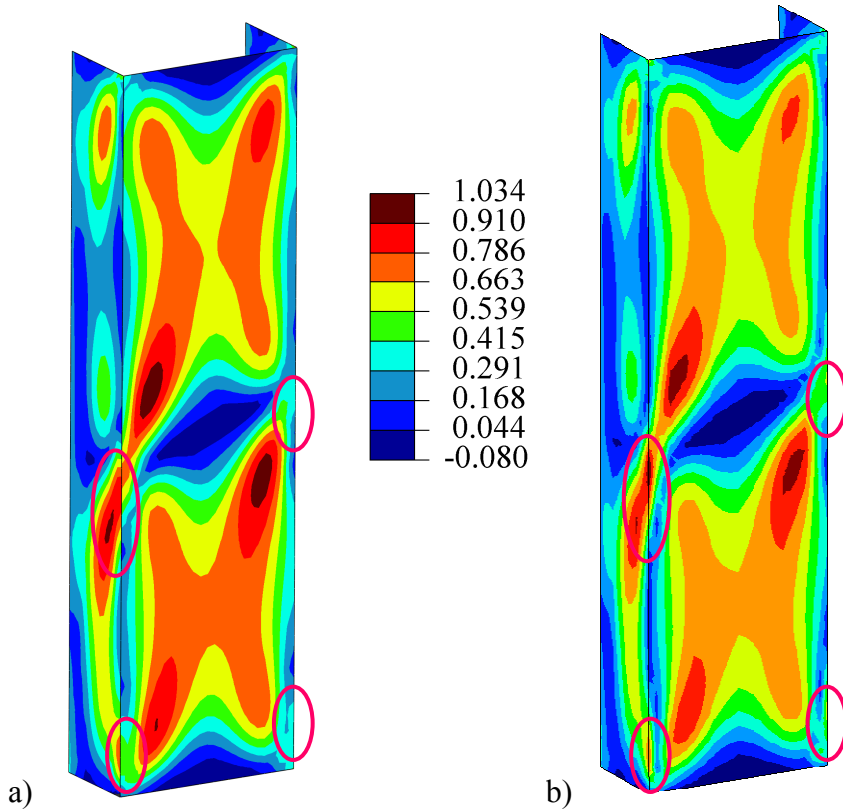
Fig. 6.41 Tsai-Wu failure indices of the U-shaped column, max value envelope in the thickness direction, classical criterion - Abaqus (a), modified criterion - CAM (b)
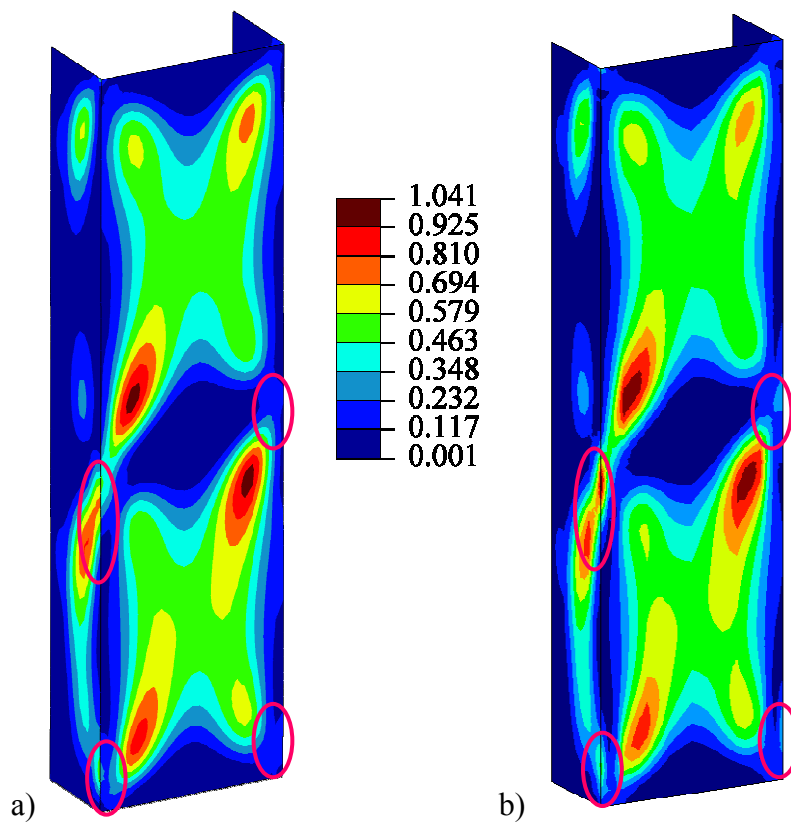

Fig. 6.42 Tsai-Hill failure indices of the U-shaped column, max value envelope in the thickness direction, classical criterion - Abaqus (a), modified criterion - CAM (b)
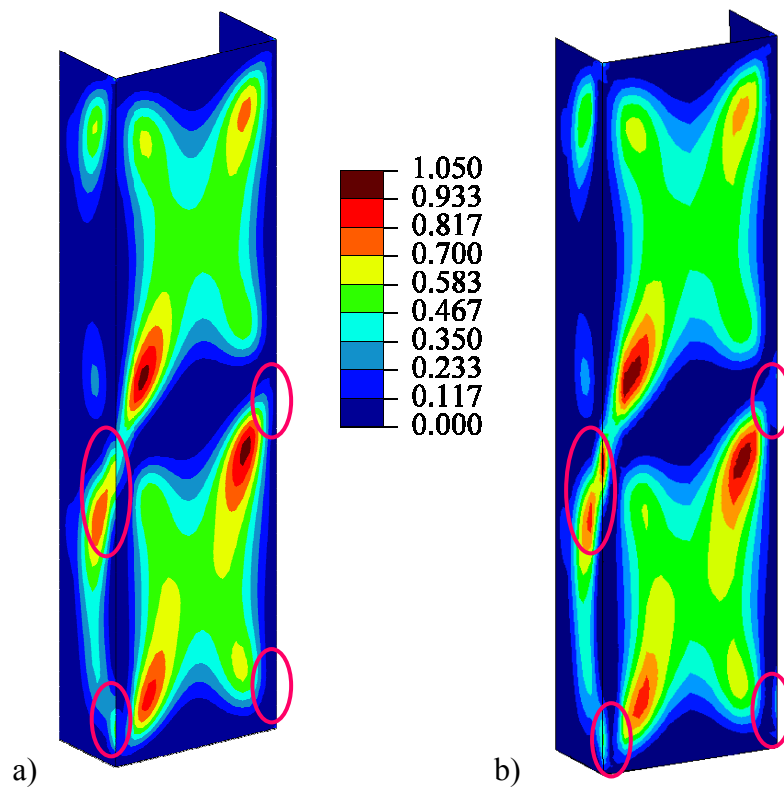
Fig. 6.43 Hashin matrix tension failure indices of the U-shaped column, max value envelope in the thickness direction, classical criterion - Abaqus (a), modified criterion - CAM (b)
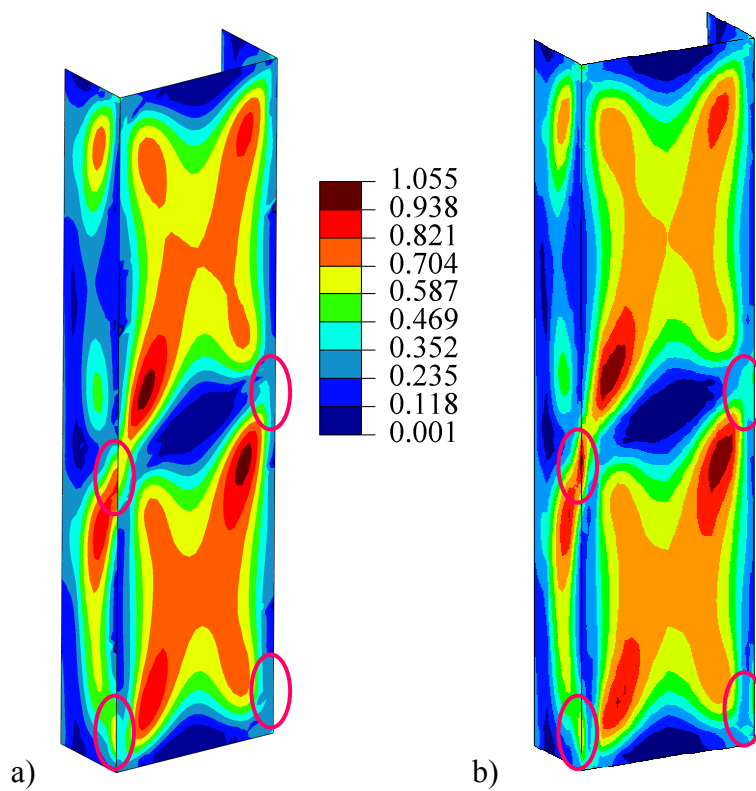

Fig. 6.44 Puck IFF failure indices of the U-shaped column, max value envelope in the thickness direction, classical criterion - Abaqus (a), modified criterion - CAM (b)

In the case of the modified Tsai-Wu criterion the in-plane shear asymmetry is so large that the damage onset location (see Fig. 6.40) is moved from the web to the web-flange intersection, in comparison with the classical one. Fig. 6.45 contains the plots of the available in-plane shear stress components as the function of cross sectional position. Location of the cross section (used in Fig. 6.45) is shown in Fig. 6.46. It contains information from the row of integration points in which FPF occurs according to the modified Tsai-Wu criterion in CAM and from the closest row in Abaqus.
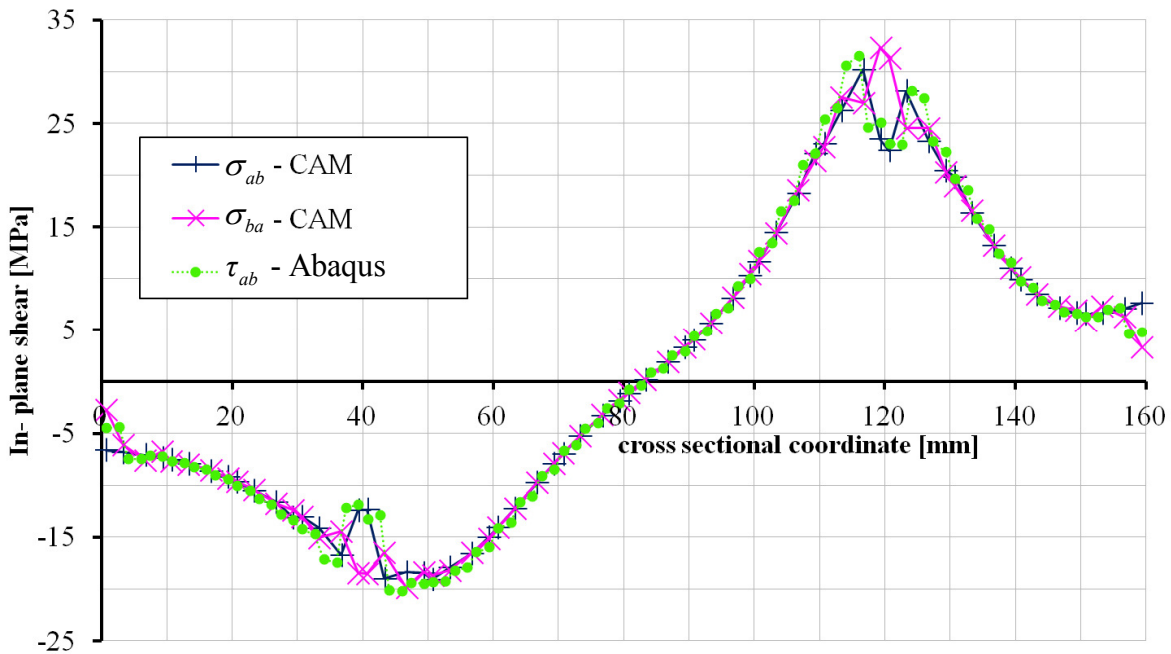

Fig. 6.45 In-plane shear stress components vs. cross sectional coordinate of the cross section shown in Fig. 6.46
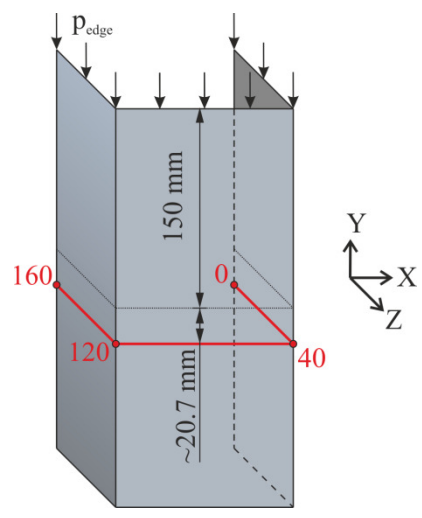

Fig. 6.46 Location of the cross section, where the in-plane shear stress components are investigated.

Although the in-plane shear asymmetry for the remaining failure initiation criteria under consideration did not change the FPF failure location and load values, the differences in failure indices distribution cannot be neglected (refer to the Fig. 6.42÷Fig. 6.44). All the calculations in this paper are performed up to the moment of FPF. Nevertheless, if LPF load capacity is considered, differences in the indices distribution may lead to different failure patterns and different behaviour of progressively damaging structure.

Summarizing, it is observed in this example, that the distributions of failure indices patterns differ for 5p and 6p theory, which is the second type of distinctions observed in this work between the considered theories. These are caused by the in-plane shear asymmetry which can be high at shell intersections under complex states of deformation.

6.7   U-shaped footbridge

Finally, U-shaped composite sandwich footbridge is analyzed. It is a full scale research object, built within the FOBRIDGE project (NCBiR, PBS/B2/6/2013) in 2015. It will be mounted over the Radunia Canal in Pruszcz Gdański, to connect cycle path between Pruszcz Gdański and Gdańsk. Its simplified numerical model is built according to the information given in Fig. 6.47 and Fig. 6.48. The pictures of the bridge are shown in Fig. 6.47 and Fig. 6.48 as well.
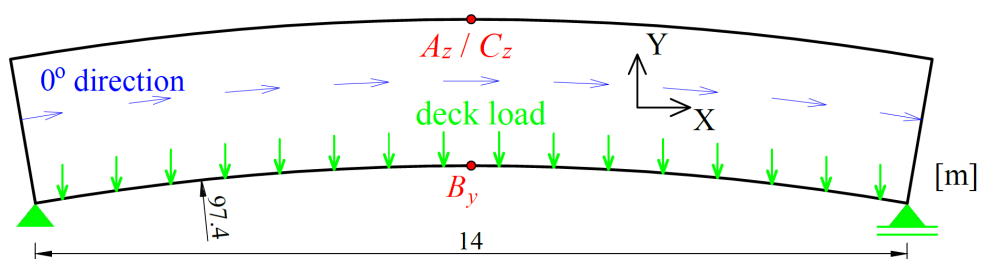

longitudinal cross section

Fig. 6.47 Side view of the FOBRIDGE bridge and the geometry of the numerical model
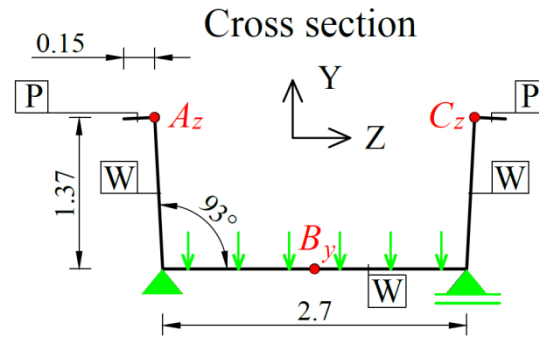
Fig. 6.48 Front view of the FOBRIDGE bridge and the geometry of the numerical model

The footbridge is made of sandwich plates with foam core and laminated parapets. The stacking sequence of the sandwich plate, denoted with W in Fig. 6.48, is [0/45/0/0/45/0/foam/0/45/0/0/45/0], while of the laminated parapets, indicated with P according to Fig. 6.48, is $[0/45/0/0/45/0]_s$. Each lamina (biaxial fabric) is 0.663 mm thick and is endowed with the following elastic and strength properties (following CHRÓŚCIELEWSKI J., KLASZTORNY M., NYCZ D., SOBCZYK B. [2014]): $E_a = 19\,\text{GPa}$, $E_b = 19\,\text{GPa}$, $G_{ab} = 3.18\,\text{GPa}$, $G_{ac} = G_{bc} = 1.49\,\text{GPa}$, $v_{ab} = 0.14$, $X_t = 449\,\text{MPa}$, $X_c = 336\,\text{MPa}$, $Y_t = 449\,\text{MPa}$, $Y_c = 336\,\text{MPa}$, $S_l = 45.2\,\text{MPa}$, $S_t = 34.7\,\text{MPa}$. The foam is approximated with an elastic isotropic material: $E = 75\,\text{MPa}$, $v = 0.4$ and has the thickness of 100mm.

Analysis of the geometrically nonlinear behaviour of the footbridge was performed in SOBCZYK B. [2016], where its response was predicted using 5p and 6p shell theories and compared. In this work these calculations are extended and FPF estimations with aid of Tsai-Wu and Tsai-Hill classical and modified criteria are carried out. It is shown in this example as well, that the 6p theory and modified criteria can be used in the analysis of real structure and support the process of structural design.

Up to this point only unidirectional laminas were considered. Hence, it was possible to use Tsai-Wu, Tsai-Hill, Hashin and Puck criteria. It is not possible to predict FPF with aid of Hashin and Puck criteria in this example, as biaxial layers are used. Moreover, since unidirectional laminas are utilised, the equation (4.9) should be used as the classical Tsai-Hill criterion and consequently modified Tsai-Hill criterion corresponding with (4.9) ought to be formulated and applied here. Nevertheless, the Z strengths of the lamina, according to the experimental data (see e.g. CHRÓŚCIELEWSKI J., KLASZTORNY M., NYCZ D., SOBCZYK B. [2014]), are almost the same as compared with the Y strengths (Z_c=348MPa). Therefore,

finally it is assumed that the (4.11) form of classical Tsai-Hill criterion and correspondingly expression (5.7) for the modified criterion are used in this example.

The numerical models are built with aid of S4 and CAMe16FI elements using edge divisions. Correspondingly, in Abaqus: 3 elements are created across each parapet, 12 across each wall, 12 across the deck and 72 along the structure: This results in the following discretization: $(3 + 12 + 12 + 12 + 3) \times 72$. In CAM the $(1 + 4 + 4 + 4 + 1) \times 24$ mesh is built.

The deck load − displacements paths, at A_z, B_y and C_z points (see Fig. 6.47 and Fig. 6.48) are presented in Fig. 6.49.
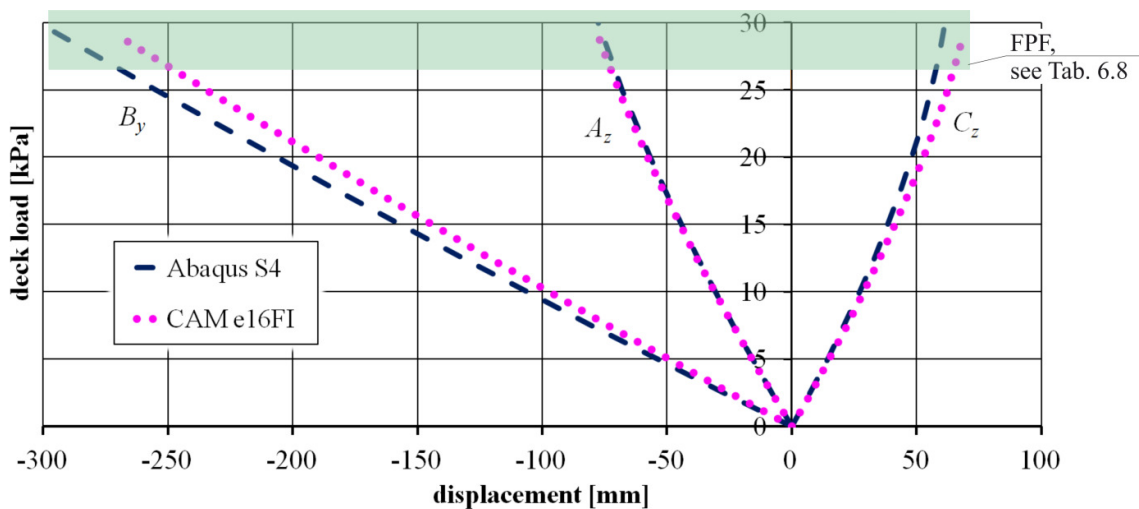
Fig. 6.49 The equilibrium paths for A_z, B_y and C_z points

The difference between the structural behaviour predicted by 5p and 6p theory, as shown in Fig. 6.49, is probably caused by the way the shell intersections are modelled. It is assumed that the CAM predictions are more precise, since in 6p theory the drilling degree of freedom is not introduced artificially like in 5p theory, but in a natural way as a consequence of theoretical foundations. Moreover, it is observed in CAM calculations that the top parapets lost their stability (see Fig. 6.50). This effect does not occur in Abaqus.

In consequence, the FPF classical and modified criteria estimations differ, as it is shown in Tab. 6.8. Nevertheless the failure initiation is observed always in laminated parapets at the bottom of the second layer, regarding the thickness coordinate.
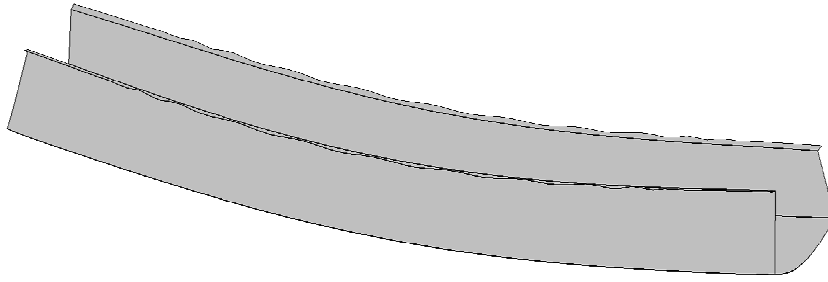
Fig. 6.50 Visualization of the deformed structure, when the deck load is equal to 20kPa in 6p theory calculations (CAM), deformations are scaled 20 times

Tab. 6.8 FPF deck loads [kPa] calculated with aid of the considered failure criteria

Criterion	Abaqus - classical criterion	CAM - modified criterion
Tsai-Wu	29.95	26.45
Tsai-Hill	31.19	27.08

The precise locations of the damage onsets for the considered criteria are shown in Fig. 6.51 and they differ as well.
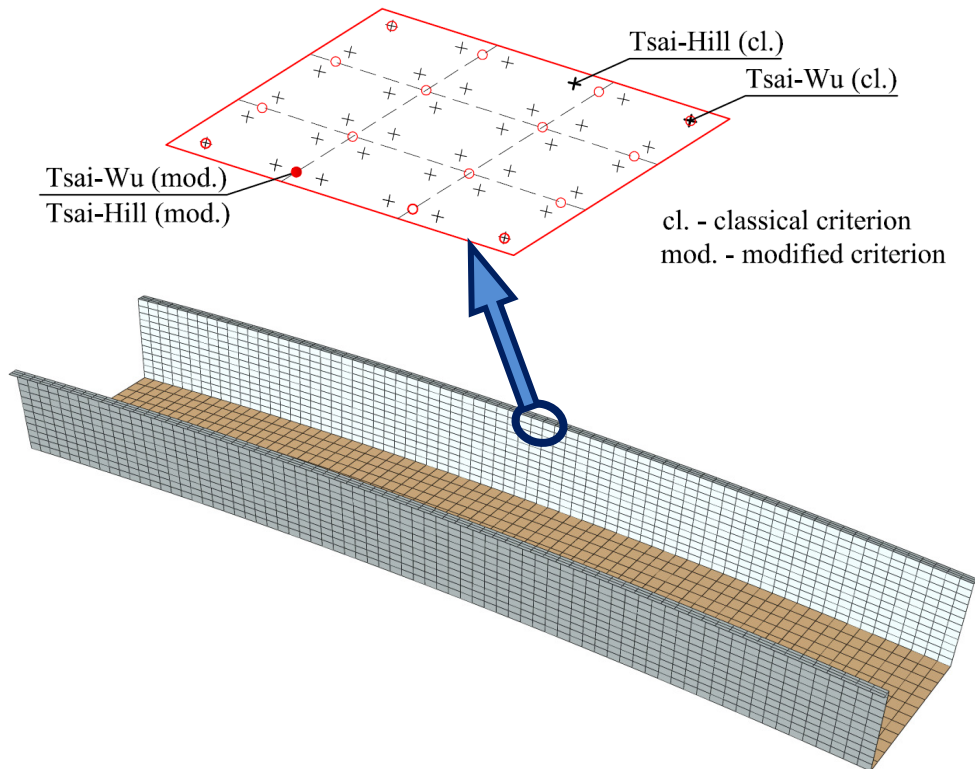
Fig. 6.51 Location of initial damage (in-plane integration points: red circles CAM, black x-marks Abaqus) and the mesh of finite elements: red lines CAMe16FI, black dashed lines S4 Abaqus

The contours of classical and modified Tsai-Wu and Tsai-Hill failure indices are shown in Fig. 6.52 and Fig. 6.53. It needs to be emphasized here, that failure indices for all

the considered criteria exceed the value of 1 in the vicinity of supports. However, these areas are excluded from FPF analysis, because in reality the supports are not of pin type but the boundary conditions are distributed, thus such a concentration would not occur. It is also observed, that in 6p theory very small in-plane shear asymmetry evolves, for example for Tsai-Hill modified criterion it yields $\sigma_{ab} = -44.61\text{MPa}$, $\sigma_{ab} = -44.88\text{MPa}$.

Fig. 6.52 Tsai-Wu failure indices for the footbridge, max value envelope in the thickness direction, classical criterion - Abaqus (a), modified criterion - CAM (b)
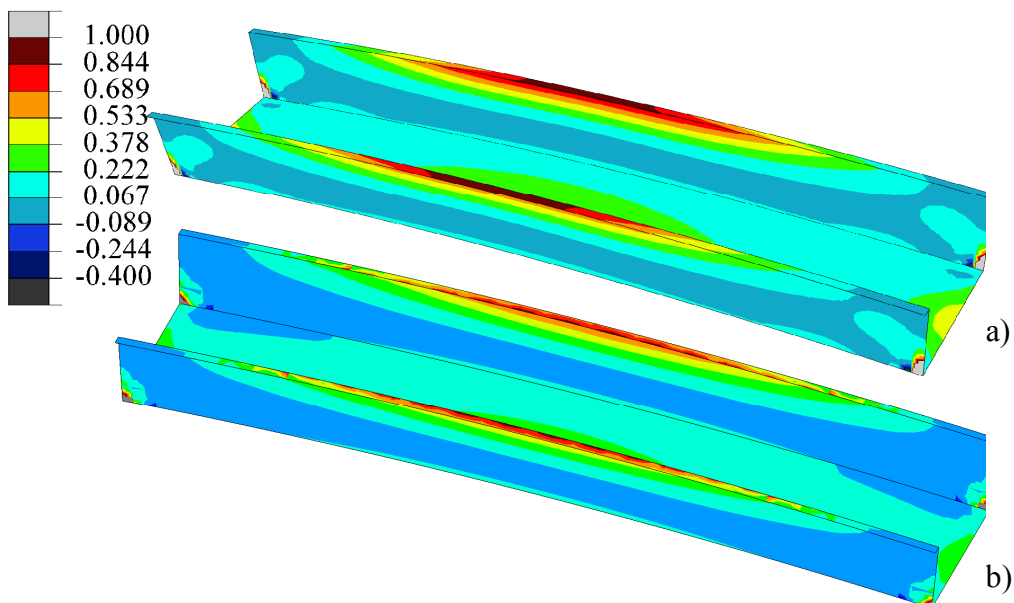
Fig. 6.53 Tsai-Hill failure indices for the footbridge, max value envelope in the thickness direction, classical criterion - Abaqus (a), modified criterion - CAM (b)

Some essential conclusions can be formulated here, which determine the third type of distinctions between classical and modified criteria predictions found in this work. It is observed 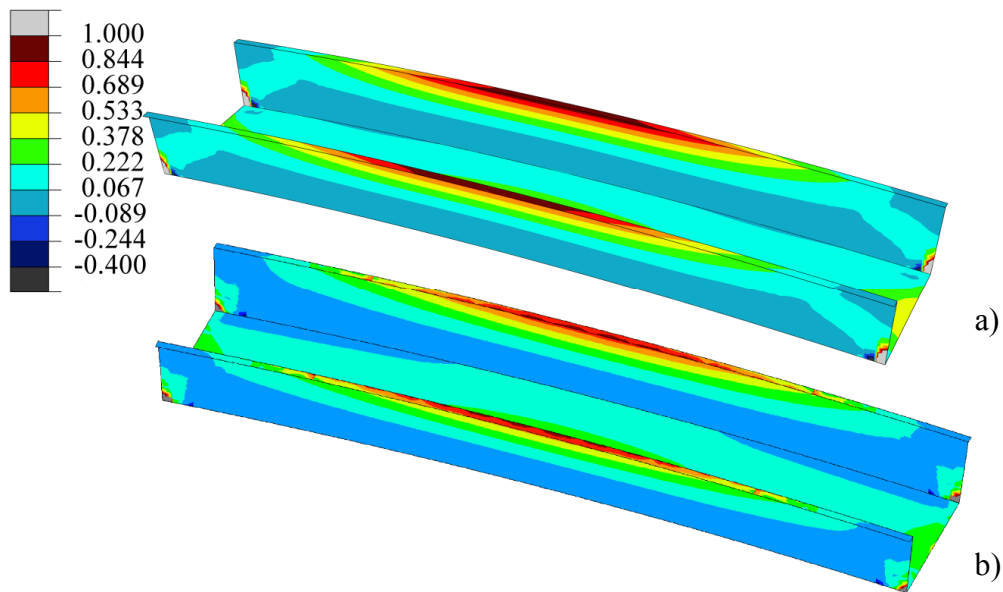in this example that the 6p theory can predict different behaviour of shells with intersections, as compared with 5p theory. As a consequence of the discrepancies in the estimated bridge responses the relative errors between classical and modified Tsai-Wu and Tsai-Hill criteria FPF deck loads are correspondingly 13.2% and 15.2%. These are the highest ones reported among all the considered numerical examples in this thesis. Although minor in-plane shear asymmetry occurs in the 6p theory the contours of the modified failure indices present some differences, as compared with the classical ones. This results from the fact that the parapets lost their stability in CAM. From this reason also the possible progressive damage estimations may vary for 5p and 6p theories. Finally, it can be stated that the 6p theory can be used in the behaviour assessment and design process of real structures. The theory enables, especially, the analysis of shells with intersection and as it was shown in this example it may give different behaviour predictions, as compared with the 5p one. Nevertheless, an experiment should be carried out in order to justify if the 6p theory is more precise or better than the 5p approach.

7. FINAL REMARKS

The problem of failure initiation in laminated composites using the nonlinear 6 parameter shell theory was studied here. This theory is especially dedicated to the analysis of shells with intersections, since the 6th degree of freedom i.e. the drilling rotation appears naturally. This is in contrast to 5 parameter shell theories, which are quite popular in application, e.g. in commercial codes like Abaqus, or Nastran where there is a need to include it artificially. The failure estimations of these two approaches were compared, since differences are expected to arise, as a consequence of the aforementioned discrepancies in the theoretical foundations.

Asymmetric strain and stress measures are the inherent ingredients of the 6p theory, as opposed to the 5p theories, where symmetric ones are incorporated. In the standard failure criteria formulation, it is assumed that the stress tensor is symmetric. Thus they cannot be utilised when 6p theory is chosen. Therefore, in this work original Author's modifications of the classical Tsai-Hill, Tsai-Wu, Hashin and Puck failure initiation criteria, that meet the requirements of the 6p theory, were proposed and described.

Consequently FPF FEM analyzes were carried out with aid of the classical and modified criteria. The classical criteria results were obtained by Abaqus calculations, while the modified criteria ones by the non-commercial FEM code named CAM, written in Fortran. The procedures that enable modified criteria failure predictions were implemented into the CAM code by the Author, which is also his achievement in this field.

The following numerical examples, using 5p and 6p theories, were analyzed to estimate FPF: pure shear test, cylindrical panel, C4 panel, blade-stiffened partially clamped panel, compressed U-shaped column, U-shaped footbridge. The results, in the case of the shells without intersections, viz.: pure shear test, cylindrical panel, C4 panel revealed that nearly the same predictions are obtained regarding the failure loads, locations and failure indices contours. Nevertheless, three essential distinctions arose when shell with intersections, namely partially clamped panel, compressed U-shaped column and U-shaped footbridge, were investigated.

The analysis of the partially clamped panel showed that the values of FPF loads were different, as a consequence of different estimations of stress values. Low in-plane shear stress asymmetry in 6p theory analysis was observed in the area of FPF location.

Nevertheless, there were parts of the structure marked with higher in-plane shear asymmetry. Since the distinctions between in-plane shear stress components in 6p theory did not contribute much into the failure initiation, the contours of failure indices calculated with aid of the modified criteria turned out to be similar to those determined by the classical ones.

It was observed in the analysis of the compressed U-shaped column, that the distributions of all the considered failure indices patterns differ for 5p and 6p theory, whereas the FPF forces are quite comparable. In the case of the Tsai-Wu criterion the failure locations predicted by the classical and modified criteria were not the same. This was caused by the in-plane shear asymmetry which was high at shell intersections under complex states of deformation. The remaining classical and modified criteria under consideration gave the same failure locations. However, it needs to be emphasized that different behaviour of such a structure would be possibly observed when progressive damage is considered, as a consequence of the aforementioned differences in the contours of failure indices.

The analysis of U-shaped footbridge brought out that the 6p theory can predict the behaviour of shells with intersections more precisely, in comparison with 5p theory. The top parapets lost their stability in the course of the 6p theory analysis, which did not happen in the 5p theory calculations. As a consequence, relative errors between classical and modified Tsai-Wu and Tsai-Hill criteria FPF estimations were correspondingly 13.2% and 15.2%, and were the highest ones calculated in all the numerical examples under consideration in this thesis. Although minor in-plane shear asymmetry occurred in the 6p theory, the contours of the modified failure indices, as compared with the classical ones, were distinct, which in case of progressive damage analysis may lead to different LPF loads and behaviour, similarly as in the analysis of compressed U-shaped column.

Finally, in view of the above, it can be stated that the thesis: *It is possible to determine the damage onset moment with aid of FEM algorithms under the nonlinear 6 parameter shell theory*, postulated at the beginning of this work was proved. What is more, the application of the modified criteria in the analysis of shells with intersections was found to be reasonable, as different predictions in comparison with classical criteria may be expected.

Future studies will address an extension of the material law used here in chapter 3. It is intended to include the effects of characteristic length in the constitutive description of a layer. Consequently it will be also necessary to supplement the failure initiation equations of the selected criteria with additional stress tensor components, in order to estimate FPF. Also the analysis of progressive damage using the actual modified initiation criteria or the planned ones will be considered.

8. REFERENCES

1. ABAQUS 6.14: Documentation.

2. AUTODESK SIMULATION COMPOSITE DESIGN 2014: Documentation.

3. ALLIX O. [2001]:A composite damage meso-model for impact problems. *Composites Science and Technology*, **61(15)**, 2193-2205.

4. ALTENBACH J., ALTENBACH H., EREMEYEV V. A. [2010]: On generalized Cosserat-type theories of plates and shells: a short review and bibliography. *Arch. Appl. Mech.*, **80 (1)**, 73-92.

5. ALTENBACH H., EREMEYEV V. A. [2014]: Vibration Analysis of Non-linear 6-parameter Prestressed Shells, *Meccanica*, **49(8)**, 1751-1761.

6. ASHBY M. F., JONES D. R. H. [2006]: *Engineering Materials 2. An Introduction to Microstructures, Processing and Design (3rd edition)*. Butterworth-Heinemann, Oxford.

7. BAKER A., DUTTON S., KELLY D. [2004]: *Composite Materials for Aircraft Structures*. AIAA.

8. BANAT D., KOŁAKOWSKI Z., MANIA R. J. [2016]: Investigations of fml profile buckling and post-buckling behaviour under axial compression. *Thin Wall. Struct.*, **107**, 335-344.

9. BAŞAR Y., DING Y. [1997]: Shear deformation models for large strain shell analysis. *Int. J. Solids Structures*, **34(14)**, 1687-1708.

10. BELYTSCHKO T., LIU K. W., MORAN B. [2003]: *Nonlinear Finite Elements for Continua and Structures*. John Wiley & Sons, Ltd.

11. BIELEWICZ E. [1998]: *Wytrzymałość Materiałów*. Wydawnictwo Politechniki Gdańskiej, Gdańsk.

12. BÎRSAN M., NEFF P. [2014a]: Existence of minimizers in the geometrically non-linear 6-parameter resultant shell theory with drilling rotations. *Math. Mech. Solids*, **19(4)**, 376-397.

13. BÎRSAN M., NEFF P. [2014b]: Shells without drilling rotations: A representation theorem in the framework of the geometrically nonlinear 6-parameter resultant shell theory. *Int. J. Eng. Sci.*, **80**, 32-42.

14. BURZYŃSKI S., CHRÓŚCIELEWSKI J., WITKOWSKI W. [2014a]: Elastoplastic material law in 6-parameter nonlinear shell theory, In: Pietraszkiewicz W.,

Górski J. (eds.), *Shell Structures: Theory and Applications, vol. 3*, CRC Press, London, 377-380.

15. BURZYŃSKI S., CHRÓŚCIELEWSKI J., WITKOWSKI W. [2014b]: Elastoplastic law of Cosserat type in shell theory with drilling rotation. *Math. Mech. Solids*, **20(7)**, 790-805.

16. BURZYŃSKI S., CHRÓŚCIELEWSKI J., WITKOWSKI W. [2015], Geometrically nonlinear FEM analysis of 6-parameter resultant shell theory based on 2-D Cosserat constitutive model, *Z. Angew. Math. Mech.*, **96(2)**, 191-204.

17. BURZYŃSKI S., CHRÓŚCIELEWSKI J., DASZKIEWICZ K., WITKOWSKI W. [2016]: Geometrically nonlinear FEM analysis of FGM shells based on neutral physical surface approach in 6-parameter shell theory. *Compos. Part B - Eng.*, **107**, 203-213.

18. CALVERT T. [2009]: Composite footbridge installed in six hours. *Reinforced plastics, materials today*, **18 June 2009**, available online at: www.materialstoday.com/composite-applications/news/composite-footbridge-installed-in-six-hours/.

19. CAMANHO P. P. [2002]: Failure criteria for fibre-reinforced polymer composites. *Secção de Mecânica Aplicada Departamento de Engenharia Mecânica e Gestão Industrial Faculdade de Engenharia da Universidade do Porto*, Porto (available online at: https://web.fe.up.pt/~stpinho/teaching/feup/y0506/fcriteria.pdf).

20. CAMPBELL F. C. [2010]: *Structural Composite Materials*. ASM International, Materials Park Ohio. Preview available online at: https://books.google.pl/books /about/Structural_Composite_Materials.html?id=D3Wta8e07t0C&redir_esc=y.

21. CARRERA E., BRISCHETTO S. [2009]: A survey with numerical assessment of classical and refined theories for the analysis of sandwich plates. *Appl. Mech. Rev.*, **62**, 010803-1–010803-17.

22. CHRÓŚCIELEWSKI J. [1996]: The family of C^0 finite elements in 6-parameter nonlinear shell theory (in Polish), *Gdańsk University of Technology research bulletin (in polish)*, **LIII**, 1-291.

23. CHRÓŚCIELEWSKI J., KREJA I., SABIK A., WITKOWSKI W. [2011]: Modeling of composite shells in 6-parameter nonlinear theory with drilling degree of freedom. *Mech. Adv. Mater. Struct.*, **18**, 403–419.

24. CHRÓŚCIELEWSKI J., MAKOWSKI J., PIETRASZKIEWICZ W. [2000]: Large overall motion of flexible branched shell structures, In: Ambrosio JAC, Kleiber M. (eds), *Computational Aspects of Nonlinear Structural Systems with Large Rigid Body Motion*, NATO ARW, Pułtusk (Poland), July 2-7, IDMEC Lisboa 201-218.

25. CHRÓŚCIELEWSKI J., MAKOWSKI J., PIETRASZKIEWICZ W. [2004]: *Statics and Dynamics of Multifold Shells: Nonlinear Theory and Finite Element Method (in polish)*. IPPT PAN, Warsaw.

26. CHRÓŚCIELEWSKI J., MAKOWSKI J., STUMPF H. [1992]: Genuinely resultant shell finite elements accounting for geometric and material non-linearity. *Int. J. Numer. Meth. Eng.*, **35**, 63-94.

27. CHRÓŚCIELEWSKI J., MAKOWSKI J., STUMPF H. [1997]: Finite element analysis of smooth, folded and multi-shell structures. *Comp. Meth. Appl. Mech. Engng.*, **141**, 1-46.

28. CHRÓŚCIELEWSKI J., WITKOWSKI W. [2006]: 4-node semi-EAS element in 6–field nonlinear theory of shells. *Int. J. Numer. Meth. Eng.*, **68**, 1137–1179.

29. CHRÓŚCIELEWSKI J., KLASZTORNY M., NYCZ D., SOBCZYK B. [2014]: Load capacity and serviceability conditions for footbridges made of fibre-reinforced polymer laminates. *Roads and Bridges - Drogi i Mosty*, **13(3)**, 189-202.

30. CHRÓŚCIELEWSKI J., WITKOWSKI W., SOBCZYK B., SABIK A. [2015]: First ply failure analysis of laminated shells undergoing large displacements − 6 parameter shell theory approach. In: Kleiber M., Burczyński T., Wilde K., Górski J., Winkelmann K., Smakosz Ł. (eds.), *3rd Polish Congress of Mechanics and 2st International Conference on Computer Methods in Mechanics Short Papers Vol. 1*, 8.09-11.09.15 Gdańsk University of Technology, Gdańsk, Poland.

31. CHRÓŚCIELEWSKI J., SABIK A., SOBCZYK B., WITKOWSKI W. [2016]: Nonlinear FEM 2D failure onset prediction of composite shells based on 6-parameter shell theory. *Thin Wall. Struct.*, **105**, 207-219.

32. COSSERAT E., COSSERAT F. [1908]: Sur la théorie des corps minces. *C. R. Acad. Sci. Paris*, **146**, 169-172.

33. COSSERAT E. AND COSSERAT F. [1909]: *Theorie des corps deformables*. Librairie Scientique, A. Hermann et Fils, Paris (english translation by D. Delphenich,

2007, PDF available online at: http://www.uni-
due.de/~hm0014/Cosserat_files/Cosserat09_eng.pdf).

34. DAVILA C. G., CAMANHO P. P., ROSE C. A. [2005]: Failure Criteria for FRP
    Laminates. *J. Compos. Mater.*, **39(4)**, 323-345.

35. DASZKIEWICZ K., CHRÓŚCIELEWSKI J., WITKOWSKI W. [2014]: Geometrically
    nonlinear analysis of functionally graded shells based on 2-d Cosserat
    constitutive model, *Engng. Trans.*, **62(2)**, 109–130.

36. DĘBSKI H. [2013]: Numerical Analysis of Stability of Thin-Walled Composite
    Column with Open Cross-Section. *Mech. Mech. Eng.*, **17(1)**, 29-35.

37. DĘBSKI H., TETER A., KUBIAK T., SAMBORSKI S. [2016]: Local buckling, post-
    buckling and collapse of thin-walled channel section composite columns
    subjected to quasi-static compression, *Compos. Struct.*, **136**, 593,601.

38. DEUSCHLE H. M. [2010]: *3D Failure Analysis of UD Fibre Reinforced
    Composites: Puck's Theory within FEA. PhD Thesis*, Universitet Stuttgart,
    Institute of Statics and Dynamics of Aerospace Structures, Stuttgart.

39. ENGELSTAD S. P., REDDY J. N., KNIGHT JR. N.F. [1992]: Postbuckling Response
    and Failure Prediction of Graphite-Epoxy Plates Loaded in Compression, *AIAA
    J.,* **30(8)**, pp. 2106-2113.

40. EREMEYEV V. A., LEBEDEV L. P. [2011]: Existence theorems in the linear theory
    of micropolar shells. *Z. Angew. Math. Mech*, **91(6)**, 468-476.

41. EREMEYEV V. A., LEBEDEV L. P., ALTENBACH H. [2013]: *Foundations of
    Micropolar
    Mechanics*, Springer, Heidelberg New York Dordrecht London.

42. EREMEYEV V. A, PIETRASZKIEWICZ W. [2011]: Thermomechanics of shells
    undergoing phase transition. *J.Mech. Phys. Solids*, vol. 59, 1395-1412.

43. EREMEYEV V. A., LEBEDEV L. P., CLOUD M. J. [2014]: The Rayleigh and Courant
    variational principles in the six-parameter shell theory. *Math. Mech. Solids*,
    20(7), 806-822.

44. EREMEYEV V. A, PIETRASZKIEWICZ W. [2015]: Material symmetry group and
    constitutive equations of micropolar anisotropic elastic solids. *Math. Mech.
    Solids.*, **21(2)**, 210-221.

45. ERHART T. [2013]: Drilling Rotation Constraint for Shell Elements in Implicit and
    Explicit Analyses. *LS-DYNA Forum 2013 Sttutgart-Filderstadt*, available

online at: https://www.dynamore.de/de/download/papers/2013-ls-dyna-forum/documents

/drilling-rotation-constraint-for-shell-elements-in-implicit-and-explicit-

analyses.

46. FAN X. L., WANG T. J., SUN Q. [2011]: Damage evolution of sandwich composite structure using a progressive failure analysis methodology. *Procedia Engineering*, **10**, 530-535.

47. GERMAN J. [2001]: *Podstawy Mechaniki Kompozytów Włóknistych*. Cracow University of Technology, Cracow.

48. GREEN A. E., NAGHDI P. M. WAINWRIGHT W. K. [1965]: A General Theory of a Cosserat Surface. *Arch. Ration. Mech. An.*, **20(4)**, 287-308.

49. GREEN A. E., NAGHDI P. M. [1982]: A Theory of Laminated Composite Plates. *J. Appl. Mech.*, **29(1)**, 1-23.

50. GUNAYDIN M., ADANUR S., ALTUNISIK A. C., SEVIM B. [2015]: Dynamic Responses of Halgavor Footbridge Using Steel and FRP Materials. *Steel Compos. Struct.*, 1**8(1)**, 51-69.

51. GURIT [2015]: Gurit's Guide to composites v.5 (available online at: www.gurit.com/files/documents/guide-to-compositesv5webpdf.pdf).

52. HASHIN Z. [1980]:, Failure criteria for unidirectional fiber composites. *J. Appl. Mech.*, **47**, 329-334.

53. HAUPT P. [2000]: *Continuum mechanics and theory of materials*. Springer, Berlin.

54. HIGHAM N. J., DENNIS M. R., GLENDINNING P., MARTIN P. A., SANTOSA F., TANNER J. (EDS.) [2015]: *The Princeton Companion to Applied Mathematics*. Princeton University Press, Princeton and Oxford.

55. HILL R. [1950]: *The Mathematical Theory of Plasticity*. Oxford University Press, London.

56. HINTON M. J., KADDOUR A. S., SODEN P. D. (EDS.) [2004]: *Failure Criteria in Fibre Reinforced Polymer Composites: The World-Wide Failure Exercise*. Elsevier, Amsterdam.

57. HINTON M. J., KADDOUR A. S., SODEN P. D. [2004]: Recommendations for designers and researchers resulting from the world-wide failure. *Compos. Sci. Technol.*, **64**, 589-604.

58. HINTON M. [2011]: Failure Criteria in Fibre Reinforced Polymer Composites : Can any of the Predictive Theories be Trusted ? *NAFEMS World Congress, 23rd-26th May, Boston, 2011*.

59. HINTON M. J., KADDOUR A. S. [2012]: The background to the Second World-Wide Failure Exercise. *J. Compos. Mater.*, **46(19-20)**, 2283-2294.

60. HOFFARD T. A., MALVAR L. J. [2005]: Fiber-Reinforced Polymer Composites in Bridges A State-of-the-Art Report. *Technical Memorandum Tm-2384-SHR*, Naval Facilities Engineering Service Center 1100 23rd Avenue Port Hueneme, CA 93043-4370 (available online at: www.dtic.mil/dtic/tr/fulltext/u2/a524794.pdf).

61. IBRAHIMBEGOVIĆ A. [2005]: Nonlinear shell theory with finite rotations and finite strains: recent achievements. In: Pietraszkiewicz W., Szymczak C. (eds.), *Shell Structures: Theory and Applications*, CRC Press, London, 19-32.

62. JASTRZĘBSKI P., MUTERMILCH J., ORŁOWSKI W. [2011]: *Wytrzymałość Materiałów*, Arkady, Warszawa.

63. JINGXUAN H., MINGFA R., SHIYONG S., QIZHONG H., XIANNIAN S. [2011]: Failure prediction on advanced grid stiffened composite cylinder under axial compression. *Compos. Struct*. **93(7)**, 1939-1946.

64. JONES R. M. [1999]: *Mechanics of Composite Materials*, Taylor & Francis, Philadelphia.

65. KADDOUR A. S., HINTON M. J., SMITH P. A., LI S. [2013]: The background to the third world-wide failure exercise. *J. Compos. Mater.*, **47(20-21)**, 2417-2426.

66. KAW A. K. [2006]: *Mechanics of Composite Materials (2nd edition)*. CRC Press - Taylor & Francis Group, Boca Raton.

67. KNOPS M. [2008]: *Analysis of Failure in Fiber Polymer Laminates*. Springer-Verlag, Berlin, Heidelberg, New York.

68. KNIGHT JR. N. F., RANKIN C. C., BROGAN F. A. [2002]: STAGS computational procedure for progressive failure analysis of laminated composite structures, *Int. J. Nonlinear Mech.*, **37**, 833-849.

69. KOLIOS A. J., PROIA S. [2012]: Evaluation of the Reliability Performance of Failure Criteria for Composite Structures. *World Journal of Mechanics*, **2(3)**, 162-170.

70. KONG C. W., LEE I. C., KIM C. G., HONG C. S. [1998]: Postbuckling and failure of stiffened composite panels under axial compression, *Compos. Struct.*, **42,** 13–21.

71. KREJA I. [2003]: *Continuum Mechanics, materials for PhD students of the Faculty of Civil and Environmental Engineering, Gdańsk University of Technology*. Centre for Urban Construction and Rehabilitation CURE, Gdańsk.

72. KREJA I. [2011]: A literature review on computational models for laminated composite and sandwich panels. *Cent. Eur. J. Eng.*, **1(1)**, 59-80.

73. KUBIAK T., MANIA R. J. [2016]: Hybrid versus FR laminate channel section columns – Buckling and postbuckling behaviour. *Compos. Struct.*, **154**, 142-149.

74. KULA K. [2007]: *Nieliniowa analiza płyt włóknokompozytowych. Rozprawa doktorska*, Uniwersytet Zielonogórski, Instytut Budownictwa, Zakład Mechaniki Budowli, Zielona Góra.

75. LADEVÈZE P., LUBINEAU G., MARSAL D. [2006]: Towards a bridge between the micro- and mesomechanics of delamination for laminated composites. *Composites Science and Technology*, **66(6)**, 698-712.

76. LEONE F. A., DAVILA C. G., GIROLAMO D. [2015]: Progressive damage analysis as a design tool for composite bonded joints. *Compos. Part B-Eng.*, **77**, 474-483.

77. LEWIŃSKI J., WILCZYŃSKI A.P., WITEMBERG-PERZYK D. [1994]: Podstawy *Wytrzymałości Materiałów*. Oficyna Wydawnicza Politechniki Warszawskiej, Warszawa.

78. LI Z. X., ZHUO X., VU-QUOC L, IZUUDDIN B. A., WEI H. Y. [2013]: A four-node corotational quadrilateral elastoplastic shell element using vectorial rotational variables. *Int. J. Numer. Meth. Engng.*, **95(3)**, 181-211.

79. LIBAI A., SIMMONDS J. G. [1998]: *The nonlinear Theory of Elastic Shells, 2nd edition*. Cambridge University Press, Cambridge.

80. LOVE A. E. H. [1889]: The small free vibrations and deformation of a thin elastic shell. *Phil. Trans. R. Soc. Lond. A*, 179, 491-546.

81. LOVE A. E. H. [1927]: *A treatise on the Mathematical Theory of Elasticity*, Cambridge University Press, Cambridge.

82. LUBINEAU G., LADEVÈZE P. [2008]: Construction of a micromechanics-based intralaminar mesomodel, and illustrations in ABAQUS/Standard. *Comp. Mater. Sci.*, **43(1)**, 137-145.

83. LUBOWIECKA I. [2001]: *Całkowanie nieliniowych dynamicznych równań ruchu w mechanice konstrukcji. Dynamika powłok sprężystych. Rozprawa doktorska.* Politechnika Gdańska, Wydział Inżynierii Lądowej, Gdańsk.

84. LUBOWIECKA I., CHRÓŚCIELEWSKI J. [2002]: On dynamics of flexible branched shell structures undergoing large overall motion using finite elements. *Comp. Struct.*, **80(9-10)**, 891-898.

85. LOPEZ-ANIDO R., TROUTMAN D. L., BUSEL J. P.: Fabrication and Installation of Modular FRP Composite Bridge Deck. *Creative Pultrusions Technical Papers* (available online at: www.creativepultrusions.com/connect-with-us/technical-papers).

86. MEYER-PIENING H.-R. [2004]: Application of the Elasticity Solution to Linear Sandwich Beam, Plate and Shell Analyses. *J. Sandw. Struct. Mater.*, **6(4)**, 295-312.

87. MOHR O. [1900]: Welche Umstände bedingen die Elastizitatsgrenze und den Bruch eines aterials? (Which circumstances are causing yield limit and fracture of a material?). *Civilingenieur*, **44**, 1524-1530 and 1572-1577.

88. NAHAS M. N. [1986]: Survey of failure and post-failure theories of laminated fiber-reinforced composites. *J. Compos. Technol. Res.*, **8,** 138-153.

89. NALI P., CARRERA E. [2012]: A numerical assessment on two-dimensional failure criteria for composite layered structures. *Compos. Part B-Eng.*, **43(2)**, 280-289.

90. NX NASTRAN 7 MANUAL.

91. PARIS F. [2001]: *A Study of Failure Criteria of Fibrous Composite Materials*, NASA technical report NASA/CR-2001-210661.

92. PIETRASZKIEWICZ W. [2011]: Refined resultant thermomechanics of shells. *Int. J. Eng. Sci.*, **49(10)**, 1112-1124.

93. PIETRASZKIEWICZ W., KONOPIŃSKA V. [2014]: Drilling couples and refined constitutive equations in the resultant geometrically non-linear theory of elastic shells. *Int. J. Solids Struct.*, **51(11-12)**, 2133-2143.

94. PIETRASZKIEWICZ W. [2016]: The resultant linear six-field theory of elastic shells: What it brings to the classical linear shell models? *Z. Angew. Math. Mech*, **96(8)**, 899-915.

95. PONETA P., KULPA M., WŁASAK L., SIWOWSKI T. [2014]: Koncepcja i badania innowacyjnego dźwigara mostowego z kompozytów FRP. *Inżynieria i Budownictwo*, **70(3)**, 147-151.

96. PRUSTY B. G., SATSANGI S. K., RAY C. [2001]: First Ply Failure Analysis of Laminated Panels Under Transverse Loading. *J. Reinf. Plast. Comp.*, **20(8)**, 671-684.

97. PUCK A., KOPP J., KNOPS M. [2002]: Guidelines for the determination of the parameters in Puck's action plane strength criterion. *Compos. Sci. Technol.*, **62(3)**, 371-378.

98. PUCK A., SCHÜRMANN H. [1998]: Failure analysis of FRP laminates by means of physically based phenomenological models. *Compos. Sci. Technol.*, **58(7)**, 1045-1067.

99. PUCK A., SCHÜRMANN H. [2002]: Failure analysis of FRP laminates by means of physically based phenomenological models. *Compos. Sci. Technol.*, **62(12-13)**, 1633-1662.

100. POTYRAŁA P. B. [2011]: *Use of Fibre Reinforced Polymer Composites in Bridge Construction. State of the Art in Hybrid and All-composite Structures.* Master of Science Thesis, Universitat Politecnica de Catalunya, Barcelona, Spain, available
online at: http://upcommons.upc.edu/bitstream/handle/2099.1/12353/Use%20o f%20Fibre%20Reinforced%20Polymer%20Composites%20in%20Bridge%20 Construction.%20State%20of%20the%20Art%20in%20Hybrid%20and%20All -Composite%20Structures..pdf?sequence=1.

101. PYRZOWSKI Ł., SOBCZYK B., WITKOWSKI W., CHRÓŚCIELEWSKI J. [2015]: Three-point bending test of sandwich beams supporting the GFRP footbridge design process - validation analysis. In: Kleiber M., Burczyński T., Wilde K., Górski J., Winkelmann K., Smakosz Ł. (eds.), *3rd Polish Congress of Mechanics and 2st International Conference on Computer Methods in Mechanics Short Papers Vol. 1*, 8.09-11.09.15 Gdańsk University of Technology, Gdańsk, Poland.

102. RACZKIEWICZ W. [2010]: Beton - materiał budowlany znany od wieków. *Przegląd Budowlany*, **83(10)**, 13-18.

103. RAMM E. [2000]: From Reissner Plate Theory to Three Dimensions in Large Deformation Shell Analysis. *Z. Angew. Math. Mech.*, **80(1)**, 61-68.

104. RATTANAWANGCHAROEN N. [2005]: First-ply Failure Analysis of Laminated Composite Cylindrical Panels. *J. Reinf. Plast. Comp.*, **24(14)**, 1521-1537.

105. REDDY J. N., PANDEY A. K. [1987]: A First-Ply Failure Analysis of Composite Laminates. *Comput. Struct.*, **25(3)**, 371-393.

106. REDDY J. N. [2004]: Mechanics of Laminated Composite Plates and Shells: Theory and Analysis, Second Edition. CRC Press, Boca Raton.

107. REDDY J. N. [2007]: Theory and Analysis of Elastic Plates and Shells, Second Edition. CRC Press, Boca Raton.

108. REISSNER E. [1974a]: Linear and nonlinear theory of shells. In: Fung Y. C., Sechler E. E. (eds.), *Thin Shell Structures*, Prentice-Hall, Engelwood Cliffs, 29-44.

109. REISSNER E. [1974b]: The Effect of Transverse Shear Deformation on the Bending of Elastic Plates. *J. Appl. Mech.*, **12**, 69-77.

110. ROHWER K. [2015]: Predicting fiber composite damage and failure. *J. Compos. Mater.*, **49(21)**, 2673-2683.

111. RYMARZ C. [1993]: *Mechanika Ośrodków Ciągłych.* Wydawnictwo Naukowe PWN, Warszawa.

112. SABIK A. [2012]: *Analiza stateczności powłok warstwowych obciążonych termicznie*. Wydawnictwo Politechniki Gdańskiej, Gdańsk.

113. SABIK A., KREJA I. [2008]: Linear analysis of laminated multilayered plates with the application of zig-zag function. *Arch. Civ. Mech. Eng.*, **VIII(4)**, 61-72.

114. SAWICKI. A. [1994]: *Mechanika Kontinuum. Wprowadzenie*. IBW PAN, Gdańsk.

115. SANTIUSTE C., SÁNCHEZ-SÁEZ S., BARBERO E. [2010]: A comparison of progressive-failure criteria in the prediction of the dynamic bending failure of composite laminated beams. *Compos. Struct.*, **92**, 2406-2414.

116. SATISH KUMAR Y. V., SRIVASTAVA A. [2003]: First ply failure analysis of laminated stiffened plates. *Compos. Struct.,* **60(3)**, 307-315.

117. SCHMIDT B., DAMRATH R., PAHL P.J. [1977]: A geometrically and physically nonlinear finite element method for the analysis of stiffened rectangular panels*, In: Bathe K.J., Oden J.T., Wunderlich W. (eds.)*, *Formulations and Computational Algorithms in Finite Element Analysis,* The MIT Press, Boston, 294-320.

118. SIMMONDS J. G. [1984]: The nonlinear thermodynamical theory of shells: Descent from 3-dimensions without thickness expansions, In: Axelrad E. L., Emmerling F. A. (eds.), *Flexible Shells, Theory and Applications*, Springer-Verlag, Berlin.

119. SLEIGHT D. W. [1999]: *Progressive Failure Analysis Methodology for Laminated Composite Structures*, NASA technical publication NASA/TP-1999-209107.

120. Smits J. [2014]: Architectural Engineering of FRP Bridges. In: *Proceedings of 37th IABSE Symposium*, Madrid.

121. Sobczyk B. [2015]: Laminated plates and shells – first ply failure analysis within 6-parameter shell theory. In: S. Elgeti, J.-W. Simon (eds.), *Proceedings of YIC GACM 2015: 3rd ECCOMAS Young Investigators Conference and 6th GACM Colloquium*, 20.07-23.07.15 RWTH Aachen University, Aachen, Germany.

122. Sobczyk B. [2016]: FEA of foam core sandwich footbridge based in 6-parameter shell theory. In: *Proceedings of ECCOMAS Congress 2016, VII European Congress on Computational Methods in Applied Sciences and Engineering*, 5.06-10.06.16, Crete Island, Greece.

123. Sun C.T., Quinn B.J., Tao J., Oplinger D.W., Hughes W. J. [1996]: Comparative Evaluation of Failure Analysis Methods for Composite Laminates. *Technical report number DOT/FAA/AR-95/109*.

124. Tessler A., Di Sciuva M., Gherlone M [2010]: A consistent refinement of first-order shear deformation theory for laminated composite and sandwich plates using improved zigzag kinematics. *J. Mech. Mater. Struct.*, **5(2)**, 341-367.

125. Tony Gee Partners [2012]: FRP footbridge at UK railway station. *Reinforced Plastics,* **56(6)**, 6.

126. Tuttle M. E. [2004]: *Structural Analysis of Polymeric Composite Materials*. Marcel Dekker inc., New York, Basel.

127. Tsai S.W., Wu E.M [1971]: A General Theory of Strength for Anisotropic Materials, J. Compos. Mater., **5(1)**, 58-80.

128. Vasiliev V. V., Morozov E. V. [2013]: *Advanced Mechanics of Composite Materials and Structural Elements*. *Third Edition*. Elsevier, Oxford.

129. Wagner W. [2010]: Modeling of failure mechanisms in laminated composite shell structures. In: Pietraszkiewicz W., Kreja I. (eds.), *Shell Structures: Theory and Applications, Vol. 2*, CRC Press, London, 25-34.

130. Wang L., Zheng Ch., Luo H., Wei S., Wei Z. [2015]: Continuum damage modeling and progressive failure analysis of carbon fiber/epoxy composite pressure vessel. *Compos Struct.*, **134**, 475-482.

131. Warren K. C., Lopez-Anido R. A., S. S. Vel, Bayraktar H. H. [2016]: Progressive failure analysis of three-dimensional woven carbon composites in single-bolt, double-shear bearing. *Compos. Part B-Eng.*, **84**, 266-276.

132. WITKOWSKI W. [2006]: *Efektywny 4-węzłowy element skończony o wzbogaconym polu odkształceń w nieliniowej 6-parametrowej teorii powłok. Rozprawa doktorska.* Politechnika Gdańska, Wydział Inżynierii Lądowej, Gdańsk.

133. WITKOWSKI W. [2009]: 4-Node combined shell element with semi-EAS-ANS strain interpolations in 6-parameter shell theories with drilling degrees of freedom. *Comput. Mech.*, **43**, 307–319.

134. YE J., QIU Y., CHEN X., MA J. [2015]: Initial and final failure strength analysis of composites based on a micromechanical method, *Compos. Struct.*, **125**, 328-335.

135. YU M.-H. [2002]: Advances in strength theories for materials under complex stress state in the 20th Century. *Appl. Mech. Rev.*, **55(3)**, 169-218.

136. ZIENKIEWICZ O. C., TAYLOR R. L. [2000]: *Finite Element Method (Vol 2), 5th ed..* Butterworth-Heinemann, Oxford.

137. ZOBEL H., KARWOWSKI W., ŻÓŁTOWSKI K., KOZAKIEWICZ A. [2005]: Badania kratownicowej kładki z kompozytu polimerowego zbrojonego włóknem szklanym. *Inżynieria i Budownictwo*, **61(4)**, 202-206.

APPENDIX A. - DERIVATION OF PUCK CRITERION

This Appendix summarise considerations of Puck and Schürmann leading to the derivation of the final form of the criterion.

The following equations are treated as the base form for further discussion:

$$f_{E,IFF0} = c_1 \frac{\sigma_n}{R_\perp^{(+)A}} + c_2 \left(\frac{\sigma_n}{R_\perp^{(+)A}} \right)^2 + \left(\frac{\tau_{nt}}{R_{\perp\perp}^A} \right)^2 + \left(\frac{\tau_{nl}}{R_{\perp\|}^A} \right)^2 = 1 \quad \text{for } \sigma_n \geq 0, \qquad (A.1)$$

$$f_{E,IFF0} = \frac{\tau_{nt}^2}{\left(R_{\perp\perp}^A \right)^2 - 2p_{\perp\perp}^{(-)}\sigma_n} + \frac{\tau_{nl}^2}{\left(R_{\perp\|}^A \right)^2 - 2p_{\perp\|}^{(-)}\sigma_n} = 1 \quad \text{for } \sigma_n < 0, \qquad (A.2)$$

assuming that:

$$\frac{p_{\perp\perp}^{(-)}}{R_{\perp\perp}^A} = \frac{p_{\perp\|}^{(-)}}{R_{\perp\|}^A} = \frac{p}{R} = \text{const.} \qquad (A.3)$$

Owing to the assumption (4.51), it is possible to simplify equation (4.53) to the following form:

$$f_{E,IFF0} = \left(\frac{\tau_{nt}}{R_{\perp\perp}^A} \right)^2 + \left(\frac{\tau_{nl}}{R_{\perp\|}^A} \right)^2 + c\sigma_n = 1 \quad \text{for } \sigma_n < 0. \qquad (A.4)$$

The shear stress components τ_{nt} and τ_{nl} can be replaced by one shear resultant $\tau_{n\psi}$, which acts on the fracture plane and is expressed as (KNOPS M. [2008]):

$$\tau_{n\psi} = \sqrt{\tau_{nt}^2 + \tau_{nl}^2} . \qquad (A.5)$$

Consequently, equations (4.52) and (A.4) can be rewritten:

$$f_{E,IFF} = c_1 \frac{\sigma_n}{R_\perp^{(+)A}} + c_2 \left(\frac{\sigma_n}{R_\perp^{(+)A}} \right)^2 + \left(\frac{\tau_{n\psi}}{R_{\perp\psi}^A} \right)^2 = 1 \quad \text{for } \sigma_n \geq 0, \qquad (A.6)$$

$$f_{E,IFF} = \left(\frac{\tau_{n\psi}}{R_{\perp\psi}^A} \right)^2 + c\sigma_n = 1 \quad \text{for } \sigma_n < 0. \qquad (A.7)$$

The constants c_1, c_2 and c can be derived from boundary conditions (see KNOPS M. [2008] or DEUSCHLE H. M. [2010] for details). In effect, equations (A.6) and (A.7) become:

$$f_{E,IFF0} = 2p_{\perp\psi}^{(+)} \frac{\sigma_n}{R_\perp^{(+)A}} + \left(1 - 2\frac{p_{\perp\psi}^{(+)}R_\perp^{(+)A}}{R_{\perp\psi}^A}\right)\left(\frac{\sigma_n}{R_\perp^{(+)A}}\right)^2 + \left(\frac{\tau_{n\psi}}{R_{\perp\psi}^A}\right)^2 = 1 \quad \text{for } \sigma_n \geq 0, \tag{A.8}$$

$$f_{E,IFF0} = \left(\frac{\tau_{n\psi}}{R_{\perp\psi}^A}\right)^2 + 2\frac{p_{\perp\psi}^{(-)}}{R_{\perp\psi}^A}\sigma_n = 1 \quad \text{for } \sigma_n < 0. \tag{A.9}$$

The left hand side of (A.8) or (A.9) is named as the failure index f_E, which is used as the measure of failure risk. If the calculated failure index is less than 1 the failure does not initiates. The expressions (A.8) or (A.9) determine particular situation of failure initiation. However, in some cases the condition for failure in Puck criterion may be more strict. Beyond a particular value of the normal stress in fibre direction σ_{aa}, the risk of IFF becomes higher. This, according to some experimental observations, occurs when e.g. $\sigma_{aa} >\sim 0.7X_T$ and is expressed by the reduction of the failure initiation limit value, namely by the introduction of a weakening factor $0 \leq \eta_{w1} \leq 1$ (PUCK A., SCHÜRMANN H. [1998]). In such a case the condition for failure initiation is $f_{E,IFF} = \dfrac{f_{E,IFF0}}{\eta_{w1}} = 1$. Different approaches to estimate η_{w1} are proposed. This problem is discussed in chapter 4.4. Up to the point, where the details of η_{w1} determination are described, it will be assumed in the considerations that the effect of high normal stress will not be included in IFF criterion description.

The stress components σ_n and $\tau_{n\psi}$, which occur in (A.8) and (A.9) form some higher order expressions. Therefore the failure indices described by (A.8) and (A.9) cannot be treated as direct measures of risk of failure (KNOPS M. [2008]). To convert them into the aforesaid measures the following transformation is proposed (DEUSCHLE H. M. [2010]):

$$f_{E,IFF0} = \frac{1}{2}\left(\Sigma L + \sqrt{(\Sigma L)^2 + 4\Sigma Q}\right), \tag{A.10}$$

where ΣL denotes the sum of all linear terms correspondingly in (A.8) and (A.9), while ΣQ the sum of quadratic terms in the aforementioned equations. This results for the (A.8)

equation in: $\Sigma L = 2 p_{\perp\psi}^{(+)} \dfrac{\sigma_n}{R_{\perp}^{(+)A}}$; $\Sigma Q = \left(1 - 2\dfrac{p_{\perp\psi}^{(+)} R_{\perp}^{(+)A}}{R_{\perp\psi}^{A}}\right)\left(\dfrac{\sigma_n}{R_{\perp}^{(+)A}}\right)^2 + \left(\dfrac{\tau_{n\psi}}{R_{\perp\psi}^{A}}\right)^2$. In effect the IFF

criterion is established (see e.g. PUCK A., SCHÜRMANN H. [2002]), for normal tensile

stressing $\sigma_n \geq 0$:

$$f_{E,IFF0} = \sqrt{\left[\left(\frac{1}{R_{\perp}^{(+)A}} - \frac{p_{\perp\psi}^{(+)}}{R_{\perp\psi}^{A}}\right)\sigma_n(\theta)\right]^2 + \left(\frac{\tau_{nt}(\theta)}{R_{\perp\perp}^{A}}\right)^2 + \left(\frac{\tau_{nl}(\theta)}{R_{\perp\|}^{A}}\right)^2} + \frac{p_{\perp\psi}^{(+)}}{R_{\perp\psi}^{A}}\sigma_n(\theta) = 1 \tag{A.11}$$
$$\text{for } \sigma_n \geq 0$$

and by analogy for normal compressive stressing $\sigma_n < 0$:

$$f_{E,IFF0} = \sqrt{\left(\frac{\tau_{nt}(\theta)}{R_{\perp\perp}^{A}}\right)^2 + \left(\frac{\tau_{nl}(\theta)}{R_{\perp\|}^{A}}\right)^2 + \left[\frac{p_{\perp\psi}^{(-)}}{R_{\perp\psi}^{A}}\sigma_n(\theta)\right]^2} + \frac{p_{\perp\psi}^{(-)}}{R_{\perp\psi}^{A}}\sigma_n(\theta) = 1 \text{ for } \sigma_n < 0, \tag{A.12}$$

where:

$$\frac{p_{\perp\psi}^{(+),(-)}}{R_{\perp\psi}^{A}} = \frac{p_{\perp\perp}^{(+),(-)}}{R_{\perp\perp}^{A}}\cos^2\psi + \frac{p_{\perp\|}^{(+),(-)}}{R_{\perp\|}^{A}}\sin^2\psi \tag{A.13}$$

and:

$$\cos^2\psi = \frac{\tau_{nt}^2}{\tau_{nt}^2 + \tau_{nl}^2}$$
$$\sin^2\psi = \frac{\tau_{nl}^2}{\tau_{nt}^2 + \tau_{nl}^2} \tag{A.14}$$

In (A.11) and (A.12) the stress components are written as θ−dependent. It is to emphasize that the particular angle of failure plane inclination needs to be found in order to predict the failure initiation. The θ−dependency was tacitly assumed in all preceding equations. The fracture angle determination is performed numerically in the case of 3D state of stress, which introduce some computational cost. The goal is to find the angle of inclination with the highest failure risk (PUCK A., SCHÜRMANN H. [1998]). However, an analytical formulation is proposed for the plane stress lamina that simplify the consideration (KNOPS M. [2008]). Thus, the final forms of the initiation criterion can be developed easier.

Since many other failure initiation criterions are written in terms referred to the lamina material coordinate system, the stress tensor components defined on the failure plane are transformed to the material system, via well-known rules (PUCK A., SCHÜRMANN H. [1998]), in order to maintain consistency and simplicity of application of the Puck criterion:

$$\sigma_n(\theta) = \sigma_{bb} \cos^2 \theta$$
$$\tau_{nt}(\theta) = -\sigma_{bb} \sin \theta \cos \theta \,. \qquad\qquad (A.15)$$
$$\tau_{nl}(\theta) = \sigma_{ba} \cos \theta$$

A proper analysis of failure mechanism, which is discussed below, allows one to use lamina strengths instead of failure plane strengths.

In the case of normal tensile stressing $\sigma_n \geq 0$, the IFF is initiated on a plane, which normal is parallel to the b material axis, so $\theta = 0°$. This finding was deduced on the basis of experimental research (see PUCK A., SCHÜRMANN H. [1998]). Therefore, the state of stress leading to failure is derived from (A.15) as: $\sigma_n = \sigma_{bb}$, $\tau_{nt} = 0$, $\tau_{nl} = \sigma_{ba}$. Moreover, if the fracture angle $\theta = 0°$, then the strengths of the failure plane can be defined using standard strengths, namely $R_\perp^{(+)A} = Y_T$ and $R_{\perp\parallel}^A = S_l$. The above findings are applied to the equation (A.12), including also expressions (A.13) and (A.14). This results in the IFF mode A condition:

$$f_{E,IFF0,A} = \sqrt{\left(1 - p_{\perp\parallel}^{(+)} \frac{Y_T}{S_l}\right)^2 \left(\frac{\sigma_{bb}}{Y_T}\right)^2 + \left(\frac{\sigma_{ba}}{S_l}\right)^2} + \frac{p_{\perp\parallel}^{(+)}}{S_l} \sigma_{bb} = 1 \qquad \text{for } \sigma_{bb} \geq 0 \,. \text{(A.16)}$$

Now the attention is focused on the normal compressive stressing $\sigma_n < 0$. According to the experimental observation, it was found that the first possible angle of fracture is $\theta = 0°$ (PUCK A., SCHÜRMANN H. [1998]). This happens if the ratio of transverse stress and the transverse compressive strength remains approximately below 0.4 ($|\sigma_{bb}/Y_T| <\sim 0.4$) (KNOPS M. [2008]). This mode of failure is called B mode. Similar conclusions, as in the case of $\sigma_n \geq 0$, can be formulated for $\theta = 0°$, regarding the state of stress and strengths of the failure plane. Therefore, mode B failure initiation condition is established, basing on the aforementioned conclusions, which are associated with (A.12), and relations (A.13) and (A.14) (PUCK A., SCHÜRMANN H. [1998]):

$$f_{E,IFF0,B} = \frac{1}{S_l}\left(\sqrt{\sigma_{ba}^2 + \left(p_{\perp\parallel}^{(-)}\sigma_{bb}\right)^2} + p_{\perp\parallel}^{(-)}\sigma_{bb}\right) = 1$$

$$\text{for } \sigma_{bb} < 0 \text{ and } 0 \leq \frac{|\sigma_{ba,crit}|}{R_{\perp\perp}^A} \leq \left|\frac{\sigma_{ba}}{\sigma_{bb}}\right|$$

(A.17)

The validity condition of (A.17) will be explained later.

If a condition $|\sigma_{bb}/Y_T| \geq \sim 0.4$ is met, then the inclination of failure plane is $\theta \neq 0°$ and has to be determined somehow. This can be achieved by finding the plane with the maximum risk of failure, namely by the solution of extremum problem $\frac{d(f_{E,IFF})}{d(\theta)} = 0$ for $\sigma_n < 0$. The first solution of this equation is $\theta = 0°$. This case was already discussed. The second solution leads to determination of the following failure angle (PUCK A., SCHÜRMANN H. [2002]):

$$\theta_f = \arccos\sqrt{\frac{1}{2\left(1 + p_{\perp\perp}^{(-)}\right)}\left[\left(\frac{\sigma_{ba}}{\sigma_{bb}}\right)^2\left(\frac{R_{\perp\perp}^A}{S_l}\right)^2 + 1\right]}$$

(A.18)

and it yields the IFF mode C damage (see e.g. PUCK A., SCHÜRMANN H. [1998] or KNOPS M. [2008]):

$$f_{E,IFF0,C} = \left[\left(\frac{\sigma_{ba}}{2\left(1 + p_{\perp\perp}^{(-)}\right)S_l}\right)^2 + \left(\frac{\sigma_{bb}}{Y_c}\right)^2\right]\frac{Y_c}{(-\sigma_{bb})} = 1.$$

(A.19)

It turned also out, during the solution resulting in mode C, that the normal stress on action plane remains constant and equal to $-R_{\perp\perp}^A$ (see e.g. PUCK A., SCHÜRMANN H. [1998] or KNOPS M. [2008]) for each combination of $\sigma_{bb} < 0$ and θ_f, whenever IFF mode C initiation is achieved. This is expressed by:

$$\sigma_n = \sigma_{bb}\cos^2\theta_f = -R_{\perp\perp}^A.$$

(A.20)

Therefore, the transition between modes B and C occurs for $\sigma_{bb} = -R_{\perp\perp}^A$. The in-plane shear component corresponding to $\sigma_{bb} = -R_{\perp\perp}^A$ can be calculated as follows:

$$\sigma_n = \sigma_{bb}\cos^2\theta_f = -R_{\perp\perp}^A.$$

(A.21)

Consequently, all points of the IFF failure envelope that lie below the line, defined by the transition point and the beginning of the coordinate system in $\sigma_{bb} - \sigma_{ba}$ space are classified to the IFF mode C. This is shown in Fig.A.1 for AS4/3501-6 Carbon/Epoxy composite lamina. Hence, the final validity condition for the mode C is expressed as $\sigma_{bb} < 0$ and

$$0 \leq \left| \frac{\sigma_{ba}}{\sigma_{bb}} \right| \leq \frac{\left| \sigma_{ba,crit} \right|}{R_{\perp\perp}^{A}}.$$
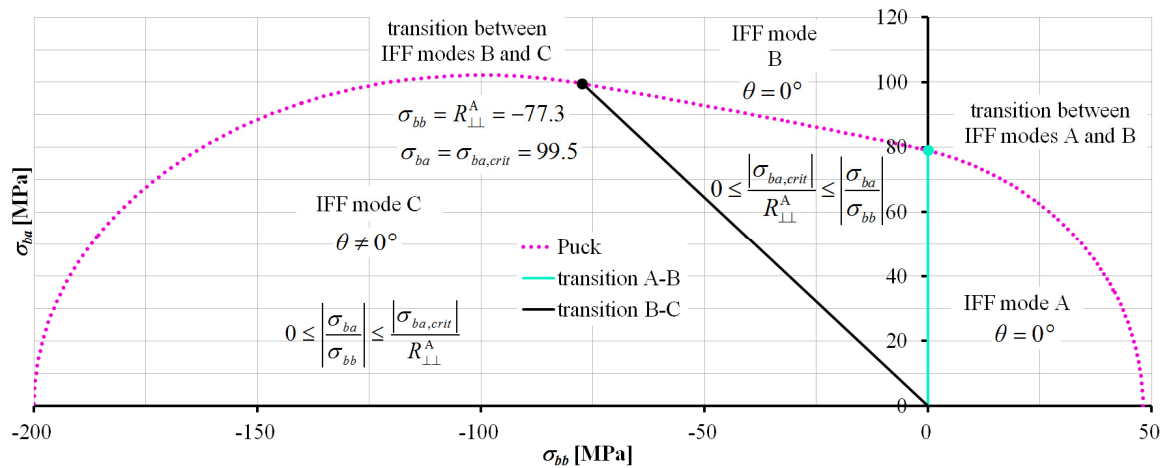

Fig.A.1 Failure initiation envelope of Puck IFF criterion in σ_{bb} - σ_{ba} space.